universität wien

DISSERTATION

Titel der Dissertation

Neuronal control of backward walking in *Drosophila melanogaster*

verfasst von

Rajyashree Sen (BSc. MSc.)

angestrebter akademischer Grad

Doctor of Philosophy (PhD)

Wien, 2017

Studienkennzahl lt. Studienblatt:	A 091 490
Dissertationsgebiet lt. Studienblatt:	Molekulare Biologie
Betreut von:	Dr. Barry J. Dickson

In loving memory of my wonderful father.

Acknowledgments

I am indebted to many people who directly or indirectly contributed to this work.

My thanks to:

My supervisor, Barry Dickson, who inspired and motivated me, and taught me to do science.

My thesis committee – Vivek Jayaraman, Gwyneth Card, Andrew Straw and Thomas Hummel – who ensured that I didn't stray.

Salil Bidaye, who helped me get started.

Ming Wu (Rubin lab, Janelia Research Campus), who I was lucky to work with, whose valuable contributions made the work in Chapter 2 possible.

Ansgar Büschges, Till Bockemühl and Michael Dübbert (University of Cologne), for insightful discussions and technical support (Chapter 3).

Kai Feng (Dickson Lab, Queensland Brain Institute), for long hours of trans-Pacific discussions on how flies walk backwards.

All Dickson lab members from 2012-2017, for valuable discussions and an excellent research and social environment.

Barry Dickson, Mark Palfreyman and Kai Feng for valuable comments on my thesis.

Marie Curie FliACT network, for funding my time in Vienna, for connecting me to scientists and peers I will value throughout my career.

HHMI Janelia Research Campus for funding my research in the United States.

Project Technical Resources (PTR) and Instrument Design and Fabrication Departments (ID&F) of Janelia Research Campus for dream technical support.

Friends from Washington Improvisational Theater (WIT) and my improv team ‘Please and Thank You’, for teaching me how to be comfortable with uncertainty.

Mark Palfreyman – without whose friendship, intellectual inputs, advice, pep-talks, and occasional stories of naked mole rats and other weird organisms, this thesis would not have been possible.

Finally, to my parents and sister for their incredible patience, love and unconditional support throughout my PhD.

This thesis is dedicated to my father, whom I miss dearly. His curiosity, creativity, sense of wonder about the world, and love for finding things out had been a constant source of inspiration over the years. It was he who instilled in me a deep love for science and a perennial longing for adventure.

Table of Contents

Zusammenfassung

In dieser Studie untersuchten wir, wie das Nervensystem sensorische Information in eine Verhaltensantwort umwandelt. Dabei konzentrierten wir uns auf ein bestimmtes Verhalten der Fruchtfliege, *Drosophila melanogaster*, das Rückwärtsgehen. Vorarbeiten hatten, durch Aktivierung umschriebener spezifischer Nervenzell-Gruppen, eine Klasse von absteigend projizierender Kommando-Nervenzellen, die sog. "Moonwalker-Zellen, identifiziert. Diese sind sowohl notwendig als auch ausreichend, um Rückwärtsgehen auszulösen. Davon ausgehend verwendeten wir in der nun hier vorliegenden Arbeit Methoden zur Verhaltensuntersuchung und Aktivitätsmessung, um zwei Fragen zu beantworten: 1) welcher Art sind die sensorischen Eindrücke und Nervenzellbahnen, welche die Moonwalker-Nervenzellen aktivieren, und 2) welche Nervenzell-Netzwerke wandeln Moonwalker-Nervenzell-Aktivität in Rückwärts-Bewegung um?

In unserer Arbeit zeigen wir nun, dass eine bestimmte Gruppe von visuellen Projektions-Nervenzellen, die Lobula Nervenzellen der Säule 16, über die Aktivierung der Moonwalker-Nervenzellen visuell-ausgelöstes Rückwärtsgehen in der Fruchtfliege bewirken. Weiterhin identifizieren wir, im Rahmen eines Inaktivierungs-Screenings, eine Nervenzell-Population, welche, wenn inaktiviert, Rückwärtsgehen beeinträchtigt. Wir entdeckten außerdem ein Paar aufsteigender Projektions-Nervenzellen, welche Information an die Moonwalker-Nervenzellen weitergeben, und einige kleinere Gruppen von Interneuronen, die anatomisch dem ventralen Nervenstrang zuzuordnen sind. Weitere Untersuchungen der Anatomie, der Aktivität und der Rolle dieser identifizierten Nervenzell-Gruppe für Verhaltenssteuerung werden dazu beitragen, die Moonwalker-Nervenzellen in das sich abzeichnende Nervenzell-Netzwerk für Rückwärtsgehen in der Fruchtfliege einzubauen.

Synopsis

In this work, I set out to understand how the nervous system transforms sensory information into action. I focused on a specific behavior in *Drosophila melanogaster*: backward locomotion. Our lab has previously identified a class of descending command neurons – the moonwalker descending neurons (MDNs) – that are both necessary and sufficient for backward walking in *Drosophila*. From this starting point, I took behavioral and functional approaches aimed at answering two broad questions: 1) what is the nature of the sensory cues and neural pathways that trigger MDN activation and 2) what are the neural circuits that transform MDN activity into the joint movements required for backward locomotion.

I demonstrated that a specific population of visual projection neurons, the lobula columnar 16 (LC16) cells, acts via the MDNs to trigger visually evoked retreat in *Drosophila*. I further undertook a neuronal silencing screen to identify neuronal populations that, when silenced, impair backward locomotion. Hits from my screen include a pair of ascending neurons that provides inputs to MDNs as well as several small populations of interneurons anatomically restricted to the ventral nerve cord. In total, these hits are likely to encompass both putative inputs and outputs of MDNs, and therefore represent an important step in understanding the circuitry governing backward locomotion. Further anatomical, behavioral, and physiological studies will incorporate these identified neurons into the emerging circuit for backward walking in *Drosophila*.

Chapter 1

Introduction

1.1 Motivation

How does the nervous system transform sensory information into appropriate locomotor action? Neural circuits that select and implement locomotor action must interact, on one hand, with circuits that process sensory information and, on the other hand, with circuits that execute the motor commands. Neural networks that execute locomotion must orchestrate multiple motor motifs, each of which in temporal isolation would not achieve any organismal goal. Furthermore, as an animal maneuvers through its natural environment, it must dynamically and flexibly modify its motor output in response to a changing environment. The pathway from sensory input to coordinated motor output thus encompasses multiple interacting circuits. These circuits must dynamically interact with the external and internal environment of the organism. A holistic understanding of adaptive behavior must therefore encompass multiple functionally distinct neuronal ensembles, and must incorporate an understanding of how these circuits interact during the behavior of the organism. In this regard, escape pathways provide an attractive platform for investigating the interactions among sensory processing, action selection and motor execution. This thesis is designed to understand the neuronal underpinnings of evasive walking in the genetic model organism *Drosophila melanogaster.*

Walking forms a crucial component of many behaviors in *Drosophila.* Fruit flies walk to find food, mates and egg-laying sites. They also walk backwards when faced with certain imminent threats [1]. A fly's backward-walking 'retreat' is tuned to specific threats and is thus the output of complex circuit computations that detect, perceive and localize the threat (sensory processing), select the appropriate action out of a repertoire of possibilities (action selection), and subsequently alter the movements of limb-joints to reverse the walking direction (motor execution). Thus, investigating the neuronal basis of backward walking forms an excellent model to understand neuronal processing at multiple levels.

1.2 Backward locomotion in the animal kingdom

In almost all organisms studied, backward locomotion is either employed as a strategy to escape or as a behavioral solution to circumvent the exigencies of the environment. Worms back up in response to aversive cues [2–7]; stick insects in response to aversive touch [8]; lampreys when encountering obstacles [9]; and flies, in response to visual threats and to maneuver out of tight spots [1,10]. There are some insects that naturally walk backwards for long bouts – desert ants [11–13], for example, drag heavy food home by walking long distances backwards. In other cases a unique environment can dictate the evolution of robust backward locomotion. For instance, the naked mole rat lives its entire life in long narrow underground burrows. To cope with this environment the naked mole rat has sensory bristles both on its nose and tail and can run just as fast backwards as it can forwards [14,15].

We have a fairly detailed circuit level understanding of backward locomotion in 3 organisms – *Caenorhabditis elegans*, lamprey and stick insects. Studies in each of these organisms have provided insights into when and how backward locomotion is selected and executed. By highlighting these organisms, I will give an overarching view of known circuits, with an aim to highlight those elements that might be generalizable. Understanding backward locomotion in other organisms will inform the relatively nascent field of *Drosophila* locomotion.

1.2.1 *Caenorhabditis elegans*

In the nematode *Caenorhabditis elegans*, the sensory inputs, command neurons and motor outputs for backward locomotion have been extensively studied at a circuit level. *C. elegans* backs up in response to nose touch, volatile chemical repellents and aversive osmotic stimuli [2–7]. Additionally, reversals are observed to occur in a probabilistic fashion during exploratory behavior [16]. Backward locomotion in worms, like in flies, is usually followed by a turn (known as the omega turn after its shape) [17,18]. This turn reorients the worm to a new direction: away from the aversive cue [16]. *C. elegans* has a numerically simple nervous system comprising 302 neurons, and its entire connectome has been delineated using electron microscopy [19–21]. The fully elucidated connectome has guided the models that aim to understand the critical concepts on the selection and execution of directed locomotion.

The core set of neurons for executing coordinated locomotion in worms includes five pairs of premotor neurons – AVA, AVB, AVD, AVE and PVC (historically referred to as command neurons). These premotor neurons integrate inputs from sensory and other upstream neurons

and innervate four distinct classes of motor neurons – VA (ventral A), VB (ventral B), DA (dorsal A) and DB (dorsal B) neurons [21]. The AVA, AVE and AVD neurons innervate the A class of motor neurons by both chemical and electrical synapses and mediate backward locomotion; the PVC and AVB neurons innervate the B class of motor neurons by chemical synapses and gap junctions respectively and mediate forward locomotion [22,23]. Among the premotor neurons, ablation of AVA and AVB neurons results in the strongest reductions in backward and forward locomotion respectively, suggesting that these neurons play the most critical roles in controlling the direction of locomotion [22,23]. One of the inputs to AVA is a nociceptive polymodal neuron – ASH – known to mediate escape reversals [2,3,5–7]. The sensory processes of ASH are exposed to the external environment through a pair of sensilla located at the nose of the worm [24]. ASH neurons receive aversive mechanical [3], chemical [2,5–7] and osmotic [2] stimuli and are monosynaptically connected to AVA [25–27]. Furthermore, the ASH-AVA synapse is graded, favoring a model that stronger inputs from ASH to AVA – presumably encoding a more dangerous aversive stimulus – would trigger more robust escapes responses [27].

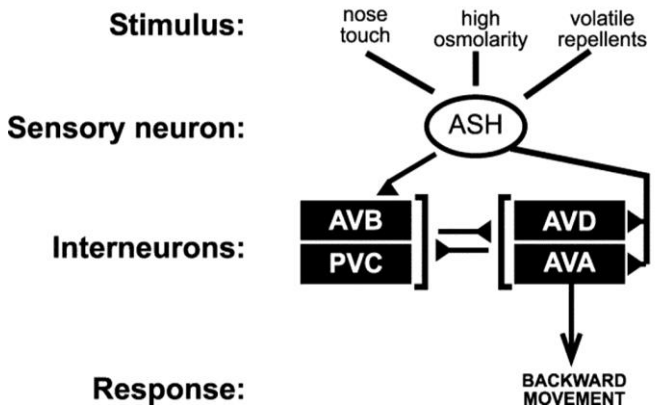

Figure 1. Aversive mechanosensory, chemical and osmolar cues mediate backward locomotion in *C. elegans* through known circuit components. **Adapted from [4].** ASH neurons receive aversive sensory stimuli from nose touch, high osmolarity and volatile repellents, and relay this information to premotor command neurons – the AVA and AVD neurons – that mediate backward locomotion.

In *C. elegans*, higher activity levels in AVA or A neurons favor backward locomotion whereas the same in AVB or B neurons favors forward locomotion. Initiations of reversals are temporally correlated with an increase in the activity of AVA and A neurons and a simultaneous decrease in the activity of AVB and B neurons, while an inverse profile is

observed during a switch to forward locomotion [28–30]. The inherent bias to move in forward direction in *C. elegans* can be explained by a gap-junction mediated shunting mechanism at the AVA-A synapse, that maintains a low output state at the levels of AVA and A neurons during locomotion [30]. It is important to note that the forward and backward circuits in *C. elegans* are highly interconnected – an observation that might be generalizable to locomotor circuits in other organisms.

To get a detailed mechanistic understanding of the nature of interaction between networks mediating forward and backward locomotion, it is important to simultaneously record the activity of multiple neurons. Advancements in recent years have enabled whole-brain imaging of neuronal activity at a single-cell-resolution in *C. elegans*. Whole-brain imaging relies on a genetically encoded reporter of calcium activity (GCaMP), whose activity can be captured with high-speed volumetric images of the entire brain in animals [18,31,32]. Interestingly, the brains of immobilized worms reliably show a finite number of 'fictive' locomotor states [18,33] – patterns of neural activity that would, if the animal were mobile, give rise to distinct locomotor behaviors (reversals and turns and forward swims). This shows that even in the absence of movement, a large fraction of the worm brain still encodes the different locomotor states. Each of these states, or patterns, of neural activity can be viewed as a dynamic system and can be visualized using plots called phase-space diagrams (Figures 2A and 2B) [18,32–34]. Remarkably, the 'fictive' locomotor states seem to fluidly (but predictably) transition from one state to the other in a cyclical fashion. Moreover, the sequence of these transitions has similarities with the sequence of actions in a freely moving animal (Figure 2C) [18,32]. Environmental input merely increases the probability of a given state, for example, increased oxygen concentration increases the frequency with which the reversal state is entered.

Presumably, the brain of a freely moving worm also oscillates between the various stable locomotor states (reversals and turns and forward swims) and environmental stimuli simply bias the probability of entering or leaving one state over the other. The phase space diagrams also reveal that large proportions of neurons in the worm brain are multi-functional and provide distributed signal to encode each locomotor state as an ensemble. It is clear that although AVA executes the command to reverse, the circuits that lead to reversal encompass a large fraction of the brain. Behaviors in *C. elegans* are thus generated by the concerted neural activity of distributed networks rather than by simple feedforward sensory-motor pathways. A variety of behaviors in other organisms (ranging from digestion in lobsters [35]

to decision making in leech [36] and primates [37]) have been shown to also rely on large distributed networks with cyclical dynamics.

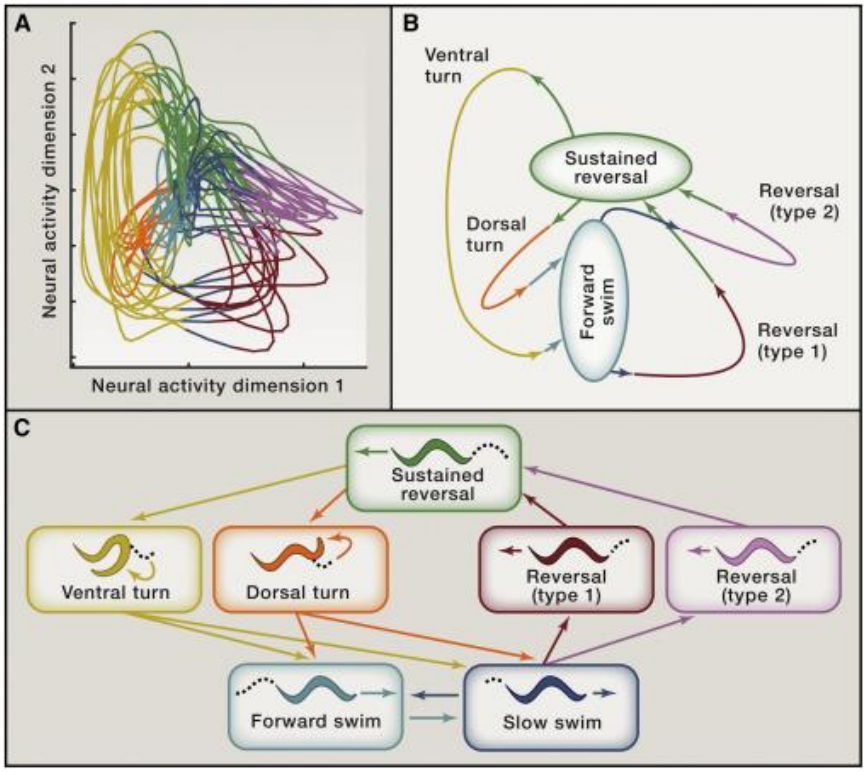

Figure 2. Large proportions of neurons in the worm brain are multi-functional and provide distributed signal to encode the different locomotor states as an ensemble. Adapted from [33].

(A) Example 2-D phase space diagram of network activity color-coded for the various fictive locomotor states. The coordinate axes represent two relevant parameters for network activity over time. In brief, the n-dimensional time series describing whole-brain activity was collapsed into a two-dimension trajectory by principal component analysis. The resultant trajectories follow a cyclical, repeatable pattern in which one stereotyped neural activity pattern follows another until the initial pattern reappears and the cycle repeats.

(B) Regions of neural activity space labeled by corresponding fictive locomotor states

(C) Types and probabilities of transitions between locomotor states in freely moving *C. elegans*

It remains to be explored if the level of multifunctionality seen in circuits in the *C elegans* nervous system is merely an adaptation for tackling relatively complex behaviors with a numerically simple nervous system, as has been suggested [38]. However, it is noteworthy that circuits in other organisms are known to show distributed control and multi-stable states and can participate in generating different behaviors [34]. Therefore, aspects of the neuronal basis of locomotion in *C. elegans* might be generalizable to circuits in other organisms.

At present the recording of whole-brain activity in an organism with defined cell types has only been accomplished in *C. elegans*. Nonetheless, multi-functional circuits existing in more than one stable state have been seen in other organisms [34,39–41]. Such circuits include central pattern generators (CPGs) – local circuits in the spinal cord or nerve cord of organisms that have intrinsically rhythmic properties and are used for locomotion in a wide range of species [42–46]. Despite being able to produce rhythmic behavior, *C. elegans* does not obviously possess autonomous CPGs [47]. In the next section we will explore those organisms where CPGs have been defined. These CPGs produce a rhythmic motor output without receiving a rhythmic input and have been shown to exist in a finite number of stable states to generate a range of related (and sometimes distinct) motor rhythms (for reviews see [35,42,48,49]).

1.2.2 Lamprey

The aquatic vertebrate lamprey usually shows episodes of backward swimming upon encounters with obstacles [9]. It has been shown that both backward and forward swimming rely on the patterned activity of a common pattern-generating circuit. Repeated individual pattern-generating circuits are distributed along the length of the animal and their communication allows for the intersegmental coordination that yield the smooth wave of muscle contraction and relaxations that undulate the body of the entire organism. Neural mechanisms switch the sequence of recruitment of the different sets of neurons within the pattern-generating network to achieve backward swimming.

The lamprey propels itself through water with an undulatory wave that passes from the head to the tailfin. During backward swimming, the wave passes in the opposite direction, from the tail to the head [50]. In lampreys, swimming relies on the alternating left-right contraction and relaxation of body muscles. The sequence of muscle contraction and relaxation is, in turn, driven by the patterned activity of intrinsically rhythmic central pattern generators (CPGs). The locomotor burst activity can be elicited equally robustly in isolated spinal cords, isolated hemicords and isolated hemisegments [51,52]. It has been shown that each hemisegment contains a unit CPG – comprising a network of excitatory glutamatergic interneurons that form connections within the network. The unit CPG outputs onto excitatory motor neurons and, contralaterally, via inhibitory glycinergic neurons, to the reciprocal unit CPG on the other side of the body. Together these unit CPGs and their outputs generate the

alternating left-right contraction and relaxations of the body that occur during swimming. The CPGs are further coordinated along the length of the body to generate the phase-lag (1% of the cycle duration) between the burst of activity in each successive hemicord unit CPG (Figure 3) [50]. Fictive backward and forward swimming elicited in an isolated lamprey spinal cord are both characterized by the constant phase lag [53]. The lag can be explained by a circuit architecture where the unit burst generators are coupled to their respective neighbors with bidirectional excitatory connections. Two different hypotheses have been proposed to account for the change in direction of the undulatory locomotor wave in backward versus forward swimming – the 'trailing oscillator' hypothesis [53,54] and the 'network reconfiguration hypothesis' [55,56].

According to the 'trailing oscillator' hypothesis, the intrinsic frequency of the unit oscillators are not the same along the spinal cord and the oscillator with the highest intrinsic frequency imposes its rhythm onto others. If the most rostral segment has a higher intrinsic frequency than the caudal segments, it would take the lead and the other segments would follow with a phase lag – generating a rostrocaudal wave. Indeed, during forward swimming, a rostrocaudal gradient in the intrinsic frequency of the oscillators is observed [50]. Further evidence for this hypothesis comes from the finding that fictive backward swimming could be elicited in isolated spinal cords when the caudal oscillators were manipulated to have higher excitability than their rostral neighbors [53,54]). One could propose that tactile stimulation at the anterior end of the lamprey activates backward-swimming neurons that, in turn, set a caudorostral gradient of intrinsic frequencies such that every oscillator has a higher intrinsic frequency than its rostral neighbor.

According to the 'network reconfiguration' hypothesis, the individual oscillators along the spinal cord have equivalent intrinsic frequency and the direction of locomotor wave propagation results from a switch in the connections of the oscillators with their neighbors. In this case, anterior-touch could evoke backward-swimming neurons that would activate the backward-specific connections in the chain of oscillators [50].

Backward swimming in lamprey is also characterized by higher amplitude and lower frequency body undulations than forward swimming [50]. It is plausible that, in addition to activating the oscillators, backward-swimming neurons modify the intrinsic properties of the oscillators to make them oscillate with appropriate frequency [50]. In fact, application of *N*-

methyl-D-aspartate in the spinal cord of lamprey has been shown to elicit two different states of rhythmic activity – a fast rhythm similar to forward swimming and a slow rhythm similar to backward swimming [51]. It has been suggested that other neuromodulators such as serotonin (5-HT) that produce more intense and longer bursts may also be involved in modifying the intrinsic properties of the oscillators during backward swimming [50,57,58].

In summary, the lamprey chain-oscillator serves as an example of a multi-functional patter-generating circuit that exists in at least 2 stable states – backward and forward swimming. The lamprey studies further show that the switch from forward to backward state can be achieved by manipulating the excitability of only a fraction of neurons in the network – the unit oscillators in the caudal segments.

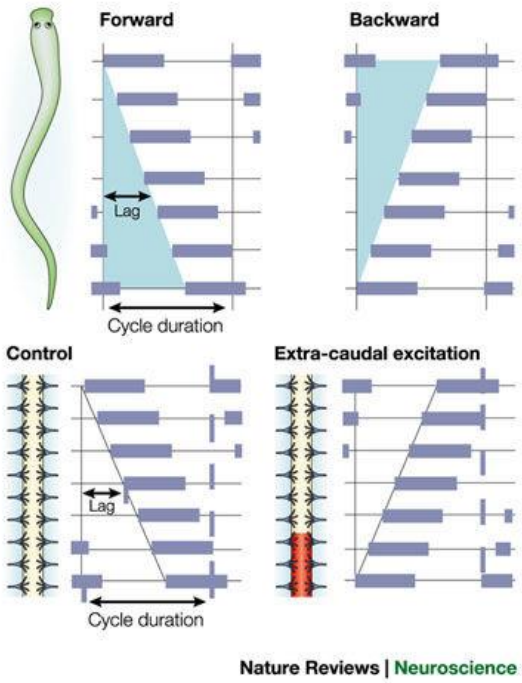

Figure 3. Bi-stable locomotor pattern-generators in lamprey. Adapted from [59].

Top: Both forward and backward swimming in lamprey are characterized by a constant phase lag between consecutive segmental unit oscillators. Bottom: Fictive backward and forward swimming generated in isolated spinal cords recapitulate the phase lag of freely swimming lamprey. Fictive backward swimming can be elicited experimentally by driving extra excitation to the caudal segments.

1.2.3 Stick insects

Much of our understanding of limbed backward locomotion comes from experimental and theoretical studies done in stick insects. Stick insects will walk backwards in response to tactile stimulation of their antennae [60], suggesting that backward locomotion might be used in these insects as a strategy to steer away from aversive touch or to get out of a confined space [10]. The reversal of walking direction results from an alteration in the phase of muscle activation at a single joint – the thoracic-coxa joint [61]. The retractor/protractor pair of antagonistic muscles controls the thoracic-coxa joint. During forward walking, the leg moves backwards while on the ground (stance phase) and forwards in the air (swing phase); during backward walking it moves forwards while on the ground (stance phase) and backwards in the air (swing phase). During forward walking, the retractor is activated during ground contact (stance) and moves the leg backwards on the ground until the posterior extreme position is reached, at which point the tarsus is lifted off. In the air (swing phase), the protractor is activated and moves the leg forwards until the anterior extreme position is reached and touch down occurs. Backward walking effectively reverses this sequence.

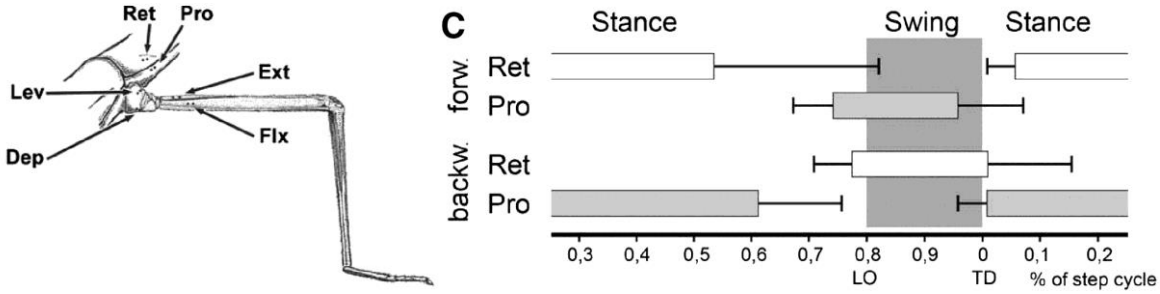

Figure 4. Backward locomotion results from an alteration in the phase of protractor and retractor muscle activation. Adapted from [61]. Left: Middle leg of a stick insect. Locations of retractor/protractor (Ret/Pro), levator/depressor (Lev/Dep) and extensor/flexor (Ext/Flx) muscle pairs are labeled. Right: Average beginning or ending of retractor (Ret) and protractor (Pro) muscle activity versus percentage of step-cycle. TD, touch-down; LO, lift-off. Gray rectangle indicates swing phase.

In stick insects, the rhythmic activation of antagonistic muscle pairs controlling the different leg joints (e.g, retractor/protractor for the thoracic-coxa joint) are driven by the patterned activity of CPGs [62,63]. While central command neurons are responsible for the choice of locomotion direction, sensory signals from the periphery (reporting the actual movement of the limbs and strains in the cuticle (sensory feedback)) play an important role in controlling

the output of the CPGs [64]. The switch in the phase of muscle activation at the thoracic-coxa joint during backward locomotion can be largely explained by a switch in the way sensory feedback is processed to modulate the output of the CPG controlling the joint [64,65].

Similar to lamprey, in which unit CPGs control the rhythmic activity of individual hemisegments, in stick insects individual CPGs control the rhythmic activity of antagonistic muscles in each leg-joint [62,63]. Each of the 6 legs in stick insects have 3 joints – which means that there are a total of 18 CPGs that control the patterned activity of limb-muscles during locomotion in these organisms (three per limb). Evidence for this comes from experiments in deafferented thoracic ganglia, where application of muscarinic agonists could reliably elicit alternating patterns of activity in antagonistic motor neuron pools of each leg joint [62]. However, in contrast to lamprey, where unit CPGs are coupled by bidirectional excitatory connections between neighbors, the CPGs in stick insects are uncoupled. The motor rhythms generated in deafferented preparation show no coupling between motor neuron pools belonging to different leg joints [62,63]. The aquatic environment through which a lamprey swims is largely uniform compared to the varied environment of a stick insect's world. In addition, in order to move, the lamprey must generate a coordinated wave that propagates through the length of the body. In response to the environment and their body morphology, lampreys have highly coupled CPGs that utilize a fast predictive component [66]. By contrast, a stick insect walks through rugged terrains and has 6 legs that need to individually respond to the local terrain. This has led to CPGs that are comparatively much more autonomous [66]. Sensory feedback, reporting the movement of limbs, plays a critical role in coordinating the CPGs of different joints in stick insects. For example, during forward locomotion, load signals from the legs activate the retractor during stance phase. But identical input during backward walking instead activates protractor activity. The neuronal basis for this switch has been explained by a neuromechanical model (Figure 5) [65].

At a circuit level, the CPG controlling the thoracic-coxa joint can be viewed as an oscillator consisting of two mutually inhibitory neurons (C1 and C2). This core CPG is connected to motor neurons by a layer of interneurons (IN1 and IN2 in Figure 5). IN1 and IN2 are key to the switch in walking direction: It is at the connection between the core CPG (the C neurons) and the interneurons (the IN neurons) that the forward and backward specific neurons act (SF and SB in Figure 5). SF and SB provide inhibitory output that enables a switch in the

connection between the CPGs and motor neurons. This switch then results in a reversal of the motor neurons that are active during the stance and swing phase, as explained further below.

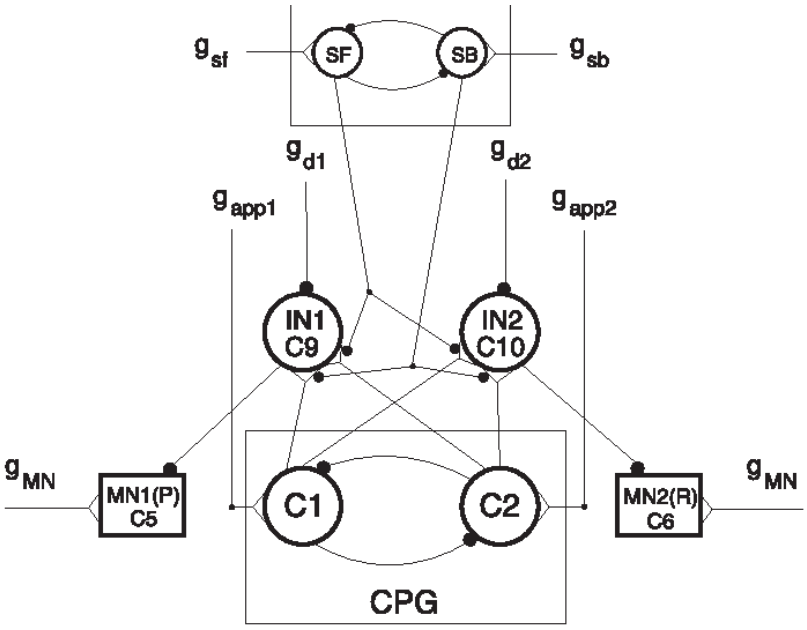

Figure 5. Neuromechanical model explaining the switch in the phase of activation of retractor/protractor during backward walking. Adapted from [65]. See text for details.

During forward walking, SF is active and SB is silent. The possibility of clashing information is eliminated by the mutual inhibition between SF and SB. SF provides simultaneous presynaptic inhibition to the connection from C2 to IN1 and C1 to IN2. C1 also receives excitatory feedback from the leg, which conveys load information (from campaniform sensilla) and somatosensory information (from the femur-tibia joint). In the stance phase of forward walking, C1 is active in phase with IN1. In this phase, the concerted activity of C1 and IN1 triggers IN1 to provide inhibitory output to the protractor motor neuron, MN1(P)C5 – simultaneously, the retractor motor neuron, MN2(R)C6, which is not receiving inhibitory input, is active. This state is reinforced by sensory feedback, which provides excitatory drive to C1 during the stance phase. Together, the circuit ensures that during the stance phase of forward walking the leg pushes backward on the substrate. This state continues until the rhythm of the CPG oscillates back from high C1 activity to high C2 activity – a state presumably reinforced by somatosensory feedback indicating that the leg has attained its extreme posterior position. The leg lifts off the substrate and enters the swing phase. In the swing phase of forward walking, C2 and IN2 are active – leading to the inhibition of MN(R)C6 and the activation of MN1(P)C5. This state is again enforced by the lack of

excitatory drive that sensory feedback would normally provide to C1 during surface contact. The leg swings forward.

With this understanding, the switch to backward locomotion is now relatively easy to comprehend. At the circuit level, SB provides inhibitory input to the connection between C1 and IN1 and the connection between C2 and IN2. This inhibition ensures that, instead of synchronous firing of C1 to IN1 and C2 to IN2 (as seen in forward walking), the neurons firing synchronously are the C1 to IN2 and the C2 to IN1 pairs. Thus, MN1(P)C5 activity is favored in the swing phase and MN2(R)C6 during the stance phase. Importantly, the sensory feedback now also has the opposite role – it reinforces the C1 and IN2 pair and MN(R)C6 activity. Thus, the sensory feedback favors retractor activity during the stance phase. The legs push forward in stance and swings backward in the air.

Importantly, the entire network exists in a bi-stable state and can be switched to forward or backward walking mode by providing excitatory input to a small fraction of the network, that is the switch neurons – SF or SB. Such excitatory drive to the switch neurons may originate from higher order centers in the brain, for example when the stick insects sense a ‘dead-end’ and decide to walk backwards and steer away.

For *C elegans*, lamprey and stick insects, it has either been experimentally demonstrated (lamprey and *C. elegans*) or suggested from theoretical studies (stick insects) that backward locomotion results from switching the bias of a circuit that exists in two or more stable modes. However, it remains to be seen if this is generalizable to all organisms. Instead of a common circuit, salamanders have been proposed to use two autonomous pattern generators for forward and backward locomotion [67]. Behavioral studies on humans walking in treadmills have shown that the pattern-generators for backward and forward locomotion are independently adaptable and hence these circuits could be largely non-overlapping [68]. However, this result contradicts a previous study in infants that argued common locomotor CPGs for both modes of walking [69]. While it is clear that locomotion requires rhythmic neuronal activity, the jury is still clearly out on the circuit elements that generate these oscillations.

1.3 Advantages of *Drosophila* as a model organism to study backward walking

There are several advantages to using *Drosophila melanogaster* to study evasive backward walking in the context of sensorimotor transformations. Drosophila has a numerically tractable nervous system comprising ~10^5 neurons. Yet, despite the relatively small number of neurons, the fruit fly displays hallmarks of complex neuronal processing including motion detection [70], feature discrimination [71,72], state dependent modulation of sensory processing [73,74] and flexibility in motor planning [75–77]. Like other invertebrates, the nervous system of flies is fairly stereotyped, such that any given neuron can be reliably identified. Most importantly, recent years have seen large advancements in our ability to genetically target small populations of neurons. Briefly, numerous groups used defined *Drosophila* genomic enhancer fragments to reproducibly express the yeast GAL4 transcription factor. When combined with reporters such as GFP, they were able to define the neurons where the enhancer element was active. This approach was further refined by intersectional genetic approaches. The GAL4 protein can be split into 2 parts – a DNA binding domain and an activation domain – each of which could be fused to interacting leucine zipper domains. When such split-derivatives are put under the control of distinct enhancers, a functional GAL4 is reconstituted in the subset of cells where the expression patterns of the two enhancers intersect. The advantage of such a collection is that it can be used in a combinatorial fashion with a collection of reporter and activator elements located downstream of a minimal promoter that includes the GAL4 DNA binding site, UAS. The collection of UAS effectors include thermosensitive [78] or light sensitive cation channels [79] (to depolarize cells) light activated anion channels [80] (to hyperpolarize cells). They also include a number of fluorescent proteins that to report on the anatomy of neurons [81]. Together, advent of genetic control of small populations of neurons affords the possibility of a cellular-level understanding of circuit function. The value of this approach has been validated in unbiased neuronal silencing and activating screens, which have identified numerous specific neurons involved in *Drosophila melanogaster* behavior [10,82–87]**.** It is this cellular level control of defined subpopulations of neurons that gives flies a comparative advantage over the lamprey and the stick insect, where neurons have so far largely been identified solely by electrophysiology. Though our understanding of premotor control of locomotion in fruitflies is currently relatively limited, genetic access to small populations of neurons will make *Drosophila* uniquely suited to deciphering this circuit, and more generally

to understanding how a nervous system transforms sensory information into action. The first steps in our endeavors will no doubt be greatly informed by the extensive literature from locomotion in other organism.

1.4 What is known about backward locomotion in *Drosophila*?

Naturally triggered backward locomotion in *Drosophila* has so far been documented in the context of escape or avoidance. Wild fruit flies retreat from ambush predators by walking a few steps backwards and steering away [1]. In lab-setting, a predator-mimicking looming stimuli can also probabilistically trigger backward walking retreat in flies [72]. In addition to visual threats, backward locomotion can also be triggered when fruit flies are forced to walk in narrow constricted grooves with dead-ends [10]. Not surprisingly, they reach the end of the groove and reverse their walking direction (much like naked mole rats reversing in their tunnels to get out of a blind alley).

At the circuit level, the activity of a cluster of 4 descending neurons – the moonwalker descending neurons (MDNs) – is necessary and sufficient for triggering backward locomotion in flies [10]. The MDNs are 4 cells, 2 on each side of the central nervous system, with soma on the central brain, extensive bilateral arborizations at the ventromedial protocerebrum, asymmetric arbors at the subesophageal ganglia (SEZ) and axons that extend to the contralateral side of the ventral nerve cord to all three leg neuropils. Presynaptic sites of MDNs are located in the three leg neuropils and in the asymmetric SEZ arbor in brain. Thermogenetic activation of MDNs is sufficient to trigger backward locomotion. This artificially induced backward locomotion is coordinated and matches the natural backward locomotion in having a reversed metachronal gait from forward locomotion (the reverse sequence of footfalls from forward locomotion) [10].

While MDNs are a central player in backward locomotion, they are not the only identified circuit components. A pair of ascending neurons – the moonwalker ascending neurons (MANs) – have been shown to facilitate sustained backward locomotion in flies in which MDNs are active – potentially by inhibiting forward walking circuits [10]. MANs have their cell bodies and extensive arborizations in the metathoracic ganglia and a partially asymmetric arbor in the SEZ. The predominant presynaptic sites of MANs are located in the SEZ, in

close proximity to MDNs. Some presynaptic sites are also observed in the metathoracic ganglia and in the wing neuropils.

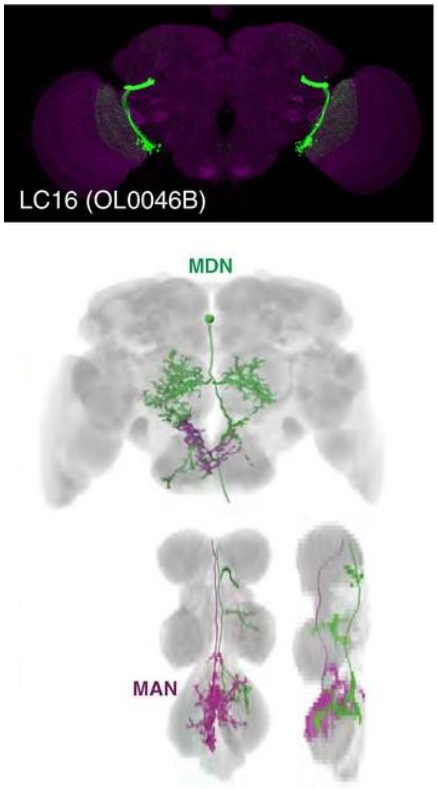

Figure 4. Circuits controlling backward locomotion in *Drosophila melanogaster*. Adapted from [72] (top) and [10] (bottom). Top: Brain of a *Drosophila* female fly expressing *CsChrimson:mVenus* in LC16 cells and stained with nc82 (magenta) and anti-GFP (green) counterstain. Bottom: Segmented MDN (green) and MAN (magenta) cells registered and overlaid onto a common reference brain and ventral nerve cord (VNC) template by non-rigid registration.

The identification of MDNs and MANs marks the starting point in understanding the neuronal underpinning of evasive walking in *Drosophila.* However, in contrast to our level of understanding of sensory inputs to backward locomotion circuits in worms, we currently have limited understanding of the underlying neural mechanisms by which MDNs get activated. From our observations of visually triggered backward walking retreat, we postulate that MDNs might receive inputs from visual threats. Recently, a population of visual projection neurons – the lobula columnar 16 (LC16) cells – has been shown to respond to looming stimuli and elicit the backward walking retreat [72] upon optogenetic activation with a red light activated cation channel CsChrimson [79]. In chapter 2 [88], we show that MDNs

receive inputs from the LC16 cells. However, apart from LC16 and MDNs, not much is known about the circuit components controlling backward walking in flies.

From our observations of flies reversing their direction and steering away from dead-ends, we envision that MDNs might also receive inputs from mechanosensory cues. However, the identity of such neurons and the nature of their interaction with MDNs remain unidentified. We also know nothing about how MDNs control putative central pattern generators in flies. Does there exist a single multi-stable pattern generating circuit like in lampreys? Or are there distinct non-overlapping backward and forward pattern generators, as suggested in humans and salamanders? Do circuits mediating backward and forward walking have extensive overlaps as in *C. elegans*? In my thesis research, I aim to use the genetic toolkit of *Drosophila melanogaster* to lay a framework within which these questions can be addressed.

1.5 Aims of the thesis

In order to address how backward locomotion is selected and executed, it is imperative to identify additional circuit components for backward locomotion. The aims of this thesis are:

1. To identify the nature of sensory cues and neuronal circuits that activate MDNs and elicit backward locomotion
2. To identify circuit components in the VNC of the fruitfly important for execution of backward locomotion

1.6 References

1. Parigi, A., Porter, C., Cermak, M., Pitchers, W.R., and Dworkin, I. (2014). How predator hunting-modes affect prey behaviour: capture deterrence in *Drosophila melanogaster*. bioRxiv, 10330. doi: https://doi.org/10.1101/010330

2. Bargmann, C.I., Thomas, J.H., and Horvitz, H.R. (1990). Chemosensory cell function in the behavior and development of *Caenorhabditis elegans*. Cold Spring Harb. Symp. Quant. Biol. *55*, 529–538.

3. Kaplan, J.M., and Horvitz, H.R. (1993). A dual mechanosensory and chemosensory neuron in *Caenorhabditis elegans*. Proc. Natl. Acad. Sci. U. S. A. *90*, 2227–2231.

4. Kass, J., Jacob, T.C., Kim, P., and Kaplan, J.M. (2001). The EGL-3 proprotein convertase regulates mechanosensory responses of *Caenorhabditis elegans.* J. Neurosci. *21*, 9265–9272.

5. Hilliard, M.A., Bergamasco, C., Arbucci, S., Plasterk, R.H., and Bazzicalupo, P. (2004). Worms taste bitter: ASH neurons, QUI-1, GPA-3 and ODR-3 mediate quinine avoidance in *Caenorhabditis elegans*. EMBO J. *23*, 1101–1111.

6. Sambongi, Y., Nagae, T., Liu, Y., Yoshimizu, T., Takeda, K., Wada, Y., and Futai, M. Sensing of cadmium and copper ions by externally exposed Adl, Ase, and Ash neurons elicits avoidance response in *Caenorhabditis elegans*. Neuroreport *10*, 753–757.

7. Troemel, E.R., Chou, J.H., Dwyer, N.D., Colbert, H.A., and Bargmann, C.I. (1995). Divergent seven transmembrane receptors are candidate chemosensory receptors in *C. elegans*. Cell *83*, 207–218.

8. Graham, D., and Epstein, S. (1985). Behaviour and motor output for an insect walking on a slippery surface: II. backward walking. J. Exp. Biol. *118*, 287–296.

9. McClellan, A.D. (1989). Control of locomotion in a lower vertebrate, the lamprey: brainstem command systems and spinal cord regeneration. Integr. Comp. Biol. *29*, 37–51.

10. Bidaye, S.S., Machacek, C., Wu, Y., and Dickson, B.J. (2014). Neuronal control of *Drosophila* walking direction. Science *344*, 97–101.

11. Ardin, P.B., Mangan, M., and Webb, B. (2016). Ant homing ability is not diminished when traveling backwards. Front. Behav. Neurosci. *10*.

12. Pfeffer, S.E., Wahl, V.L., and Wittlinger, M. (2016). How to find home backwards? Locomotion and inter-leg coordination during rearward walking of *Cataglyphis fortis* desert ants. J. Exp. Biol. *219*, 2110–2118.

13. Pfeffer, S.E., and Wittlinger, M. (2016). How to find home backwards? Navigation during rearward homing of *Cataglyphis fortis* desert ants. J. Exp. Biol. *219*, 2119–2126.

14. Sherman, P.W., Jarvis, J.U.M., Alxander, R.D. eds. (2017). The biology of the naked mole-rat. (Princet: Univ. Press).

15. Eilam, D., and Shefer, G. (1992). Reversal of interleg coupling in backward locomotion implies a prime role of the direction of locomotion. J. Exp. Biol. *173*, 155–163.

16. Gray, J.M., Hill, J.J., and Bargmann, C.I. (2005). A circuit for navigation in *Caenorhabditis elegans*. Proc. Natl. Acad. Sci. U. S. A. *102*, 3184–3191.

17. Croll, A. N. (2009). Components and patterns in the behavior of the nematode *Caenorhabditis elegans*. J. Zool. *176*, 159–176.

18. Kato, S., Kaplan, H.S., Schrödel, T., Skora, S., Lindsay, T.H., Yemini, E., Lockery, S., and Zimmer, M. (2015). Global brain dynamics embed the motor command sequence of *Caenorhabditis elegans*. Cell *163*, 656–669.

19. Chen, B.L., Hall, D.H., and Chklovskii, D.B. (2006). Wiring optimization can relate neuronal structure and function. Proc. Natl. Acad. Sci. U. S. A. *103*, 4723–4728.

20. White, J.G., Southgate, E., Thomson, J.N., and Brenner, S. (1986). The structure of the nervous system of the nematode *Caenorhabditis elegans*. Phil Trans R Soc Lond B *314*, 1–340.

21. White, J.G., Southgate, E., Thomson, J.N., Brenner, S., and S, F.R. (1976). The structure of the ventral nerve cord of *Caenorhabditis elegans*. Phil Trans R Soc Lond B *275*, 327–348.

22. Chalfie, M., Sulston, J.E., White, J.G., Southgate, E., Thomson, J.N., and Brenner, S. (1985). The neural circuit for touch sensitivity in *Caenorhabditis elegans*. J. Neurosci. *5*, 956–964.

23. Wicks, S.R., Roehrig, C.J., and Rankin, C.H. (1996). A dynamic network simulation of the nematode tap withdrawal circuit: predictions concerning synaptic function using behavioral criteria. J. Neurosci. *16*, 4017–4031.

24. Perkins, L.A., Hedgecock, E.M., Thomson, J.N., and Culotti, J.G. (1986). Mutant sensory cilia in the nematode *Caenorhabditis elegans*. Dev. Biol. *117*, 456–487.

25. Hilliard, M.A., Apicella, A.J., Kerr, R., Suzuki, H., Bazzicalupo, P., and Schafer, W.R. (2005). In vivo imaging of *C. elegans* ASH neurons: cellular response and adaptation to chemical repellents. EMBO J. *24*, 63–72.

26. Mellem, J.E., Brockie, P.J., Zheng, Y., Madsen, D.M., and Maricq, A.V. (2002). Decoding of polymodal sensory stimuli by postsynaptic glutamate receptors in *C. elegans*. Neuron *36*, 933–944.

27. Lindsay, T.H., Thiele, T.R., and Lockery, S.R. (2011). Optogenetic analysis of synaptic transmission in the central nervous system of the nematode *C. elegans*. Nat. Commun. *2*, 306.

28. Ben Arous, J., Tanizawa, Y., Rabinowitch, I., Chatenay, D., and Schafer, W.R. (2010). Automated imaging of neuronal activity in freely behaving *Caenorhabditis elegans*. J. Neurosci. Methods *187*, 229–234.

29. Chronis, N., Zimmer, M., and Bargmann, C.I. (2007). Microfluidics for in vivo imaging of neuronal and behavioral activity in *Caenorhabditis elegans*. Nat. Methods *4*, 727–731.

30. Kawano, T., Po, M.D., Gao, S., Leung, G., Ryu, W.S., and Zhen, M. (2011). An imbalancing act: gap junctions reduce the backward motor circuit activity to bias *C. elegans* for forward locomotion. Neuron *72*, 572–586.

31. Schrödel, T., Prevedel, R., Aumayr, K., Zimmer, M., and Vaziri, A. (2013). Brain-wide 3D imaging of neuronal activity in *Caenorhabditis elegans* with sculpted light. Nat. Methods *10*, 1013–1020.

32. Nichols, A.L.A., Eichler, T., Latham, R., and Zimmer, M. (2017). A global brain state underlies *C. elegans* sleep behavior. Science *356*, eaam6851.

33. Branson, K., and Freeman, J. (2015). Imaging the neural basis of locomotion. Cell *163*, 541–542.

34. Briggman, K.L., and W.B. Kristan, J. (2008). Multifunctional pattern-generating circuits. Annu. Rev. Neurosci. *31*, 271–294.

35. Marder, E., and Calabrese, R.L. (1996). Principles of rhythmic motor pattern generation. Physiol. Rev. *76*, 687–717.

36. Briggman, K.L., Abarbanel, H.D.I., and Kristan, W.B. (2005). Optical imaging of neuronal populations during decision-making. Science *307*, 896–901.

37. Churchland, M.M., Cunningham, J.P., Kaufman, M.T., Foster, J.D., Nuyujukian, P., Ryu, S.I., and Shenoy, K.V. (2012). Neural population dynamics during reaching. Nature *487*, nature11129.

38. Riddle, D.L., Blumenthal, T., Meyer, B.J., and Priess, J.R. eds. (1997). *C. elegans* II 2nd ed. (Cold Spring Harbor (NY): Cold Spring Harbor Laboratory Press)

39. Getting, P.A. (1989). Emerging principles governing the operation of neural networks. Annu. Rev. Neurosci. *12*, 185–204.

40. Getting, P.A., and Dekin, M.S. (1985). Tritonia swimming. In model neural networks and behavior. (Springer, Boston, MA), pp. 3–20.

41. Marder, E. (1994). Invertebrate neurobiology: polymorphic neural networks. Curr. Biol. *4*, 752–754.

42. Kiehn, O. (2006). Locomotor circuits in the mammalian spinal cord. Annu. Rev. Neurosci. *29*, 279–306.

43. Brown, T.G. (1911). The intrinsic factors in the act of progression in the mammal. Proc. R. Soc. Lond. B Biol. Sci. *84*, 308–319.

44. Büschges, A., Schmitz, J., and Bässler, U. (1995). Rhythmic patterns in the thoracic nerve cord of the stick insect induced by pilocarpine. J. Exp. Biol. *198*, 435–456.

45. Chrachri, A., and Clarac, F. (1987). Induction of rhythmic activity in motoneurons of crayfish thoracic ganglia by cholinergic agonists. Neurosci. Lett. *77*, 49–54.

46. Pearson, K.G. (1972). Central programming and reflex control of walking in the cockroach. J. Exp. Biol. *56*, 173–193.

47. de Bono, M., and Maricq, A.V. (2005). Neuronal substrates of complex behaviors in *C. elegans*. Annu. Rev. Neurosci. *28*, 451–501.

48. Grillner, S. (2006). Biological pattern generation: the cellular and computational logic of networks in motion. Neuron *52*, 751–766.

49. Marder, E. (2000). Motor pattern generation. Curr. Opin. Neurobiol. *10*, 691–698.

50. Islam, S.S., Zelenin, P.V., Orlovsky, G.N., Grillner, S., and Deliagina, T.G. (2006). Pattern of motor coordination underlying backward swimming in the lamprey. J. Neurophysiol. *96*, 451–460.

51. Cangiano, L., and Grillner, S. (2005). Mechanisms of rhythm generation in a spinal locomotor network deprived of crossed connections: the lamprey hemicord. J. Neurosci. *25*, 923–935.

52. Grillner, S., and Wallén, P. (2002). Cellular bases of a vertebrate locomotor system–steering, intersegmental and segmental co-ordination and sensory control. Brain Res. Rev. *40*, 92–106.

53. Matsushima, T., and Grillner, S. (1992). Neural mechanisms of intersegmental coordination in lamprey: local excitability changes modify the phase coupling along the spinal cord. J. Neurophysiol. *67*, 373–388.

54. Matsushima, T., and Grillner, S. (1990). Intersegmental co-ordination of undulatory movements--a "trailing oscillator" hypothesis. Neuroreport *1*, 97–100.

55. Kopell, N., and Ermentrout, G.B. (1986). Symmetry and phaselocking in chains of weakly coupled oscillators. Commun. Pure Appl. Math. *39*, 623–660.

56. Kopell, N., and Ermentrout, G.B. (1988). Coupled oscillators and the design of central pattern generators. Math. Biosci. *90*, 87–109.

57. Harris-Warrick, R.M. (2011). Neuromodulation and flexibility in central pattern generator networks. Curr. Opin. Neurobiol. *21*, 685–692.

58. Wallén, P., Buchanan, J.T., Grillner, S., Hill, R.H., Christenson, J., and Hökfelt, T. (1989). Effects of 5-hydroxytryptamine on the afterhyperpolarization, spike frequency regulation, and oscillatory membrane properties in lamprey spinal cord neurons. J. Neurophysiol. *61*, 759–768.

59. Grillner, S. (2003). The motor infrastructure: from ion channels to neuronal networks. Nat. Rev. Neurosci. *4*, 573–586.

60. Graham, D., and Epstein, S. (1985). Behaviour and Motor Output for an Insect Walking on a Slippery Surface: II. Backward Walking. J. Exp. Biol. *118*, 287–296.

61. Rosenbaum, P., Wosnitza, A., Büschges, A., and Gruhn, M. (2010). Activity patterns and timing of muscle activity in the forward walking and backward walking stick insect *Carausius morosus*. J. Neurophysiol. *104*, 1681–1695.

62. Büschges, A. (1995). Role of local nonspiking interneurons in the generation of rhythmic motor activity in the stick insect. J. Neurobiol. *27*, 488–512.

63. Bässler, U., and Büschges, A. (1998). Pattern generation for stick insect walking movements—multisensory control of a locomotor program. Brain Res. Rev. *27*, 65–88.

64. Akay, T., Ludwar, B.C., Göritz, M.L., Schmitz, J., and Büschges, A. (2007). Segment specificity of load signal processing depends on walking direction in the stick insect leg muscle control system. J. Neurosci. *27*, 3285–3294.

65. Toth, T.I., Knops, S., and Daun-Gruhn, S. (2012). A neuromechanical model explaining forward and backward stepping in the stick insect. J. Neurophysiol. *107*, 3267–3280.

66. Buschges, A. (2004). Sensory control and organization of neural networks mediating coordination of multisegmental organs for locomotion. J. Neurophysiol. *93*, 1127–1135.

67. Ashley-Ross, M.A., and Lauder, G.V. (1997). Motor patterns and kinematics during backward walking in the pacific giant salamander: evidence for novel motor output. J. Neurophysiol. *78*, 3047–3060.

68. Buford, J.A., Zernicke, R.F., and Smith, J.L. (1990). Adaptive control for backward quadrupedal walking. I. Posture and hindlimb kinematics. J. Neurophysiol. *64*, 745–755.

69. Lamb, T., and Yang, J.F. (2000). Could different directions of infant stepping be controlled by the same locomotor central pattern generator? J. Neurophysiol. *83*, 2814–2824.

70. Borst, A., and Helmstaedter, M. (2015). Common circuit design in fly and mammalian motion vision. Nat. Neurosci. *18*, nn.4050.

71. Seelig, J.D., and Jayaraman, V. (2013). Feature detection and orientation tuning in the *Drosophila* central complex. Nature *503*, nature12601.

72. Wu, M., Nern, A., Williamson, W.R., Morimoto, M.M., Reiser, M.B., Card, G.M., and Rubin, G.M. (2016). Visual projection neurons in the *Drosophila* lobula link feature detection to distinct behavioral programs. eLife *5*, e21022.

73. Maimon, G., Straw, A.D., and Dickinson, M.H. (2010). Active flight increases the gain of visual motion processing in *Drosophila*. Nat. Neurosci. *13*, 393–399.

74. Suver, M.P., Mamiya, A., and Dickinson, M.H. (2012). Octopamine neurons mediate flight-induced modulation of visual processing in *Drosophila*. Curr. Biol. *22*, 2294–2302.

75. Card, G., and Dickinson, M.H. (2008). Visually mediated motor planning in the escape response of *Drosophila*. Curr. Biol. *18*, 1300–1307.

76. Gibson, W.T., Gonzalez, C.R., Fernandez, C., Ramasamy, L., Tabachnik, T., Du, R.R., Felsen, P.D., Maire, M.R., Perona, P., and Anderson, D.J. (2015). Behavioral responses

to a repetitive visual threat stimulus express a persistent state of defensive arousal in *Drosophila*. Curr. Biol. *25*, 1401–1415.

77. Reyn, C.R. von, Breads, P., Peek, M.Y., Zheng, G.Z., Williamson, W.R., Yee, A.L., Leonardo, A., and Card, G.M. (2014). A spike-timing mechanism for action selection. Nat. Neurosci. *17*, nn.3741.

78. Hamada, F.N., Rosenzweig, M., Kang, K., Pulver, S.R., Ghezzi, A., Jegla, T.J., and Garrity, P.A. (2008). An internal thermal sensor controlling temperature preference in *Drosophila*. Nature *454*, nature07001.

79. Klapoetke, N.C., Murata, Y., Kim, S.S., Pulver, S.R., Birdsey-Benson, A., Cho, Y.K., Morimoto, T.K., Chuong, A.S., Carpenter, E.J., Tian, Z., *et al.* (2014). Independent optical excitation of distinct neural populations. Nat. Methods *11*, 338–346.

80. Mohammad, F., Stewart, J.C., Ott, S., Chlebikova, K., Chua, J.Y., Koh, T.-W., Ho, J., and Claridge-Chang, A. (2017). Optogenetic inhibition of behavior with anion channelrhodopsins. Nat. Methods *14*, 271–274.

81. Tsien, R.Y. (1998). The Green Fluorescent Protein. Annu. Rev. Biochem. *67*, 509–544.

82. Robie, A.A., Hirokawa, J., Edwards, A.W., Umayam, L.A., Lee, A., Phillips, M.L., Card, G.M., Korff, W., Rubin, G.M., Simpson, J.H., *et al.* Mapping the neural substrates of behavior. Cell *170*, 393–406.e28.

83. Feng, K., Palfreyman, M.T., Häsemeyer, M., Talsma, A., and Dickson, B.J. (2014). Ascending sag neurons control sexual receptivity of *Drosophila* females. Neuron *83*, 135–148.

84. Hampel, S., Franconville, R., Simpson, J.H., and Seeds, A.M. (2015). A neural command circuit for grooming movement control. eLife *4*.

85. Häsemeyer, M., Yapici, N., Heberlein, U., and Dickson, B.J. (2009). Sensory neurons in the *Drosophila* genital tract regulate female reproductive behavior. Neuron *61*, 511–518.

86. von Philipsborn, A.C., Liu, T., Yu, J.Y., Masser, C., Bidaye, S.S., and Dickson, B.J. (2011). Neuronal control of *Drosophila* courtship song. Neuron *69*, 509–522.

87. Yapici, N., Cohn, R., Schusterreiter, C., Ruta, V., and Vosshall, L.B. (2016). A taste circuit that regulates ingestion by integrating food and hunger signals. Cell *165*, 715–729.

88. Sen, R., Wu, M., Branson, K., Robie, A., Rubin, G.M., and Dickson, B.J. (2017). Moonwalker descending neurons mediate visually evoked retreat in *Drosophila*. Curr. Biol. *27*, 766–771.

Chapter 2

Moonwalker Descending Neurons Mediate Visually Evoked Retreat in *Drosophila*

Published: February 23, 2017.

Cite as: Sen, R., Wu, M., Branson, K., Robie, A., Rubin, G.M., and Dickson, B.J. (2017). Moonwalker descending neurons mediate visually evoked retreat in *Drosophila*. Curr. Biol. *27*, 766–771. doi: 10.1016/j.cub.2017.02.008.

2.1 Highlights

- Optogenetic activation of LC16 or MDN cells triggers backward locomotion
- Optogenetic activation of LC16 is sufficient to elicit calcium responses in MDNs
- Silencing the activity of MDNs eliminates LC16-triggered backward turning
- Asymmetric activation of MDNs induces directed backward turns

2.2 Summary

Insects, like most animals, tend to steer away from imminent threats [1-7]. *Drosophila melanogaster*, for example, generally initiate an escape take-off in response to a looming visual stimulus, mimicking a potential predator [8]. The escape response to a visual threat is, however, flexible [9-12] and can alternatively consist of walking backward away from the perceived threat [11], which may be a more effective response to ambush predators such as nymphal praying mantids [7]. Flexibility in escape behavior may also add an element of unpredictability that makes it difficult for predators to anticipate or learn the prey's likely response [3-6]. Whereas the fly's escape jump has been well studied [8; 9; 13-18], the neuronal underpinnings of evasive walking remain largely unexplored. We previously reported the identification of a cluster of descending neurons—the moonwalker descending neurons (MDNs)—the activity of which is necessary and sufficient to trigger backward walking [19], as well as a population of visual projection neurons—the lobula columnar 16 (LC16) cells—that respond to looming visual stimuli and elicit backward walking and turning [11]. Given the similarity of their activation phenotypes, we hypothesized that LC16 neurons induce backward walking via MDNs and that turning while walking backward might reflect asymmetric activation of the left and right MDNs. Here, we present data from functional imaging, behavioral epistasis, and unilateral activation experiments that support these hypotheses. We conclude that LC16 and MDNs are critical components of the neural circuit that transduces threatening visual stimuli into directional locomotor output.

Keywords

Drosophila; behavior; locomotion; visual processing; escape; evasive walking; descending neuron; visual projection neuron

2.3 Results and Discussion

In our first series of experiments, we revisited the neuronal activation phenotypes of lobula columnar 16 (LC16) and moonwalker descending neuron (MDN) cells by acutely depolarizing them using a red-light-activated cation channel, CsChrimson [20], in an optogenetic behavioral assay. We used two different split-GAL4 driver lines that label the identical LC16 population (LC16-1 and LC16-2 GAL4s) and three different lines that label the identical MDN cells (MDN-1, MDN-2, and MDN-3 GAL4s; see the list of genotypes in the Supplemental Experimental Procedures). Bilateral activation of either LC16 cells or MDNs elicited backward locomotion, as previously observed [11; 19], but a closer examination revealed subtle differences between the LC16- and MDN-triggered motor programs (Figure 1). In order to quantify these behaviors, we used computer vision software to extract two distinct features of locomotion: translation and rotation (see the Supplemental Experimental Procedures). During the 2 s stimulation window, LC16 cells triggered transient backward locomotion that included a strong turning component eventually leading the fly to resume forward walking in a direction different from its original heading (Figures 1A–1C; Movie S1). Upon LC16 activation, the resumption of forward locomotion would often begin during the 2 s light stimulation. By contrast, MDNs triggered slower, straight or slightly curved backward walking that persisted until the end of the stimulation period (Figures 1A–1C; Movie S1).

We used hysteresis-based thresholds [21; 22] to define six distinct behavioral states based on translational and angular velocities: straight backward walking, backward turning, straight forward walking, forward turning, stall, and pivot (i.e., turning without translation; see the Supplemental Experimental Procedures). Consistent with our qualitative observation, we observed that flies in which LC16 was activated predominantly showed backward turning and pivots, whereas flies with MDNs activated showed substantially more straight backward walking (Figures 1D and S1).

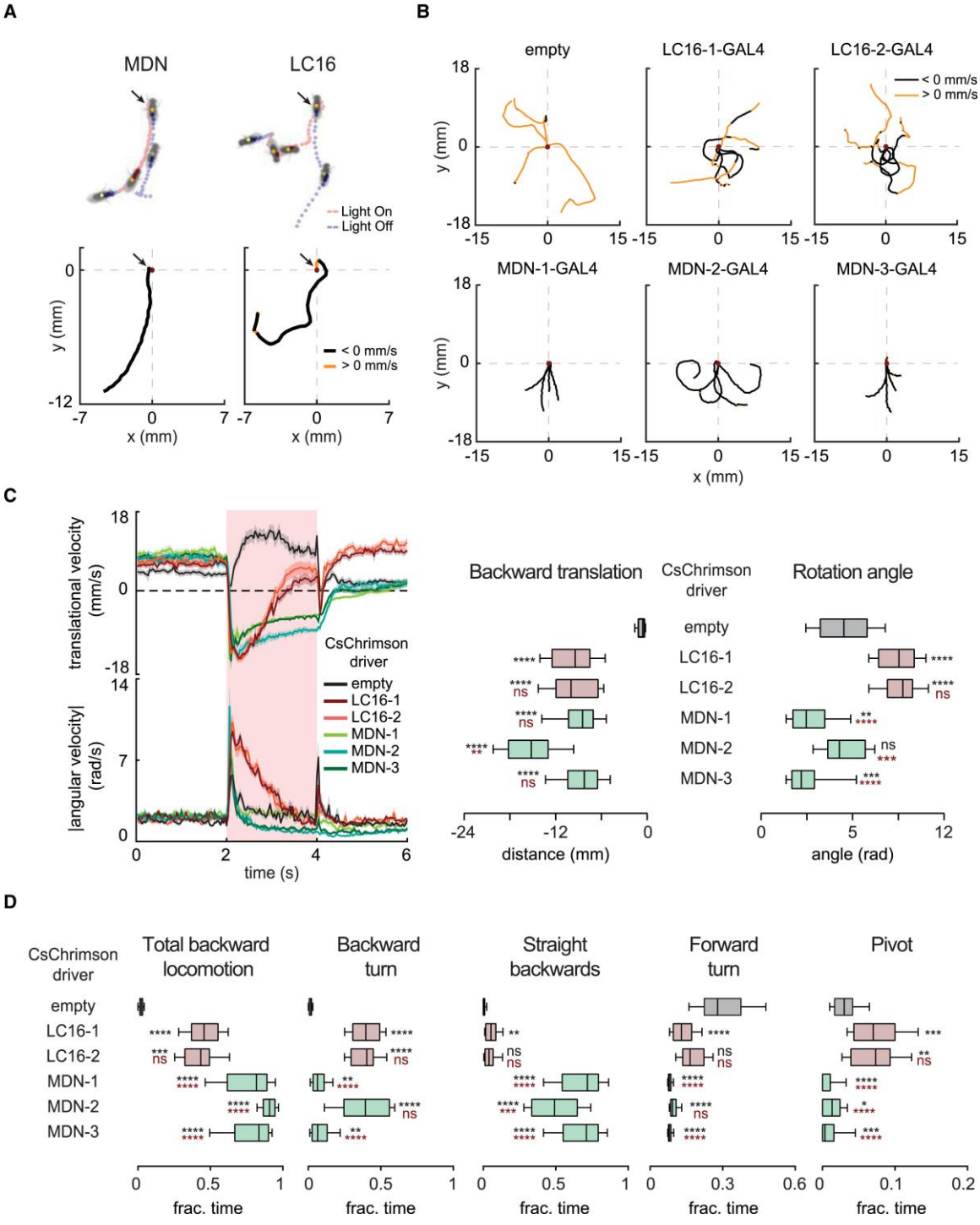

Figure 1. Similar but Distinct Features of Backward Locomotion upon Optogenetic Activation of MDNs or LC16 Cells

Figure 1. Similar but Distinct Features of Backward Locomotion upon Optogenetic Activation of MDNs or LC16 Cells

(A) Representative motion traces upon optogenetic activation of MDNs and LC16 cells, using the *MDN-2* and *LC16-1* split-GAL4 driver lines, respectively, to drive the expression of *UAS-CsChrimson*. Top: trajectories before, during, and after stimulation. Blue traces, light off; red traces, light on. Arrows indicate position at start of stimulation. Bottom: trajectories of the same flies during the 2 s stimulation window, now color-coded for backward (<0 mm/s) or forward (>0 mm/s) translational velocity. Translational velocity in this and other panels is defined as the projection of the fly's locomotion vector onto its orientation direction.

(B) Representative trajectories during the 2 s stimulation window of four flies for each of the various cell-type specific drivers.

(C) Left: translational and angular velocities versus time. Dark traces indicate mean of per-fly means (five trials per fly), and envelopes indicate ±SEM. Red rectangles in this and other panels signify optogenetic stimulation with red light. Right: per-fly mean, over five trials, of total backward translation distances and rotation angles during 2 s of optogenetic stimulation (n = 26–56 flies). Box-and-whisker plots in this and other panels show 10^{th}, 25^{th}, 50^{th}, 75^{th}, and 90^{th} percentiles. Statistical significance was assessed using the Kruskal-Wallis test ($p < 0.0001$ for both panels), followed by Dunn's post hoc test for pairwise comparisons against the empty GAL4 (black) and LC16-1 (red) controls. In this and other panels, $^{****}p < 0.0001$, $^{***}p < 0.001$, $^{**}p < 0.01$, and $^{*}p < 0.05$; ns, not significant.

(D) Per-fly mean, over five trials, of the fraction of time spent in the indicated behavioral states during the 2 s window of optogenetic activation. Kruskal-Wallis tests ($p < 0.0001$ for all panels) were followed by Dunn's post hoc test for pairwise comparisons against empty GAL4 (black) and LC16-1 (red) controls. Data for straight forward and stalled states are shown in Figure S1.

See also Movie S1.

Next we asked whether LC16 could trigger neuronal responses in MDNs. We optogenetically activated the LC16 neuronal population with CsChrimson while simultaneously imaging calcium transients in the dendritic arbors of MDNs using GCaMP6m [23] (Figure 2A). In an explanted central nervous system (CNS), optogenetic activation of LC16 cells was sufficient to trigger calcium responses in MDNs (Figures 2B and 2C). The response was mostly abolished by bath application of mecamylamine—an inhibitor of cholinergic synaptic transmission (Figures 2B and 2C). These results suggest that LC16 neurons activate MDNs via an excitatory cholinergic input. This input is unlikely to be a direct synaptic connection since the arborizations of LC16 and MDN cells do not overlap (Figure 2A; Movie S2).

Is MDN activity necessary for LC16-triggered backward locomotion? To address this question, we activated LC16 with CsChrimson in a background in which MDNs were inactivated by expression of the tetanus toxin light chain (TNT), an inhibitor of synaptic transmission [24]. As a positive control, we included flies in which TNT was expressed in LC16 rather than MDNs. As a negative control, we used flies in which an empty vector controlled TNT expression. We observed that the backward component of LC16-triggered retreat was dramatically reduced in all experimental and positive control genotypes, but not in the negative controls (Figure 3; Movie S3). The residual backward translation of the experimental flies was not significantly different from that of the positive control, suggesting that it reflects incomplete neuronal silencing with TNT rather than an MDN-independent component to LC16-triggered backward locomotion (Figures 3B–3D).

By contrast, the turning component resulting from LC16 activation was partially suppressed when MDNs were silenced (Figures 3C–3D; Movie S3), suggesting that LC16 neurons induce turning via both MDN-dependent and MDN-independent pathways. Quantification of the six behavioral states revealed that LC16-trigged backward turns were effectively and similarly suppressed by silencing of either MDNs or the LC16 cells themselves (Figures 3D and S2). The MDN-dependent pathway thus mediates the backward turns elicited by LC16 activation. Forward turns were more weakly and variably suppressed by MDN silencing (Figure 3D), suggesting that they rely primarily on the MDN-independent pathway. Pivots were increased upon both MDN and LC16 silencing (Figure 3D), perhaps in both cases as an indirect consequence of the inability to retreat.

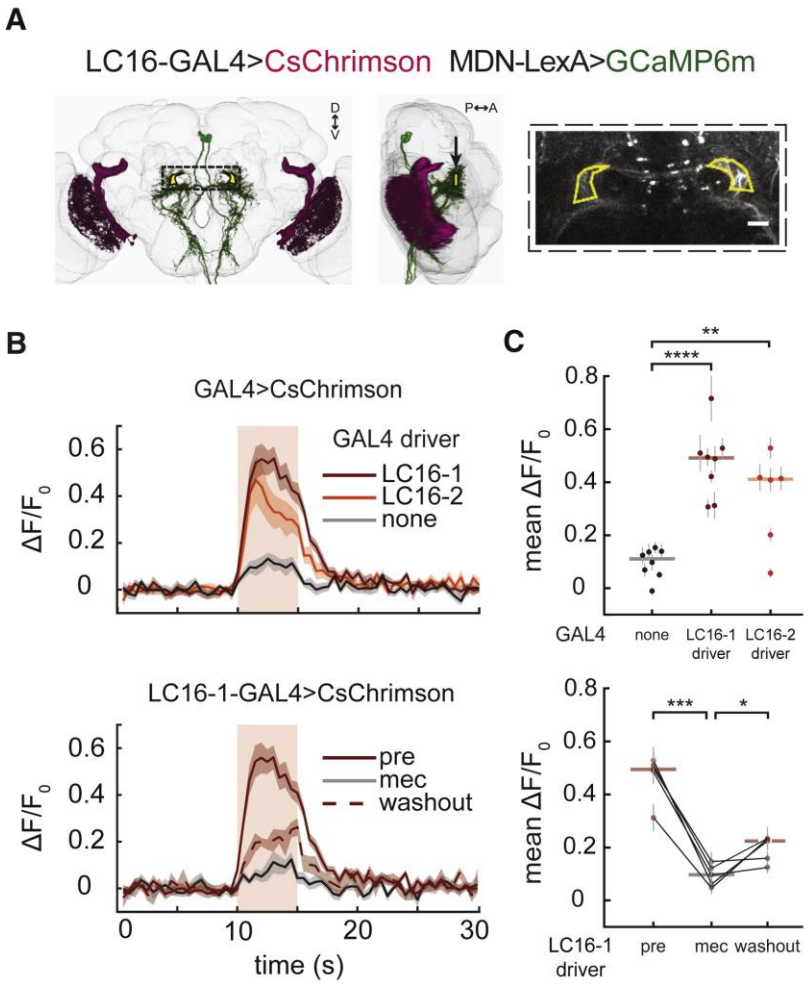

Figure 2. Optogenetic Activation of LC16 Cells Elicits Calcium Responses in MDNs
(A) Left and center: schematic of the brain showing LC16 neurons (magenta, expressing CsChrimson) and MDNs (green, expressing GCaMP6m). Yellow polygons within the dotted rectangle show regions of interest for functional imaging. Right: regions of interest overlaid on MDN arbors in a projection image of a representative sample. Scale bar, 20 μm.
(B) Top: time series for calcium responses in MDNs upon optogenetic activation of LC16 cells (n = 6–8 flies). Bottom: responses of MDNs to LC16 activation upon application and washout of mecamylamine (n = 5 flies). Dark traces indicate mean of per-fly means (20 trials per fly, ten on each side of the brain) versus time, and envelopes indicate ±SEM.
(C) Top: per-fly means of average MDN $\Delta F/F_0$ values during 5 s of LC16 activation (n = 6–8 flies), shown in jitter plots in which each dot represents per-fly mean of 20 trials and whiskers represent ±SEM. Horizontal bars indicate median values. p values are for comparisons to no GAL4 control (unpaired Student's t test with Bonferroni correction). Bottom: quantification of responses upon application and washout of mecamylamine (mec; n = 5 flies). p values are for paired comparisons to mecamylamine-treated samples (paired Student's t test).
See also Movie S2 and Tables S1 and S2.

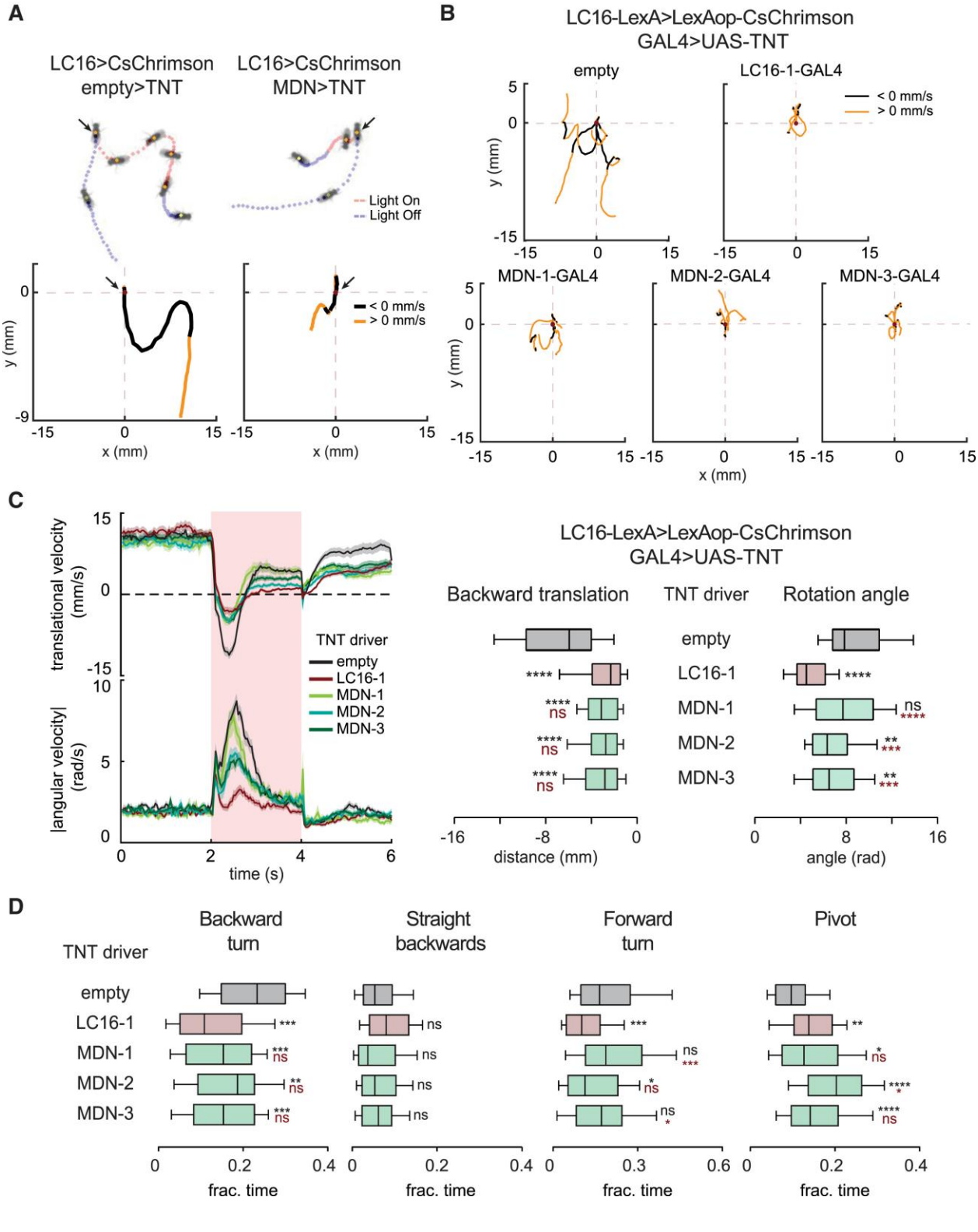

Figure 3. LC16 Neurons Act via MDNs to Trigger Backward Locomotion

Figure 3. LC16 Neurons Act via MDNs to Trigger Backward Locomotion

(A) Top: optogenetic activation of LC16 cells in combination with either *MDN-3* or the empty GAL4 control driving expression of TNT. Motion traces of representative flies are indicated. Blue traces, light off; red traces, light on. Arrows indicate position at the start of optogenetic stimulation. Bottom: trajectories during the 2 s window of optogenetic stimulation, now color-coded for backward (<0 mm/s) or forward (>0 mm/s) translational velocity.

(B) Representative trajectories of four flies for various genotypes used in the neuronal epistasis experiments. The traces include only the 2 s stimulus window.

(C) Left: translational and angular velocities versus time upon optogenetic stimulation of LC16 cells. Dark traces indicate mean of per-fly means (five trials per fly), and envelopes indicate ±SEM (n = 45–70 flies). Right: per-fly mean, over five trials, of total backward translation distances and rotation angles during the 2 s of optogenetic stimulation of LC16 cells. Statistical significance was assessed using the Kruskal-Wallis test ($p < 0.0001$ for both panels), followed by Dunn's post hoc test for pairwise comparisons against the empty GAL4 (black) and LC16-1 (red) controls.

(D) Per-fly mean, over five trials, of fraction of time spent in each behavioral state during the 2 s stimulus window. Kruskal-Wallis tests ($p < 0.0001$ for backward turn, forward turn, and pivot; $p = 0.07$ for backward straight) were followed by Dunn's post hoc test in pairwise comparisons against the negative (empty; black) and positive (LC16-1; red) controls. Data for forward straight and stalled states are shown in Figure S2.

See also Movie S3.

There are four MDN cells, two on each side of the CNS, with axons that project contralaterally to all three leg neuropils of the thoracic ganglia [19]. We speculated that asymmetric activation of the left and right MDNs might result in backward turning. To address this possibility, we applied a genetic approach to stochastically activate subsets of the four MDN cells [11] (see the Supplemental Experimental Procedures). In individual flies, the stochastically activated cells can be anatomically identified and correlated to the fly's behavior (Figures 4A–4C; Movie S4). We found that, overall, the extent of backward translation correlated with the total number of MDNs activated and the amount of turning correlated with the asymmetry of activation (Figure 4C). Asymmetric MDN activation consistently favored backward turning to the contralateral side (with respect to the location of the MDN soma in the brain). These results suggest that each of the four MDNs can act independently and that collectively they control both the magnitude and direction of backward locomotion.

In conclusion, our results suggest that LC16 cells and MDNs mediate visually evoked retreat via an excitatory feedforward circuit (Figure 4D). The four MDN cells can elicit a range of related motor outputs, depending on the pattern of their activity: symmetric activation of all four MDNs elicits straight backward walking, whereas asymmetric activation favors backward turning. Under natural conditions, a visual threat is likely to preferentially activate the ipsilateral LC16 cells, which we infer would lead to stronger activation of the ipsilateral MDNs and hence contralateral (evasive) turning. Even in the absence of pronounced asymmetry in LC16 activation, intervening circuits may introduce or amplify left-right differences to result in primarily unilateral MDN activation. We anticipate that MDNs also receive input from other sensory pathways. Mechanosensory cues, for example, might activate MDNs in response to a physical obstruction, and these too might differentially activate ipsilateral and contralateral MDNs to determine both the direction and extent of backward walking. The descending neurons that control forward walking and turning in *Drosophila* have not yet been identified, but once they are, it will be interesting to determine whether these cells employ an analogous logic to that of the MDNs to direct forward, rather than backward, walking and turning.

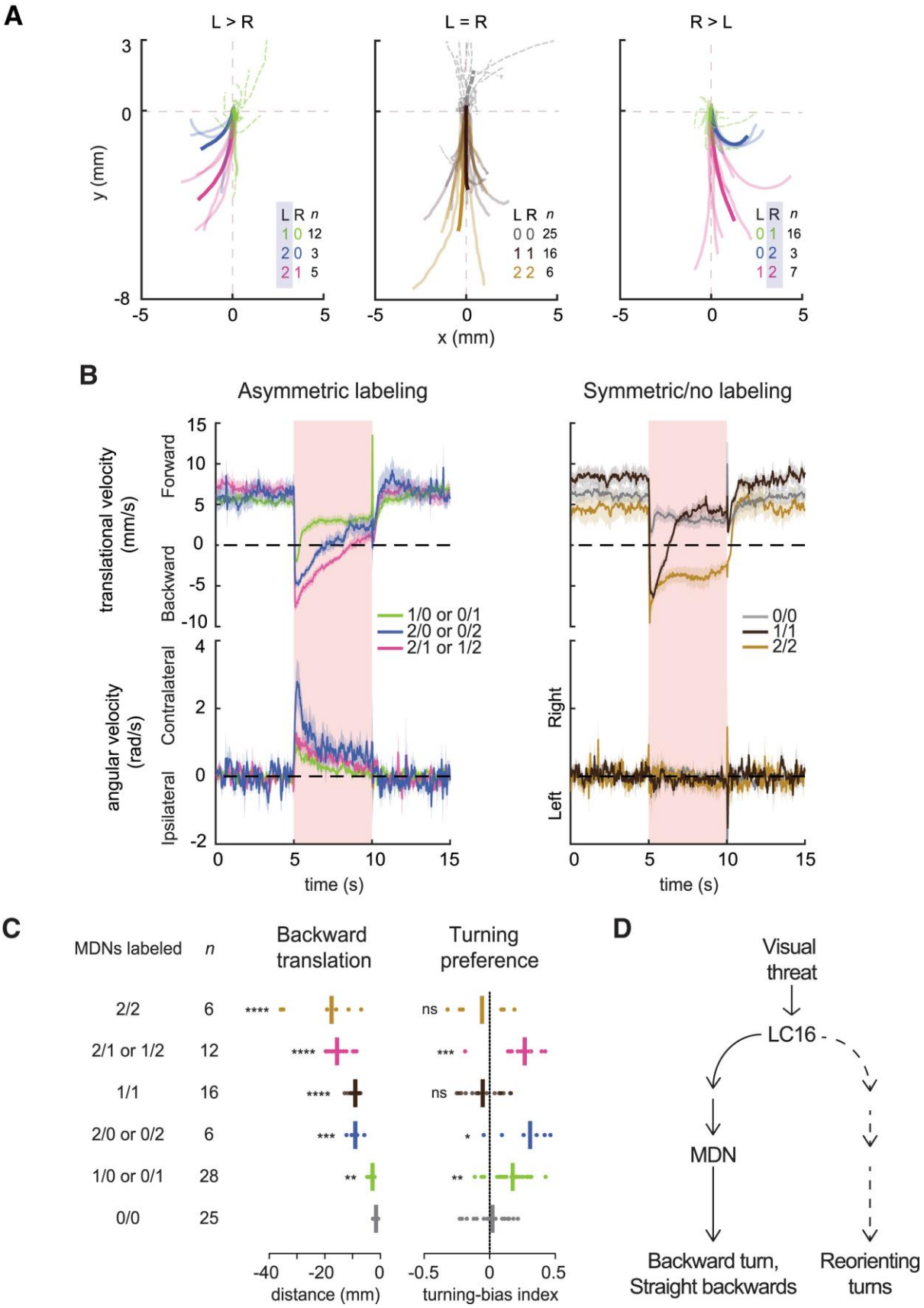

Figure 4. Asymmetric Activation of MDNs Causes Contralateral Backward Turns

Figure 4. Asymmetric Activation of MDNs Causes Contralateral Backward Turns
(A) Trajectories of all flies during the first 1 s of MDN activation. Left: categories with more left (L) than right (R) MDN cells labeled. Middle: categories with no or an equal number of MDN cells labeled in the two brain hemispheres. Right: categories with more right than left MDN cells labeled. Per-fly mean trajectories over 15 trials (faded lines) and per-category mean trajectories (bold lines) are indicated. Solid and dotted lines indicate backward (<0 mm/s) and forward (>0 mm/s) translation, respectively. "*n*" indicates the number of flies tested in each category.
(B) Time series for stochastic activation of MDNs. Positive and negative values for translational velocity indicate forward and backward locomotion, respectively. Positive and negative values for angular velocity indicate contralateral and ipsilateral turns (with respect to the side where more MDNs were labeled), respectively, for asymmetric labeling classes, and right and left turns, respectively, for symmetric/no labeling classes. Dark traces indicate means of per-fly means (15 trials per fly), pooled from all flies of a given labeling category, and envelopes indicate ±SEM (n = 6–28 flies).
(C) Per-fly mean of backward translation distances and turning-bias indices for flies with varying numbers of MDNs activated (15 trials per fly). Vertical bars indicate median values. Turning-bias indices are defined as either the ratio of contralateral / (contralateral + ipsilateral) angular distances (with respect to the side where more MDN cells were labeled; asymmetric labeling) or as right / (left + right) angular distances (symmetric/no labeling). Ratios are normalized by subtraction of light-off turning preferences to correct for any inherent left-right bias in a given fly. A Kruskal-Wallis test ($p < 0.0001$ for both panels) was followed by Dunn's post hoc test of pairwise comparisons against the category with no activated MDN cells (0/0; p values indicated).

2.4 Author Contributions

R.S. and M.W. performed the behavioral experiments. R.S. performed the antibody staining and the calcium imaging experiments and analyzed all data. K.B. generated the script for tracking fly directionality and contributed to the script for video analysis. A.R. advised the engineering of the optogenetic fly chamber and contributed to the video analysis script. R.S., M.W., and B.J.D. designed the experiments and wrote the manuscript. B.J.D. and G.M.R. supervised the project.

2.5 Acknowledgments

We thank Barret Pfeiffer for pJFRC35; Heather Dionne for 28F07-LexAp65; Romain Franconville and Kaiyu Wang for assisting with the calcium imaging experiments; Ines Ribeiro and Allen Lee for assisting in data analysis; William Rowell, Teri Ngo, and Jon-Michael Knapp for technical assistance; Aljoscha Nern, Yoshi Aso, Zhiyong Liu, and Wyatt Korff for technical advice; Vivek Jayaraman for CsChrimson stocks; and Steve Sawtelle, Igor Negrashov, and Jinyang Liu for engineering the optogenetic fly chamber. M.W. was a Helen Hay Whitney Postdoctoral Fellow. This work was funded by the Howard Hughes Medical Institute.

2.6 References

1. Tauber, E., and Camhi, J. (1995). The wind-evoked escape behavior of the cricket Gryllus bimaculatus: integration of behavioral elements. J. Exp. Biol. 198, 1895-1907.

2. Kanou, M., Ohshima, M., and Inoue, J. (1999). The air-puff evoked escape behavior of the cricket Gryllus bimaculatus and its compensational recovery after cercal ablations. Zoolog. Sci. 16, 71-79.

3. Domenici, P., Booth, D., Blagburn, J., and Bacon, J.P. (2008). Cockroaches keep predators guessing by using preferred escape trajectories. Curr. Biol. 18, 1792-1796.

4. Domenici, P., Booth, D., Blagburn, J.M., and Bacon, J.P. (2009). Escaping away from and towards a threat: the cockroach's strategy for staying alive. Commun. Integr. Biol. 2, 497-500.

5. Domenici, P., Blagburn, J.M., and Bacon, J.P. (2011). Animal escapology ii: escape trajectory case studies. J. Exp. Biol. 214, 2474-2494.

6. Card, G.M. (2012). Escape behaviors in insects. Curr. Opin. Neurobiol. 22, 180-186.

7. Parigi, A., Porter, C., Cermak, M., Pitchers, W.R., and Dworkin, I. (2014). How predator hunting-modes affect prey behaviour: capture deterrence in Drosophila melanogaster. bioRxiv.

8. Allen, M.J., Godenschwege, T.A., Tanouye, M.A., and Phelan, P. (2006). Making an escape: development and function of the Drosophila giant fibre system. Semin. Cell Dev. Biol. 17, 31-41.

9. Reyn, C.R.v., Breads, P., Peek, M.Y., Zheng, G.Z., Williamson, W.R., Yee, A.L., Leonardo, A., and Card, G.M. (2014). A spike-timing mechanism for action selection. Nat. Neurosci. 17, 962-970.

10. Gibson, William T., Gonzalez, Carlos R., Fernandez, C., Ramasamy, L., Tabachnik, T., Du, Rebecca R., Felsen, Panna D., Maire, Michael R., Perona, P., and Anderson, David J. (2016). Behavioral responses to a repetitive visual threat stimulus express a persistent state of defensive arousal in Drosophila. Curr. Biol. 25, 1401-1415.

11. Wu, M., Nern, A., Williamson, W.R., Morimoto, M.M., Reiser, M.B., Card, G.M., and Rubin, G.M. (2016). Visual projection neurons in the Drosophila lobula link feature detection to distinct behavioral programs. eLife 5, e21022.

12. Herberholz, J., and Marquart, G.D. (2012). Decision making and behavioral choice during predator avoidance. Front. Neurosci. 6, 125.

13. Tanouye, M.A., and Wyman, R.J. (1980). Motor outputs of giant nerve fiber in *Drosophila*. J. Neurophysiol. 44, 405-421.

14. Hammond, S., and O'Shea, M. (2007). Escape flight initiation in the fly. J. Comp. Physiol. A Neuroethol. Sens. Neural Behav. Physiol. 193, 471-476.

15. Card, G., and Dickinson, M.H. (2008). Visually mediated motor planning in the escape response of Drosophila. Curr. Biol. 18, 1300-1307.

16. Card, G., and Dickinson, M. (2008). Performance trade-offs in the flight initiation of Drosophila. J. Exp. Biol. 211, 341-353.

17. Fotowat, H., Fayyazuddin, A., Bellen, H.J., and Gabbiani, F. (2009). A novel neuronal pathway for visually guided escape in Drosophila melanogaster. J. Neurophysiol. 102, 875-885.

18. de Vries, S.E., and Clandinin, T.R. (2012). Loom-sensitive neurons link computation to action in the Drosophila visual system. Curr. Biol. 22, 353-362.

19. Bidaye, S.S., Machacek, C., Wu, Y., and Dickson, B.J. (2014). Neuronal control of Drosophila walking direction. Science 344, 97-101.

20. Klapoetke, N.C., Murata, Y., Kim, S.S., Pulver, S.R., Birdsey-Benson, A., Cho, Y.K., Morimoto, T.K., Chuong, A.S., Carpenter, E.J., Tian, Z., et al. (2014). Independent optical excitation of distinct neural populations. Nat. Methods 11, 338-346.

21. Robie, A.A., Straw, A.D., and Dickinson, M.H. (2010). Object preference by walking fruit flies, Drosophila melanogaster, is mediated by vision and graviperception. J. Exp. Biol. 213, 2494-2506.

22. Ramdya, P., Lichocki, P., Cruchet, S., Frisch, L., Tse, W., Floreano, D., and Benton, R. (2014). Mechanosensory interactions drive collective behaviour in Drosophila. Nature 519, 233-236.

23. Chen, T.-W., Wardill, T.J., Sun, Y., Pulver, S.R., Renninger, S.L., Baohan, A., Schreiter, E.R., Kerr, R.A., Orger, M.B., Jayaraman, V., et al. (2013). Ultrasensitive fluorescent proteins for imaging neuronal activity. Nature 499, 295-300.

24. Sweeney, S.T., Broadie, K., Keane, J., Niemann, H., and O'Kane, C.J. (1995). Targeted expression of tetanus toxin light chain in Drosophila specifically eliminates synaptic transmission and causes behavioral defects. Neuron 14, 341–351.

2.7 Supplemental Materials

2.7.1 Supplemental Figures and Tables

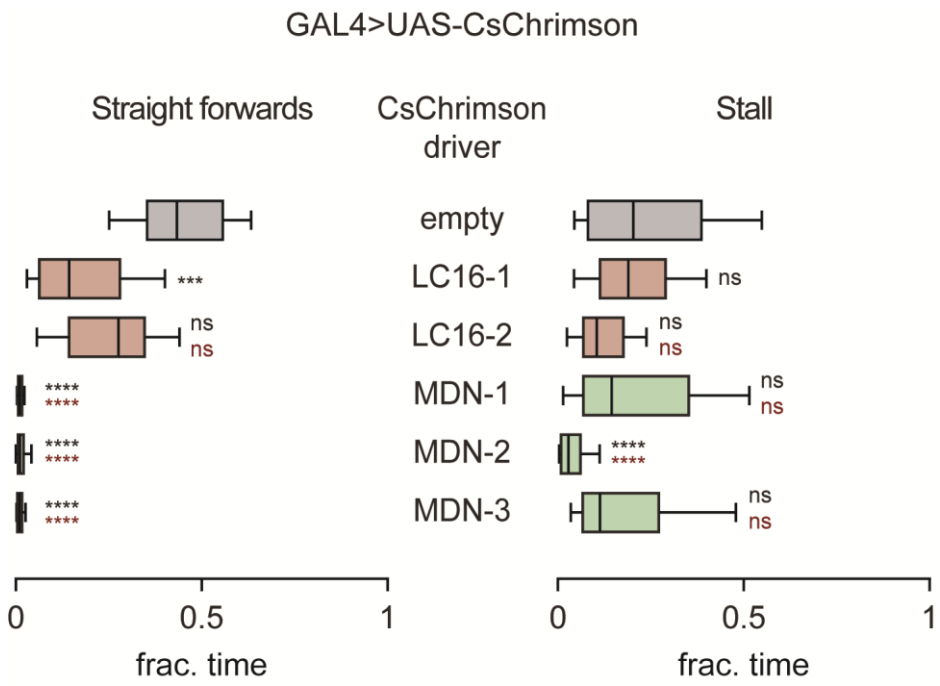

Figure S1. Fraction of time in forwards straight and stalled states upon optogenetic neuronal activation of LC16 or MDN cells. Related to Figure 1.
Per-fly mean over 5 trials, of fraction of time spent in forwards straight and stalled behavioral states during the 2 s window of optogenetic activation. Kruskal-Wallis tests ($P < 0.0001$ for both states) were followed by Dunn's post-hoc test for pairwise comparisons against empty GAL4 (black) and LC16-1 (red) controls.

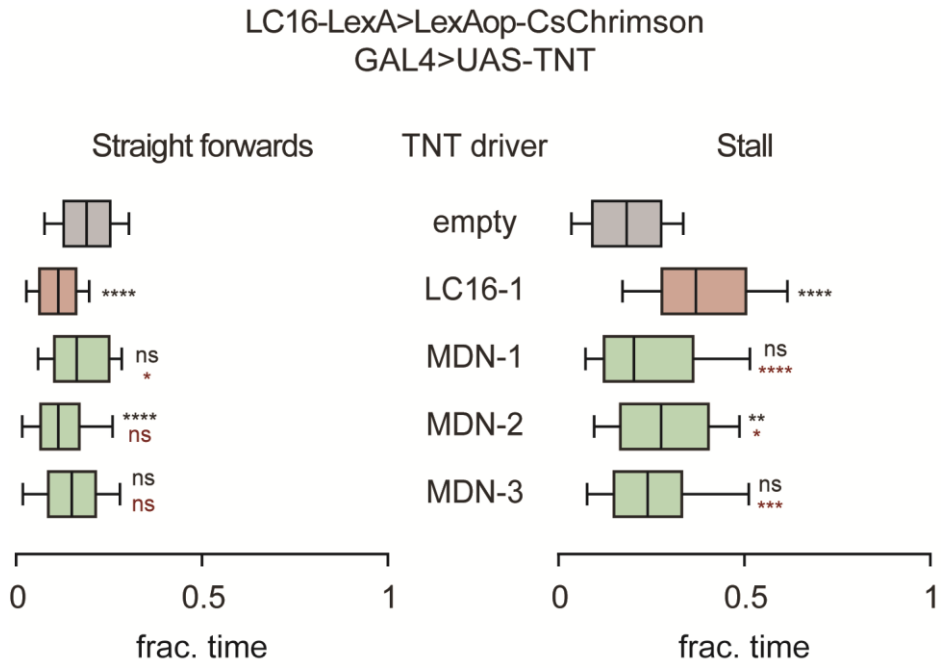

Figure S2. Fraction of time in forwards straight and stalled states in neuronal epistasis experiments. Related to Figure 3.
Per-fly mean over 5 trials, of fraction of time spent in forwards straight and stalled behavioral states during the 2 s window of optogenetic activation of LC16 cells. Kruskal-Wallis tests ($P < 0.0001$ for both states), were followed by Dunn's post-hoc test in pairwise comparisons against the negative (empty, black) and positive (LC16-1, red) controls.

GAL4:	**None**	***LC16-2***	***LC16-1***	***LC16-1* (mec)**	***LC16-1* (wash-out)**
	Mean±SEM	Mean±SEM	Mean±SEM	Mean±SEM	Mean±SEM
fly#1	0.14±0.03	0.42±0.04	0.49±0.05	0.10±0.04	0.13±0.02
fly#2	0.14±0.03	0.53±0.04	0.53±0.04	0.07±0.01	0.23±0.04
fly#3	0.13±0.03	0.06±0.02	0.50±0.03	0.15±0.04	0.16±0.03
fly#4	0.10±0.03	0.21±0.02	0.51±0.07	0.12±0.03	0.23±0.04
fly#5	0.16±0.02	0.43±0.05	0.31±0.05	0.05±0.02	0.23±0.02
fly#6	0.07±0.03	0.41±0.04	0.30±0.03		
fly#7	-0.01±0.01		0.42±0.02		
fly#8	0.06±0.01		0.72±0.09		

Table S1. Per-fly means of average $\Delta F/F_0$ in MDNs upon optogenetic stimulation of LC16 cells. Related to Figure 2.
For each fly carrying the indicated split-GAL4 driver together with *UAS-CsChrimson MDN-LexAp65 LexAop-GCaMP6m*, the mean $\Delta F/F_0$ in MDNs during each trial of LC16 activation was calculated. The mean of these per-trial mean $\Delta F/F_0$ values (over 20 trials) yielded the per-fly means tabulated above.

GAL4 driver	***n***	**Mean±SEM**	**Median**
None	8	0.10±0.02	0.12
LC16-2	6	0.34±0.07	0.41
LC16-1	8	0.47±0.05	0.49
LC16-1 (With MEC)	5	0.07±0.02	0.07
LC16-1 (MEC Wash-out)	5	0.20±0.02	0.23

Table S2. Mean of per-fly means of average $\Delta F/F_0$ in MDNs upon optogenetic activation of LC16 cells. Related to Figure 2.
Per-fly means of $\Delta F/F_0$ values, calculated as described above, were averaged over all flies of a given genotype; *n* indicates the number of flies tested for each genotype.

2.7.3 Supplemental Movie Legends

Movies are available in the accompanying CD, or online at
http://www.sciencedirect.com/science/article/pii/S0960982217301446

Movie S1. Optogenetic Activation of MDN or LC16 Cells Triggers Backward Locomotion. Related to Figure 1.
Optogenetic stimulation of flies carrying the empty GAL4 control vector (left), *LC16-1-GAL4* (middle), or *MDN-2-GAL4* (right) driver in combination with *UAS-CsChrimson*. Blue traces, light off; red traces, light on; red squares, LED indicator.

Movie S2. LC16 Cells and MDNs Are Not Directly Connected. Related to Figure 2.
Overlaid segmentations of LC16 neurons (green) and MDNs (blue) onto common reference template, following non-rigid registration.

Movie S3. MDNs Are Necessary for LC16-Triggered Backward Locomotion. Related to Figure 3.
Optogenetic stimulation of flies carrying either the empty control vector or the indicated split-GAL4 driver in combination with *UAS-TNT LC16-LexAp65 LexAop-CsChrimson*. Blue traces, light off; red traces, light on; red squares, LED indicator.

Movie S4. Asymmetric Activation of MDNs Causes Contralateral Backward Turns. Related to Figure 4.
Optogenetic stimulation of *MDN-1-GAL4 hs-FLP UAS-FRT>-STOP-FRT>-CsChrimson-mVenus* flies in which either all four (left) or two right (right) MDN cells are labeled and activated. Blue traces, light off; red traces, light on; red squares, LED indicator.

2.7.4 Supplemental Experimental Procedures

2.7.4.1 List of genotypes

Figure	Genotype	Driver(s)
Figure 1A	20XUAS-CsChrimson-mVenus (attP18); R26A03-p65ADZp (attP40)/+; R54A05-ZpGAL4DBD (attP2)/+	LC16-1-GAL4
	20XUAS-CsChrimson-mVenus (attP18); 037220-p65ADZp (attP40)/+; 044845-ZpGAL4DBD (attP2)/+	MDN-2-GAL4
Figure 1B,C,D	20XUAS-CsChrimson-mVenus (attP18); ; pBDPGAL4 (attP2)/+	empty
	20XUAS-CsChrimson-mVenus (attP18); R26A03-p65ADZp (attP40)/+; R54A05-ZpGAL4DBD (attP2)/+	LC16-1-GAL4
	20XUAS-CsChrimson-mVenus (attP18); R82D11-p65ADZp (attP40)/+; R54A05-ZpGAL4DBD (attP2)/+	LC16-2-GAL4
	20XUAS-CsChrimson-mVenus (attP18); 044845-ZpGAL4DBD (attP40)/+; 050660-p65ADZp (attP2)/+	MDN-1-GAL4
	20XUAS-CsChrimson-mVenus (attP18); 037220-p65ADZp (attP40)/+; 044845-ZpGAL4DBD (attP2)/+	MDN-2-GAL4
	20XUAS-CsChrimson-mVenus (attP18); 050660-p65ADZp (attP40)/+; 044845-ZpGAL4DBD (attP2)/+	MDN-3-GAL4
Figure 2B,C	5XUAS-CsChrimson-mCherry (su(Hw)attP5), 044845-LexAp65 (attP40)/+; LexAop2-IVS-GCaMP6m-p10 (VK00005)/+	MDN-LexAp65 (none)
	5XUAS-CsChrimson-mCherry (su(Hw)attP5), 044845-LexAp65 (attP40)/R26A03-p65ADZp (attP40); LexAop2-IVS-GCaMP6m-p10 (VK00005)/R54A05-ZpGAL4DBD (attP2)	LC16-1-GAL4, MDN-LexAp65
	5XUAS-CsChrimson-mCherry (su(Hw)attP5), 044845-LexAp65 (attP40)/R82D11-p65ADZp (attP40); LexAop2-IVS-GCaMP6m-p10 (VK00005)/R54A05-ZpGAL4DBD (attP2)	LC16-2-GAL4, MDN-LexAp65
Figure 3A	13XLexAop2-IVS-CsChrimson-mVenus (attP18); 26A03-LexAp65 (JK22C)/+; pJFRC35-10XUAS-DSCP-E86tetLC (VK00005)/pBDPGAL4 (attP2)	pBDPGAL4 (empty), LC16-LexAp65
	13XLexAop2-IVS-CsChrimson-mVenus (attP18); 26A03-LexAp65 (JK22C)/050660-p65ADZp (attP40); pJFRC35-10XUAS-DSCP-E86tetLC (VK00005)/044845-ZpGAL4DBD (attP2)	MDN-3-GAL4, LC16-LexAp65
Figure 3B,C,D	13XLexAop2-IVS-CsChrimson-mVenus (attP18); 26A03-LexAp65 (JK22C)/+; pJFRC35-10XUAS-DSCP-E86tetLC (VK00005)/pBDPGAL4 (attP2)	pBDPGAL4 (empty), LC16-LexAp65

	13XLexAop2-IVS-CsChrimson-mVenus (attP18); 26A03-LexAp65 (JK22C)/R26A03-p65ADZp (attP40); pJFRC35-10XUAS-DSCP-E86tetLC (VK00005)/R54A05-ZpGAL4DBD (attP2)	LC16-1-GAL4, LC16-LexAp65
	13XLexAop2-IVS-CsChrimson-mVenus (attP18); 26A03-LexAp65 (JK22C)/044845-ZpGAL4DBD (attP40); pJFRC35-10XUAS-DSCP-E86tetLC (VK00005)/050660-p65ADZp (attP2)	MDN-1-GAL4, LC16-LexAp65
	13XLexAop2-IVS-CsChrimson-mVenus (attP18); 26A03-LexAp65 (JK22C)/037220-p65ADZp (attP40); pJFRC35-10XUAS-DSCP-E86tetLC (VK00005)/044845-ZpGAL4DBD (attP2)	MDN-2-GAL4, LC16-LexAp65
	13XLexAop2-IVS-CsChrimson-mVenus (attP18); 26A03-LexAp65 (JK22C)/050660-p65ADZp (attP40); pJFRC35-10XUAS-DSCP-E86tetLC (VK00005)/044845-ZpGAL4DBD (attP2)	MDN-3-GAL4, LC16-LexAp65
Figure 4	pJFRC300-20XUAS-FRT>-dSTOP-FRT>-CsChrimson-mVenus (attP18), hs-FLP-PESTOpt (attP3)/+; 044845-ZpGAL4DBD (attP40)/+; 050660-p65ADZp (attP2)/+	MDN-1-GAL4

2.7.4.2 Fly genetics

The *LC16-LexAp65 and MDN-LexAp65* lines were derived respectively from the *26A03-GAL4* and *VT044845-GAL4* lines by gateway cloning, and correspondingly inserted into the JK22C [S1] and attP40 [S2] landing sites by phiC31-mediated recombination. These lines reliably targeted the LC16 and MDN cell populations and could recapitulate the corresponding activation phenotypes established with GAL4 and split-GAL4 drivers (data not shown). Split-GAL4 driver lines *MDN-1*, *MDN-2* and *MDN-3* were as described in [S3], and *LC16-1* and *LC16-2* correspond to *0L0046B* and *0L0017B*, respectively, as described in [S4]. Other stocks used were (1) *pJFRC35-10XUAS-DSCP-E86tetLC* (VK00005), abbreviated as *UAS-TNT*, a gift from Barret Pfeiffer; (2) *13XLexAop2-IVS-CsChrimson-mVenus* (attP18), Bloomington stock #55137 [S5]; (3) *20XUAS-CsChrimson-mVenus* (attP18) [S5]; (4) *hs-FLP-PESTOpt* (attP3) [S6]; (5) *pJFRC300-20XUAS-FRT>-dSTOP-FRT>-CsChrimson-mVenus* (attP18) [S4], *pBPDGAL4U* (attP2) [S7]; (6) *5XUAS-CsChrimson-mCherry* (su(Hw)attP5), a gift from Vivek Jayaraman; (7) *LexAop2-IVS-GCaMP6m-p10* (VK00005), Bloomington stock #44276 [S8].

All flies were raised in the dark at 50% relative humidity on standard cornmeal-molasses food, supplemented with all-trans-retinal (0.2 mM prior to eclosion, and 0.4 mM post-eclosion).

For activation with CsChrimson, epistasis and calcium imaging experiments, flies were raised at 25°C and aged for 5-7 days before testing. For the stochastic activation experiments, animals were heat-shocked during the 1st instar larval stage and reared at 22°C as described in [S4], with the following modifications: flies were either heat-shocked once for 2 hours, or twice for 2 hours with a 2-hour time interval in between, and were aged for 13-15 days, prior to testing.

2.7.4.3 Behavioral assays and analysis

All behavioral experiments were performed at 25°C and 50% relative humidity in the dark. The fly chamber used in the assays was designed after previously published works [S9-S11] and consists of an arena within which the flies are constrained in their movements to a plane in which they can be continuously monitored. For optogenetic activation of neurons with CsChrimson, the entire arena was uniformly illuminated with 627 nm LEDs (Red-Orange LUXEON Rebel LED – l22 lm; Luxeon Star LEDs) through a 3 mm thick diffuser. Flies were allowed to walk freely for 1-2 mins before start of the first activation trial. Behavior was recorded under backlit transmitted infrared (IR) 850nm LEDs (Osram SFH 4050) using a camera (ROHS 1.3 MP B&W Flea3 USB 3.0 Camera; POINT GREY) with a 760 nm long-pass filter (NEEWER IR filter, 52 mm) at 30 frames per second (fps) and 1024x1024 pixel resolution. For activation using CsChrimson and in epistasis experiments, groups of ~20 male flies were loaded in the arena and illuminated with red light of intensity ~5.6 mW/cm^2, for five trials. Each trial comprised a 2 s light stimulus followed by a 20 s light-off period. In the stochastic activation experiments, flies of both sexes were tested individually for fifteen trials, with a light intensity of ~20.1 mW/cm^2. Each trial comprised a 5 s light stimulus, followed by a 20 s light-off period. Individual flies were retrieved for post-hoc histology. During the light stimulations, control flies experienced an initial startle response and either moved faster (activation experiments) or moved slower (stochastic activation experiments) depending on the intensity of light.

Videos of freely walking flies were tracked with a modified version of Ctrax [S9] that used wing shape to determine the orientation of flies. Only flies with complete or continuous tracking throughout the videos were considered for analysis. For each trial, we analyzed a time window that centered on the duration of red-light illumination. This was 6 s total (2 s each before, during and after stimulus) for the activation and epistasis experiments, and 15 s total (5 s each before, during and after stimulus) for the stochastic activation experiments. The tracking fits an ellipse to the fly, and angular velocity and forward velocity for every frame were calculated as in [S11]. Angular velocity was defined as the change in the body angle relative to the global coordinate system. Positive and negative values for angular velocity indicated right and left turns respectively. Forward velocity (for simplicity, referred to as 'translational velocity' in figures) was the projection of the fly's velocity on its orientation direction. We linearly interpolated the time-points when forward velocity became 0 mm/sec. 'Backward translation' distance was calculated as the total integrated area from the interpolated time-series plots whenever forward velocity was negative. Total 'rotation angle' for the epistasis and activation experiments was calculated by integrating the area under the angular velocity (i.e., |angular velocity|) vs. time plots. For the stochastic activation experiments, we linearly interpolated the time-points when angular velocity became 0 rad/s and separately calculated the total angles turned left and right in each trial for a given fly. Turns from the cases where more right MDN cells were labeled were sign-reversed and converted into right turns. We thus defined 6 distinct categories: (1) no MDN cells, (2) 1 cell on one side, (3) 2 cells on one side, (4) 1 cell on each side, (5) 2 cells on each side, and (6) 3 cells, with 2 on one side and 1 on the other. We pooled data from all flies of a given category of expression pattern, and defined turning indices as the ratio of contralateral/(contralateral+ipsilateral) angular distances (with respect to the side where more MDN cells were labeled) for the asymmetric classes, and right/(left+right) angular distances for the symmetric/no labeling classes. We separately calculated the mean turning indices before and during stimulation for each fly over fifteen trials, and defined a per-fly 'turning-bias index', which was the mean subtracted turning index between light on and off.

For analyses of behavioral states, we manually annotated a subset of the data when the flies were in a given walking mode. Treating these classifications as ground-truth, we used hysteresis-based thresholds [S12, S13] on translational and angular velocities for a given behavioral state. A behavioral bout began when velocity increased beyond an upper threshold and ended when it fell below a lower threshold. Short bouts and pauses (<3 frames, or <100 ms at 30 fps) were removed and merged with the fly's state in neighboring frames. Frames in which angular or translational velocity exceeded 50 units/s or dipped below -50 units/s were recognized as jumps and eliminated from the analyses [S12]. A backward locomotion bout began when translational velocity fell below a threshold of -1.75 mm/s and ended when it rose above a threshold of -1.5 mm/s. A forward locomotion bout began when translational velocity exceeded 2 mm/s and ended when it fell below 1.5 mm/s. A turning bout began when |angular velocity| exceeded 2 rad/s and ended when it dipped below a lower threshold of 1.75 rad/s. Thus, periods when |angular velocity| fell below 1.75 rad/s were considered as 'not turning' and periods when translational velocity varied between -1.5 mm/s and 1.5 mm/s were considered as 'not translating'. These thresholds thus defined the 6 behavioral states of stalled (neither translating nor turning), pivot (turning without translation), forwards or backwards straight (translating without turning), and forward or backward turn (both translating and turning). Fraction of time spent in each of these behavioral states was calculated as the trial-averaged ratio of the total number of frames the flies spent in the given state to the total number of frames in the respective optogenetic trial. Fraction-time for 'total backward locomotion' was defined as the sum of the fraction-times for 'straight backwards' and 'backward turns'.

2.7.4.4 Immunohistochemistry and imaging

Immunohistochemistry of the first batch of stochastic activation experiments was performed as described in [S14] with minor modifications: flies were fixed overnight at 4°C in 1.2% PFA, and the central nervous systems (CNSs) were stained with rabbit anti-GFP (1:500, Invitrogen), mouse mAb nc82 (1:50, Hybridoma Bank) and secondary Alexa 488 and 647 antibodies (1:300, Life Technologies). Subsequent batches used a higher throughput immunohistochemistry protocol, as described in https://www.janelia.org/sites/default/files/Project%20Teams/Fly%20Light/FL%20Protocol%20-%20Adult%20IHC%20-%20Split%20Screen_0.pdf. Confocal stacks of the stained brains and ventral nerve cords were acquired with a Zeiss LSM 710 with a 20X air objective. Movie S2 showing overlaid segmentations of LC16 neurons and MDNs onto common reference template was generated using Fluorender [S15], a 3D image rendering software.

2.7.4.5 Calcium imaging and analysis

The CNSs of female flies were dissected using minimal illumination - in extracellular solution containing (in millimoles): 103 NaCl, 3 KCl, 5 N-Tris (hydroxymethyl) methyl-2-aminoethanesulfonic acid, 10 trehalose, 10 glucose, 2 sucrose, 26 $NaHCO_3$, 1 NaH_2PO_4, 1.5 $CaCl_2$, and 4 $MgCl_2$ (pH near 7.3 when bubbled with 95% (vol/vol) O_2 and 5% (vol/vol) CO_2, ~295 mOsm). We used female flies because *MDN-LexAp65* labeled MDN cells more strongly in females. Imaging was done using a 2-photon scanning microscope (Zeiss MP710), with a 20X water immersion objective of N.A. 1 (Objective W Plan-Apochromat) at a wavelength of 920 nm and an image acquisition frequency of 2 Hz. Throughout the experiment, the sample was perfused in saline bubbled with 95% O_2 (v/v) and 5% CO_2 (v/v) at a speed of ~80-100 ml/hour. The imaging plane spanned the entire area of the brain with an optical slice in which we could reliably identify MDN dendritic arbors on both sides of the brain. An LED (660 nm) light-source collimated with an optic fiber of diameter 400 μm and

N.A. 0.39 was used to activate CsChrimson. The location of the optic fiber with respect to the brain was controlled by a micromanipulator targeting the center of the brain. The distance between the sample and the optic fiber ranged from 0.5-1 mm. Light powers were measured directly from the LED light source using a power-meter (Thorlabs). Intensity measures ranged from 1.06-2.17 mW/mm^2 for an imaging plane 0.5-1 mm away from the source. Each trial comprised 5 s of continuous red light stimulation, followed by 35 s of light-off period. Each fly was tested for 10 trials. For blocking nicotinic transmission, 10-15 µl of mecamylamine stock (5 mM) was added directly to a ~5 ml static bath to generate a final concentration of 10-15 µM. Perfusion was stopped for ~10 mins to allow time for action. Preliminary experiments established that stopping the perfusion alone does not eliminate responses in MDNs. For wash-out experiments, samples were perfused with ~50 ml of saline prior to imaging.

For analysis, regions of interest (ROIs) on MDN dendrites from left and right sides of brain were hand-drawn in Fiji (http://fiji.sc). The ROIs were located in the lower lateral accessory lobe (LLAL), near the lateral accessory lobe commissure (LALC). This brain region could be reliably identified from the baseline GCaMP6m signal and by using the location of other neurons labeled in the *MDN-LexAp65* driver line as landmarks. The areas of the left and right ROIs were kept the same for all flies. Absolute fluorescence was calculated as the average pixel intensity in each ROI, for every frame of the video. $\Delta F/F_0$ (F_0 is the average signal over 10 s before the stimulation) was calculated for each video in these ROIs. Data from the left and right ROIs were pooled together since MDN has symmetric dendritic arborizations in the brain. For each trial, the average $\Delta F/F_0$ values over the 5 s red light stimulation was calculated, and the mean of these average $\Delta F/F_0$ over 20 trials yielded a per-fly mean.

2.7.5 Supplemental References

S1. Knapp, J.M., Chung, P., and Simpson, J.H. (2015). Generating customized transgene landing sites and multi-transgene arrays in *Drosophila* using phiC31 integrase. Genetics *199*, 919-934.

S2. Markstein, M., Pitsouli, C., Villalta, C., Celniker, S.E., and Perrimon, N. (2008). Exploiting position effects and the gypsy retrovirus insulator to engineer precisely expressed transgenes. Nat. Genet. *40*, 476-483.

S3. Bidaye, S.S., Machacek, C., Wu, Y., and Dickson, B.J. (2014). Neuronal control of *Drosophila* walking direction. Science *344*, 97-101.

S4. Wu, M., Nern, A., Williamson, W.R., Morimoto, M.M., Reiser, M.B., Card, G.M., and Rubin, G.M. (2016). Visual projection neurons in the *Drosophila* lobula link feature detection to distinct behavioral programs. eLife *5*, e21022.

S5. Klapoetke, N.C., Murata, Y., Kim, S.S., Pulver, S.R., Birdsey-Benson, A., Cho, Y.K., Morimoto, T.K., Chuong, A.S., Carpenter, E.J., Tian, Z., et al. (2014). Independent optical excitation of distinct neural populations. Nat. Methods *11*, 338-346.

S6. Nern, A., Pfeiffer, B.D., and Rubin, G.M. (2015). Optimized tools for multicolor stochastic labeling reveal diverse stereotyped cell arrangements in the fly visual system. Proc. Natl. Acad. Sci. U S A *112*, E2967-2976.

S7. Pfeiffer, B.D., Ngo, T.T., Hibbard, K.L., Murphy, C., Jenett, A., Truman, J.W., and Rubin, G.M. (2010). Refinement of tools for targeted gene expression in *Drosophila*. Genetics *186*, 735-755.

S8. Chen, T.-W., Wardill, T.J., Sun, Y., Pulver, S.R., Renninger, S.L., Baohan, A., Schreiter, E.R., Kerr, R.A., Orger, M.B., Jayaraman, V., et al. (2013). Ultrasensitive fluorescent proteins for imaging neuronal activity. Nature *499*, 295-300.

S9. Branson, K., Robie, A.A., Bender, J., Perona, P., and Dickinson, M.H. (2009). High-throughput ethomics in large groups of *Drosophila*. Nat. Methods *6*, 451-457.

S10. Simon, J.C., and Dickinson, M.H. (2010). A new chamber for studying the behavior of *Drosophila*. PLoS ONE *5*, e8793.

S11. Kabra, M., Robie, A.A., Rivera-Alba, M., Branson, S., and Branson, K. (2013). JAABA: interactive machine learning for automatic annotation of animal behavior. Nat Methods *10*, 64-67.

S12. Robie, A.A., Straw, A.D., and Dickinson, M.H. (2010). Object preference by walking fruit flies, *Drosophila melanogaster*, is mediated by vision and graviperception. J. Exp. Biol. *213*, 2494-2506.

S13. Ramdya, P., Lichocki, P., Cruchet, S., Frisch, L., Tse, W., Floreano, D., and Benton, R. (2014). Mechanosensory interactions drive collective behaviour in *Drosophila*. Nature *519*, 233-236.

S14. Yu, J.Y., Kanai, M.I., Demir, E., Jefferis, G.S., and Dickson, B.J. (2010). Cellular organization of the neural circuit that drives *Drosophila* courtship behavior. Curr. Biol. *20*, 1602-1614.

S15. Wan, Y., Otsuna, H., Chien, C.B., and Hansen, C. (2012). FluoRender: An application of 2D image space methods for 3D and 4D confocal microscopy data visualization in neurobiology research. IEEE Pac. Vis. Symp., 201-208.

Appendix

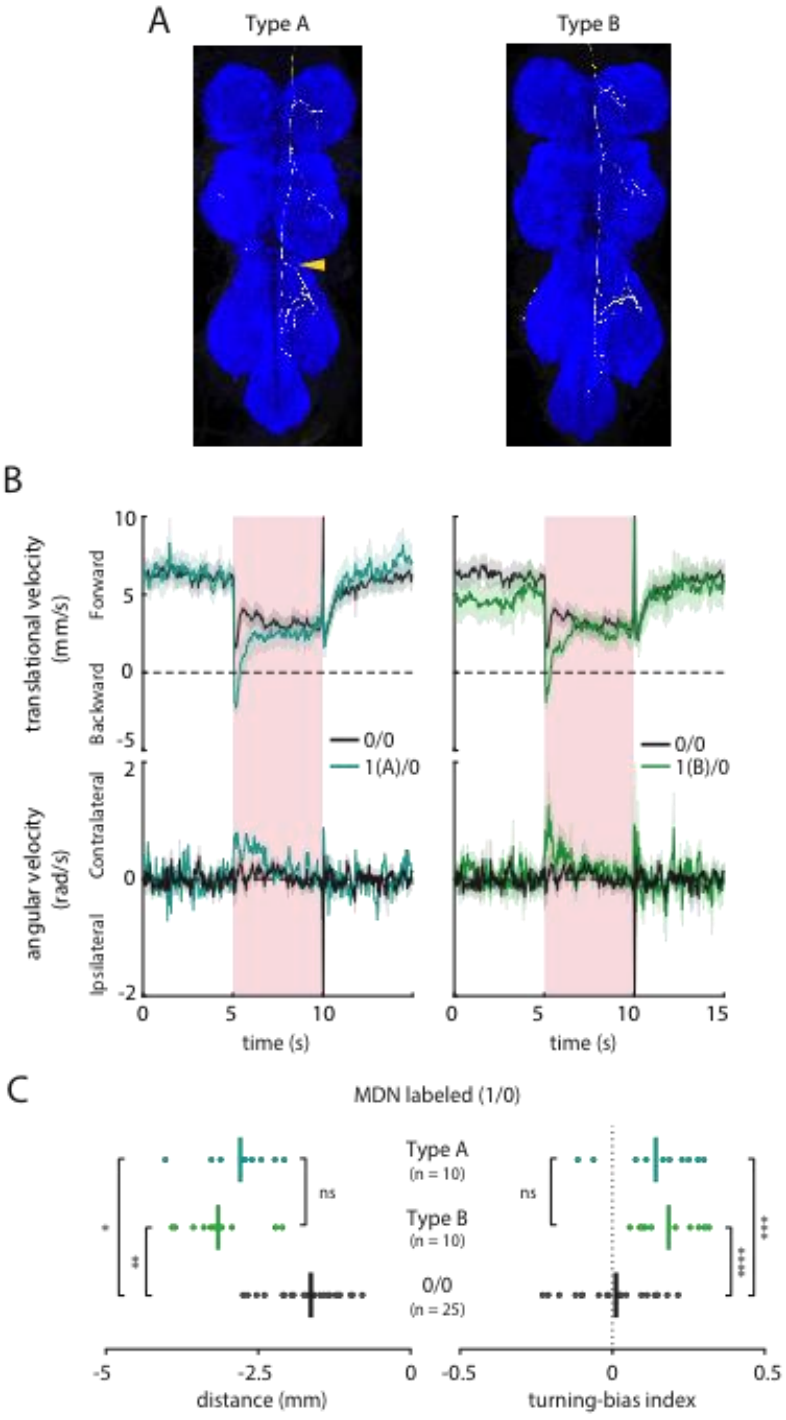

Figure A1

Figure A1. The 2 MDNs on each side of the central nervous system are functionally equivalent with respect to the extent of backward locomotion in our assay. (See Chapter 2 for further details on methods)

(A) The ventral nerve cords (VNCs) of two samples labeling a single right MDN cell from the stochastic activation experiments in Chapter 2. Left: A single type A MDN cell that has the anterior branch in the metathoracic ganglion indicated by the yellow arrowhead. Right: A single type B MDN that lacks the anterior branch (right).

(B) Time series for stochastic activation of samples with either a single Type A (left) or a single Type B (right) MDN labeled. Positive and negative values for translational velocity represent forward and backward translation. Positive and negative values for angular velocity represent contralateral or ipsilateral turns (with respect to the MDN soma in the brain). Dark traces represent the per-fly mean over 15 trials and envelopes indicate ± SEM (n = 10-25 flies).

(C) Per-fly mean of backward translational distances (left) and turning bias indices (right) for flies with either a single type A or a single type B MDN activated. Median values are represented by vertical bars. Turning bias indices are defined as ratio of contralateral to total angles turned and are normalized by subtracting light-off turning preferences. Statistical analysis was done using Kruskal Wallis test ($p < 0.0001$) followed by Dunn's post-hoc test (n = 10-25 flies). ****$p < 0.0001$, ***$p < 0.001$, **$p < 0.01$ and *$p < 0.05$; ns, not significant.

Chapter 3

A neuronal silencing screen identifies interneurons critical for backward locomotion in *Drosophila*

3.1 Highlights

- Silencing defined populations of interneurons impairs backward locomotion
- Hierarchical clustering identifies distinct categories of backward walking defects
- Identified neurons important for backward walking have diverse anatomy
- John Cleese Neuron, a T3 local interneuron, is necessary for backward locomotion

3.2 Summary

A walking animal adjusts its walking direction in response to external stimuli and changing behavioral goals. Locomotor central pattern generators (CPGs) that underlie rhythmic activation of leg muscles during walking thus need to be made flexible to the exigencies of the environment and the current goals of the animal. *Drosophila melanogaster* serves as a genetically tractable model to explore how CPGs in the ventral nerve cord (VNC) are modulated to control walking direction. Flies usually walk forwards, but can reverse their walking direction in response to specific sensory cues. We recently showed that the activity

of a cluster of 4 descending neurons, the Moonwalker Descending Neurons (MDNs), is necessary and sufficient for backward locomotion in flies. However, the nature of neuronal computations in the VNC in response to MDN activity remains poorly understood. Here we conduct an unbiased neuronal silencing screen to identify candidate interneurons in the central nervous system that are important for backward locomotion in flies. Our identified neurons mostly express in the VNC, and include a cluster of local interneurons in the metathoracic ganglia, the John Cleese Neurons (JCNs), that are anatomically close to MDNs and appear to be involved in the return stroke of backward-stepping hindlegs. Importantly, these identified neurons provide key entry points to VNC circuits that execute and coordinate backward locomotion.

3.3 Introduction

Walking is a complex, adaptive and crucial behavior in legged organisms. Walking relies on rhythmic activation of leg muscles, triggered by patterned activity of intrinsically rhythmic local circuits within the nerve cord called central pattern generators (CPGs). CPGs can produce robust and periodic output without receiving any phasic input, and their outputs are further refined by sensory feedback from leg mechanosensors that ensures the accurate timing and sequence of joint movements. Locomotor CPGs have been extensively studied in a wide variety of species [1–6]. However, it remains poorly understood how the rhythmic outputs of CPGs are modified and made flexible to changes in environmental conditions and goals of the animal.

Backward locomotion in *Drosophila melanogaster* serves as a genetically tractable model to address this question. The advent of genetic control of small populations of neurons affords the possibility of a cellular-level understanding of sensory processing, action selection and motor execution. Backward locomotion is usually a common response to aversive cues and has been studied in this and other contexts in animals including worms [7], lamprey [8–12], dogfish [13], crustaceans [14,15], scorpions and spiders [16], stick insects [17–19], ants [20–23], flies [24–27], and humans [28–30]. While flies usually walk forwards, they can alter or reverse their walking direction in response to visual threats [25–27] or when faced with physical obstructions [24]. Backward walking appears to employ the same rhythmic gaits as forward walking but alters the timing of specific muscle activation. Both forward and backward walking may rely on shared CPGs to generate rhythmic leg movements – the

change from forward to reverse mode relying on descending control from the brain and potentially higher order centers in the VNC. Previous works in cockroaches [31,32], stick insects [17] and flies [33] have suggested that inputs from the brain may cause a few critical state-dependent changes in the processing of sensory feedback in the VNC (reflex reversals) to control walking states.

We recently showed that a cluster of 4 descending neurons, the Moonwalker Descending Neurons (MDNs), are necessary and sufficient to trigger backward locomotion in flies [24], and that asymmetric activation of the left and right MDNs causes contralateral backward turns [26]. Neuronal activation of MDNs seems to switch both the sequence of leg movements and the phase of muscle activation in legs, indicating that it causes a critical flip in the premotor circuits in the VNC [24]. In addition to MDNs, we also identified a pair of ascending neurons, the Moonwalker Ascending Neurons (MANs) that facilitate backward walking induced by MDNs, possibly by inhibiting forward walking circuits [24]. However, the mechanism by which MDNs and MANs control VNC circuits to execute and coordinate backward locomotion remains poorly understood. With few exceptions [26], the nature of sensory cues and neuronal circuits that triggers MDN activity and backward locomotion also remains largely unexplored. As a necessary first step, we conducted a neuronal silencing screen to identify candidate interneurons in the brain and VNC essential for backward locomotion in *Drosophila*. These identified cells comprise numerous local, intersegmental and ascending neurons in the VNC, and include a cluster of local interneurons in the metathoracic ganglia (T3), the John Cleese Neurons, that appears to be specifically involved in return strokes of backward-stepping hindlegs. These neurons provide valuable footholds for understanding the neuronal computations essential for initiation, sustenance and coordination of backward locomotion in flies, which is likely generalizable to other legged organisms.

3.4 Results

3.4.1 A neuronal silencing screen for backward locomotion

We conducted a high-throughput unbiased neuronal silencing screen, searching for neurons which when inactivated specifically impair backward locomotion in flies. Flies were forced to walk in narrow linear groove-shaped chambers that restricted the vast majority of their lateral movement, while allowing them to move forwards and backwards. A computer vision software tracked the orientation and velocity of flies at every frame of each video, and a variant of the Viterbi algorithm was used to assign forward, backward and stalled states to flies [24] (Figure 1A). We initially used 3000 lines from the VT-GAL4 collection [34] to express the chronic synaptic silencer tetanus toxin light chain (TNT) [35] in random but defined populations of neurons, and searched for lines that had significant impairment in backward locomotion in the linear assay (data not shown). This screen yielded 83 hits that had broad expression patterns in the nervous system (Figure 1B). In an attempt to further refine the expression patterns and effectively parse the relevant neurons from the non-specific ones, we utilized the split-GAL4 intersectional system [36,37]. We generated split-GAL4 derivatives for a subset of the 83 hits by exchanging the GAL4 portion of the VT enhancer tile with either a GAL4 DNA binding domain (DBD) or a p65 activation domain (AD), each of which were fused to interacting leucine-zipper domains. A functional GAL4 would thus be reconstituted only in the subset of neurons where the expression patterns of the two enhancer tiles intersect. In total, we generated 52 GAL4-DBD and 36 p65-AD split-derivatives from the original 83 GAL4 hits. We built a collection of stocks by combining each of the 52 GAL4-DBD derivatives with the reporters *UAS-TNT* and *UAS-mCD8*-GFP, the latter expressing a membrane targeted green fluorescent protein (GFP). We aimed to generate intersections by individually crossing each of these 52 stocks to the 36 p65-AD derivatives, such that for each successful GAL4-DBD ∩ p65-AD intersection the co-expression of mCD8-GFP and TNT would allow us to both inactivate and visualize cells at the same time. In our primary screen, we tested 1741 distinct split-GAL4 pairs in the linear assay (n = 12 flies/genotype), looking for intersections in which TNT impaired backward locomotion (Figure 1C). We identified several intersections in which backward locomotion was impaired to similar extents as our positive controls, i.e. flies expressing TNT in MDNs (Figure 1C). We picked the 20^{th} percentile value for ‘distance backwards’ from the entire dataset of the screen as an upper threshold for determining hits with backward walking defects. 289 split-GAL4 combinations, whose median values for ‘distance backwards’ fell below this 20^{th}

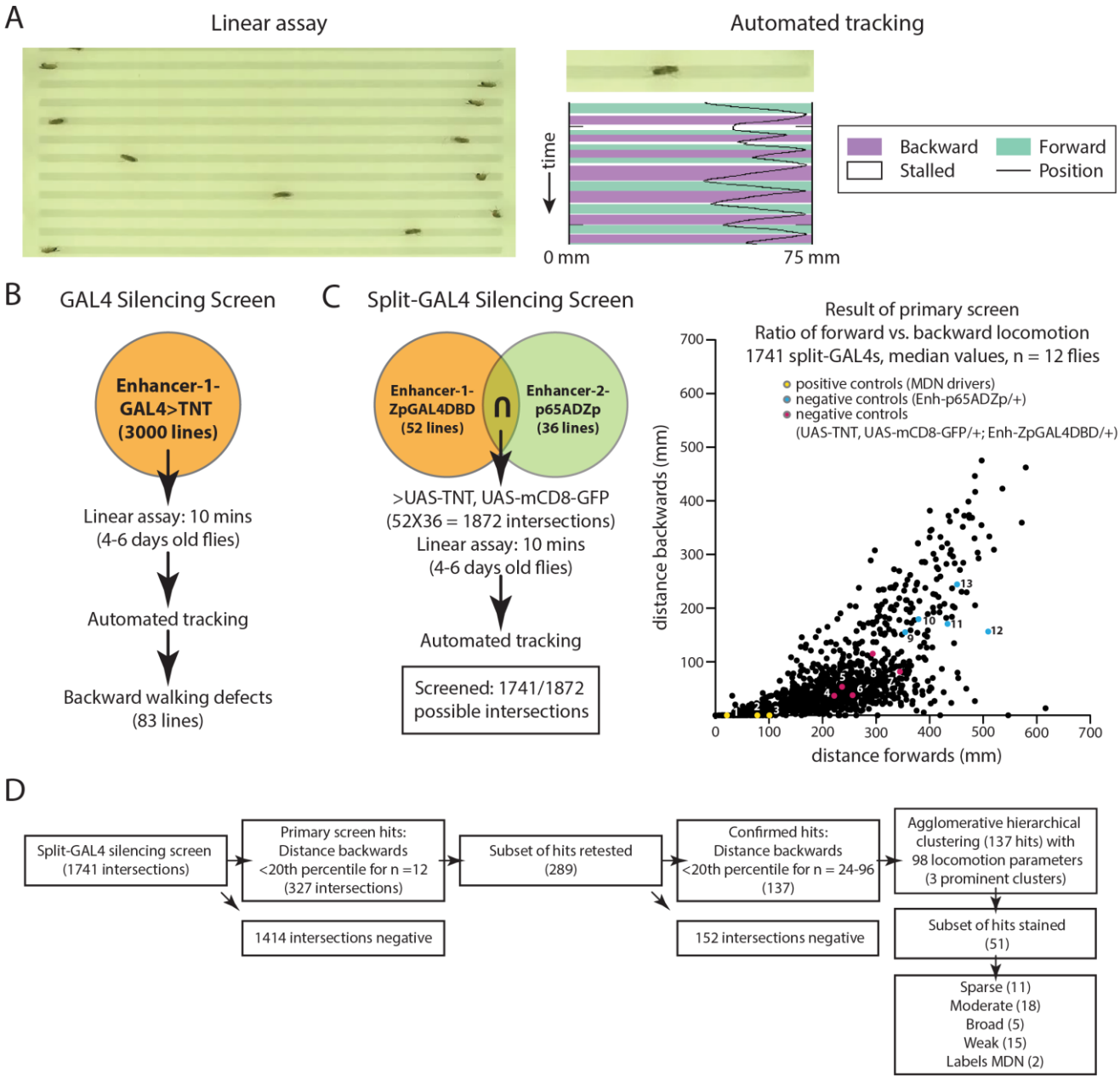

Figure 1. Neuronal silencing screen for backward locomotion

(A) Left: Linear chambers for high-throughput walking assay. Right: Representative tracking data of a single control male fly. Colors indicate walking states: magenta, backwards; green, forwards; white, stalled.

(B) Workflow and overview of initial GAL4 silencing screen.

(C) Left: Workflow of split-GAL4 silencing screen. Right: Result of primary split-GAL4 silencing screen with 1741 split-combinations. Distance backwards versus distance forwards in linear assays. Each point represents median of n = 12 flies for a single split-GAL4 combination. Positive controls (1-3; yellow) include 3 MDN drivers driving the expression of the neuronal silencer, *UAS-TNT*, along with *UAS-mCD8-GFP*. Negative controls include 5 representative *enhancer-ZpGAL4DBDs* (4-8; magenta) driving *UAS-TNT* and *UAS-mCD8-GFP*, and 5 representative *enhancer-p65ADZps* (9-13; blue). See also Table S1 for detailed genotypes of controls.

(D) Overview of the results from the split-GAL4 silencing screen.

percentile threshold, were considered ‘hits’ from the primary screen and retested 2-4 times. For 137 of these 289 intersections, the medians for ‘distance backwards’ (n = 24–96 flies/genotype) fell below our previously determined threshold again, and these were thereby selected for further analysis.

3.4.2 Agglomerative hierarchical clustering identifies distinct categories of backward walking defects

We observed that the attributes ‘distance backwards’ and ‘distance forwards’ were not sufficient to describe the entire repertoire of behavioral phenotypes observed in the linear assay. While wild-type flies easily backed up in this assay and subsequently resumed forward motion, flies with defects in either forward or backward locomotion stalled more often, or were stuck in long transitions from one state to the other. In order to identify distinct categories of backward walking defects based on the complete range of behavioral phenotypes in the assay, we extracted additional attributes from the tracker (Table S2) and used these to cluster our 137 hits into distinct groups. Assuming that distinct circuit-components underlie distinct behaviors, we anticipated that closely linked genotypes from these clusters might have similar expression patterns, enabling the efficient identification of specific cell-types for interesting phenotypes.

We identified 4 main transitions between forward and backward walking states in the linear assay: 1) turns, 2) flips, 3) reversals, (Figures S1A and S1B) and 4) stalls. A turn was defined as a change in the heading direction of the fly, with no change in its walking state. For example, a forward turn occurred when a fly moving forwards with a net displacement towards the left of the linear chamber squeezed around its body to continue walking forwards but now with a net displacement towards the right of the chamber (Figures S1A and S1B). A flip was defined as a change in both the heading direction and walking state of the fly. For example, a forward flip occurred when a fly moving forwards with a net displacement towards the left of the chamber squeezed around its body to initiate backward locomotion with a net leftward displacement (Figures S1A and S1B). A reversal was defined as a change in the walking state of the fly with no change in its heading direction. For example, a forward reversal occurred when a fly moving forwards with a net leftward displacement reversed its walking direction to initiate backward locomotion with a net rightward displacement (Figures S1A and S1B). Stalls were defined as a state when the translational velocity of the fly fell below a threshold of 1.5 mm/s [24]. We calculated the number of bouts and bout duration for each state, transition and stalls, absolute forward and backward displacements without

considering velocity thresholds, and assembled a list of 98 attributes constituting these parameters and their various meaningful ratios (Table S2).

These attributes, taken together, described almost the entire range of behavioral phenotypes that we observed in the linear assay. We next sought to use an unbiased clustering approach to cluster our 137 hits from the silencing screen into groups with similar phenotypes. We assembled a dataset of median values (n = 24 – 96 flies) of the 98 attributes for 137 genotypes, and normalized this dataset by calculating the z-score for every attribute. This normalized dataset constituted a 137X98 matrix, which we hereafter refer to as the phenotype matrix.

We clustered the phenotype matrix using agglomerative hierarchical clustering with Ward's linkage method (Figure 2). The degree of phenotypic similarity between genotypes is reflected in the linkage-distances, i.e. the branch lengths of the dendrogram (Figure 2). Values for Ward's joining costs are low at initial rounds of clustering when relatively more similar groups exist and are joined together. Values rise in later iterations, when more and more distinct groups are forced to merge. For our data, a plot of Ward's joining costs with respect to the number of clusters at a given iteration showed that the joining cost increased dramatically when less than 3 clusters were forced (Figure S1C). The slope provided further hint that the data could indeed be clustered into 3 distinct groups (Figure S1D). Additionally, local minima also existed at 6 and 10 clusters in the plot of slope versus the number of clusters (Figure S1D). As a trade-off between comprehensively describing all possible phenotypes and identifying biologically interesting phenotypic clusters, we first clustered the entire dataset into 3 distinct groups and then explored each cluster for possibilities of sub-clustering or recognizing individual outliers. Specifically, after an initial clustering into 3 main groups, we clustered the entire data again into 6 clusters. The latter revealed that the 1st main cluster had 3 sub-clusters, the 2nd had none, and the 3rd had 2.

Cluster 1 predominantly comprised phenotypes that represented specific backward walking defects. These hits preferred turning to stalling when they reached the end of the linear grooves (Figure 2). There were three variations to this phenotype, and hence 3 distinguishable sub-clusters 1A, 1B and 1C (Figure S2). Hits in sub-cluster 1A reversed relatively more than the other two sub-clusters in Cluster 1. 7 hits in our entire phenotype matrix showed flipping and were included in Cluster 1; sub-cluster 1A comprised 5 out of 7 of these hits. Sub-clusters 1B and 1C comprised hits that preferred turning to both reversing and stalling, and these two sub-clusters were more closely linked. Most of the intersections labeling MDNs (all but MDN-2 from our positive controls shown in Figure 1B and 2 new

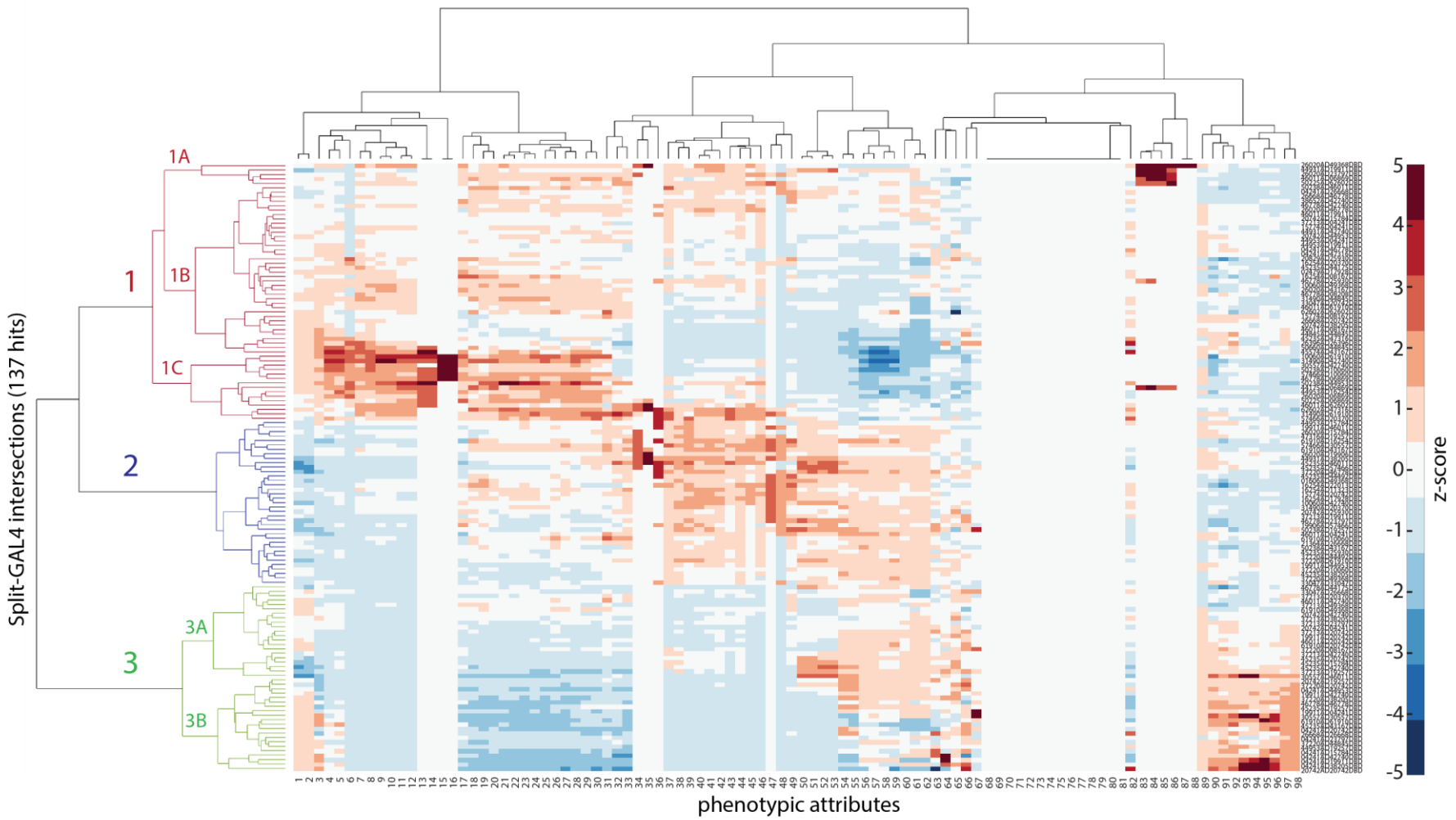

Figure 2. Hierarchical agglomerative clustering identifies three major clusters of backward walking defects
Agglomerative hierarchical clustering of the 137 X 98 phenotype matrix using a threshold of Ward's linkage cost shows that backwards walking defects fall into three major clusters. Clustered data is shown as a heatmap where values range from -5 z-score (pure blue) to +5 z-score (pure red).The three clusters are marked by different colors on the dendogram. Cluster 1 and 3 can also be broken up into further sub-clusters, which are respectively numbered. See also Key for 1-98 attributes (next page), Figures S1, S2, S3 and S4, and Tables S1 and S2.

Key for 1-98 phenotypic attributes

1. time forwards/(time forwards + backwards)
2. distance forwards/(distance forwards + backwards)
3. forward/total movement in center
4. forward/total movement
5. forward/total movement in periphery
6. (#turns forced + #flips forced)/#transitions forced
7. total turn duration
8. #turns/#transitions
9. #turns
10. #forward turns
11. #turns in periphery
12. #forwards turns in periphery
13. #forward turns forced
14. #turns forced
15. #forward turns in center
16. #turns in center
17. #heading changes
18. #stalls in center
19. total movement in center
20. total forward movement in center
21. distance forwards
22. distance forwards + backwards
23. time forwards + backwards
24. time forwards
25. #forward bouts
26. #stalls
27. total movement
28. total forward movement
29. total forward movement in periphery
30. total movement in periphery
31. #stalls in periphery
32. total backward movement in periphery
33. total backward movement
34. #reversals forced
35. #backward reversals forced
36. #forward reversals in periphery
37. #forward reversals
38. #reversals/#transitions
39. total reversal duration
40. distance backwards
41. time backwards
42. #backward bouts
43. #reversals in periphery
44. #reversals
45. #backward reversals
46. #backward reversals in periphery
47. #forward reversals in center
48. #reversals in center
49. total backward movement in center
50. distance backwards/distance forwards
51. distance backwards/(distance forwards+backwards)
52. time backwards/(time backwards+forwards)
53. time backwards/time forwards
54. backward/forward movement in center
55. backward/total movement in center
56. backward/forward movement
57. backward/total movement
58. backward/total movement in periphery
59. backward/forward movement in periphery
60. #reversals/(#turns + #reversals)
61. #reversals forced / (#turns forced + #reversals forced)
62. #reversals forced / (#turns forced + #reversals forced + #flips forced)
63. mean backward bout duration
64. mean reversal duration
65. mean body size
66. mean turn duration
67. mean flip duration
68. #backward turns in center
69. #backward flips in periphery
70. #forward flips forced
71. #backward flips forced
72. #backward turns
73. #backward turns in periphery
74. #forward reversals forced
75. #backward turns forced
76. #flips forced
77. #flips in center
78. #backward reversals in center
79. #backward flips
80. #backward flips in center
81. #forward flips in center
82. mean forward bout duration
83. #flips/#transitions
84. #flips
85. #forward flips
86. total flip duration
87. #forward flips in periphery
88. #flips in periphery
89. #stalls forced
90. stuckness
91. time in periphery
92. time in outer periphery
93. #stalls forced/#stalls
94. total stall duration forced
95. mean stall duration
96. mean stall duration forced
97. #stalls/#transitions
98. total stall duration

reagents that we uncovered from our screen (see Section 3.4.3)) were grouped together as part of sub-cluster 1B. Sub-cluster 1C had a stronger turning phenotype than 1B, and involved more forced turns at the ends of the chambers. Their forward motion was also least affected compared to all other clusters in the phenotype matrix.

Cluster 2 was mostly composed of phenotypes that represented decreased forward locomotion in the linear assay (Figures 2 and S3). Backward locomotion was also affected in these lines with respect to the entire silencing screen, since the subset of hits we pre-selected for clustering included only those that reproducibly fell below our assigned threshold for distance covered in backward walking mode. But, interestingly, in comparison to the rest of the 137 hits in our phenotype matrix, these hits showed less impairment in backward locomotion. Flies reversed more, walked longer times and distances backwards, had higher number of backward bouts and showed higher ratios for backward to forward and backward to total distance and time. It should be noted that flies with specific but potentially incomplete forward walking defects might show reductions in backward walking in this assay. Such flies would take longer to reach the end of the linear chamber and would thus have an overall decreased stimulus for reversal. While it is possible that long, failed attempts at forward locomotion might eventually transition to backward locomotion, it is likely that the level of backward locomotion resulting from this transition would be reduced compared to flies that have collided with the end of the chamber. Together, the specific decreases in forward locomotion would therefore result in an overall decrease in backward locomotion with higher ratio of backward to forward locomotion. Numerous genotypes in cluster 2 showed exactly these characteristics; we therefore infer that this cluster might contain lines with specific defects in forward locomotion. Flies in cluster 2 might provide important insights on how the forward and backward circuits are independently controlled.

Cluster 3 predominantly comprised hits that stalled more at the ends of the chamber instead of reversing or turning (Figure 2). Since flies were stalled for the majority of the assay, further tests are necessary to segregate this cluster into distinct groups constituting specific backward walking defects and general locomotion defects. The cluster could be subdivided into sub-clusters 3A and 3B, with sub-cluster 3A representing a weaker version of the phenotype (Figure S4). Interestingly, MDN-2 was grouped in Cluster 3 and sub-cluster 3B, instead of Cluster 1B where the rest of the hits labeling MDNs were grouped. It is to be noted that this apparent discrepancy in the silencing phenotype of *MDN-2* driver and other hits labeling MDNs is consistent with their corresponding activation phenotypes. We have recently shown that optogenetic activation of MDNs with *MDN-2* driving a red-light

activated cation channel CsChrimson [38] causes increased backward turning compared to other MDN drivers [26]. This can perhaps be attributed to the additional neurons labeled by the MDN-2 split-combination in the VNC [24]. Owing to its distinct activation phenotype, it is not surprising that silencing neurons labeled in MDN-2 caused a reduction in turning, and therefore resulted in MDN-2 clustering independently from the other MDN drivers.

While agglomerative hierarchical clustering helped us build intuition about the nature of our hits, we qualitatively observed that a recurrent limitation of the linear assay was the inability to conclusively segregate specific backward walking defects from general locomotion defects. To address this, we picked representative hits from Cluster 1 and Cluster 3, and allowed flies to walk forwards for 10 minutes in a previously described ring-shaped chamber [24]. 1 out of 6 of the representatives picked from Cluster 1, and 3 out of 5 picked from Cluster 3, indeed, had defects in aspects of forward locomotion (Figures S5).

3.4.3 Split-GAL4 hits from silencing screen have diverse expression patterns and show enrichment in the VNC

We next sought to identify the underlying neuronal components that explained the reductions in backward locomotion in our hits. Since mCD8-GFP and TNT reporters were co-expressed by the split-GAL4 combinations tested in our screen, we could use the same genotypes to visualize the cells that were inactivated in our intersections of interest. In total, we stained 51 hits from our screen. Out of these 51 hits, we identified 11 ‘sparse’ intersections, 23 ‘moderate’ to ‘broad’ intersections, and 2 split-GAL4 combinations that labeled MDNs and were not described previously (Figure 1D). 26 out of 51 of the stained hits had interesting expression patterns, either because they were sparsely expressed or because they expressed in regions of the nervous system implicated in locomotion. We hereafter (affectionately) refer to these as SillyWalkers (SW) (after Monty Python’s famous sketch, ‘the Ministry of Silly Walks’).

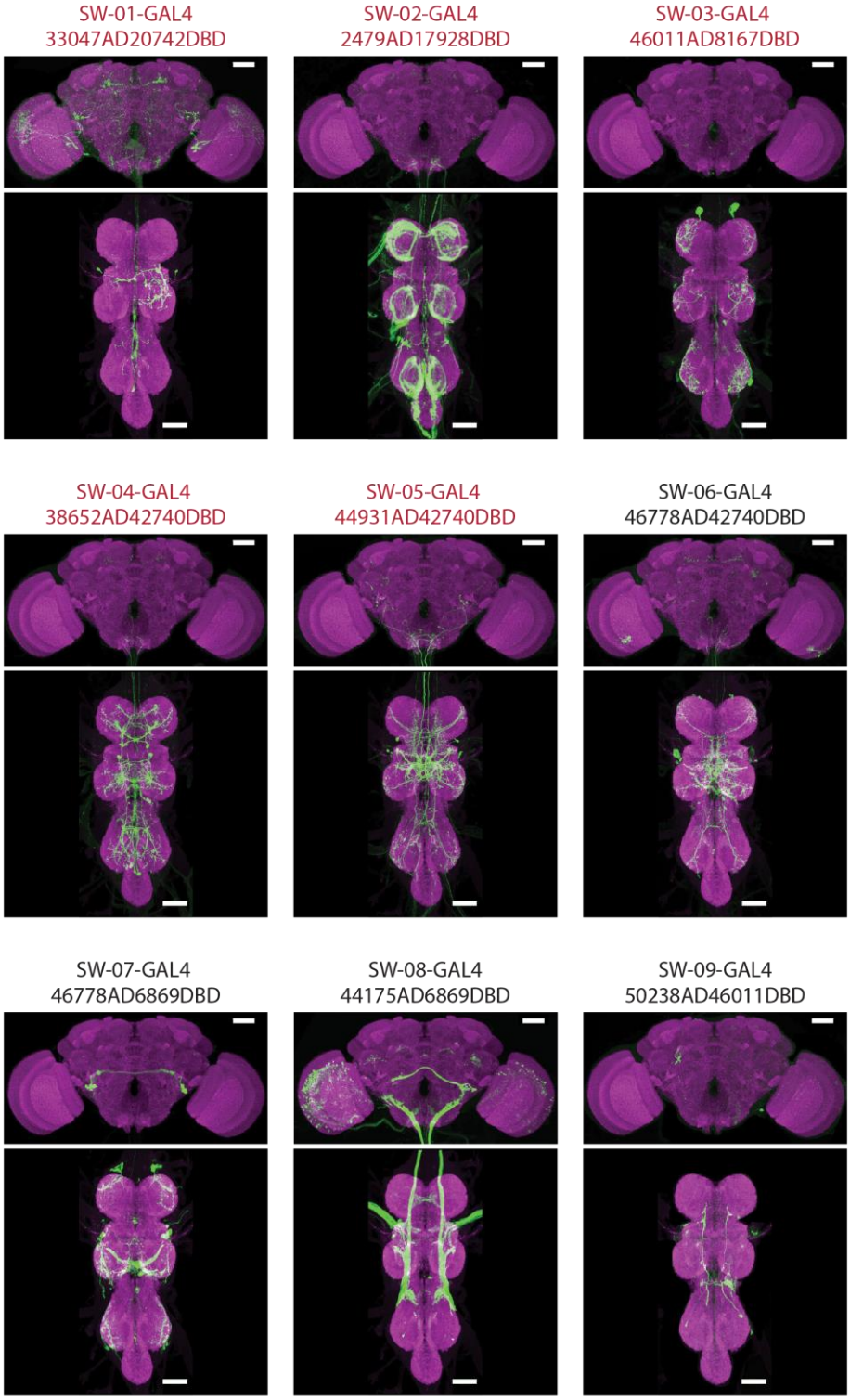

Figure 3. Expression patterns of representative SillyWalker neurons from Cluster 1
Expression patterns of representative hits from Cluster 1. Each image shows the central nervous system of a male fly, carrying the indicated split-GAL4 combination driving *UAS-mCD8-GFP* and *UAS-TNT* expression. The brain is shown at the top and the VNC at the bottom. Flies are stained with anti-GFP (green), which indicates the silenced neurons, and nc82 (magenta), which labels neuropil and acts as a counterstain. All images have been registered onto a common reference template. Lines marked in red are further tested for general locomotion defects in the ring assay. Scale bar, 50 μ. See also Figure S5 and Table S1.

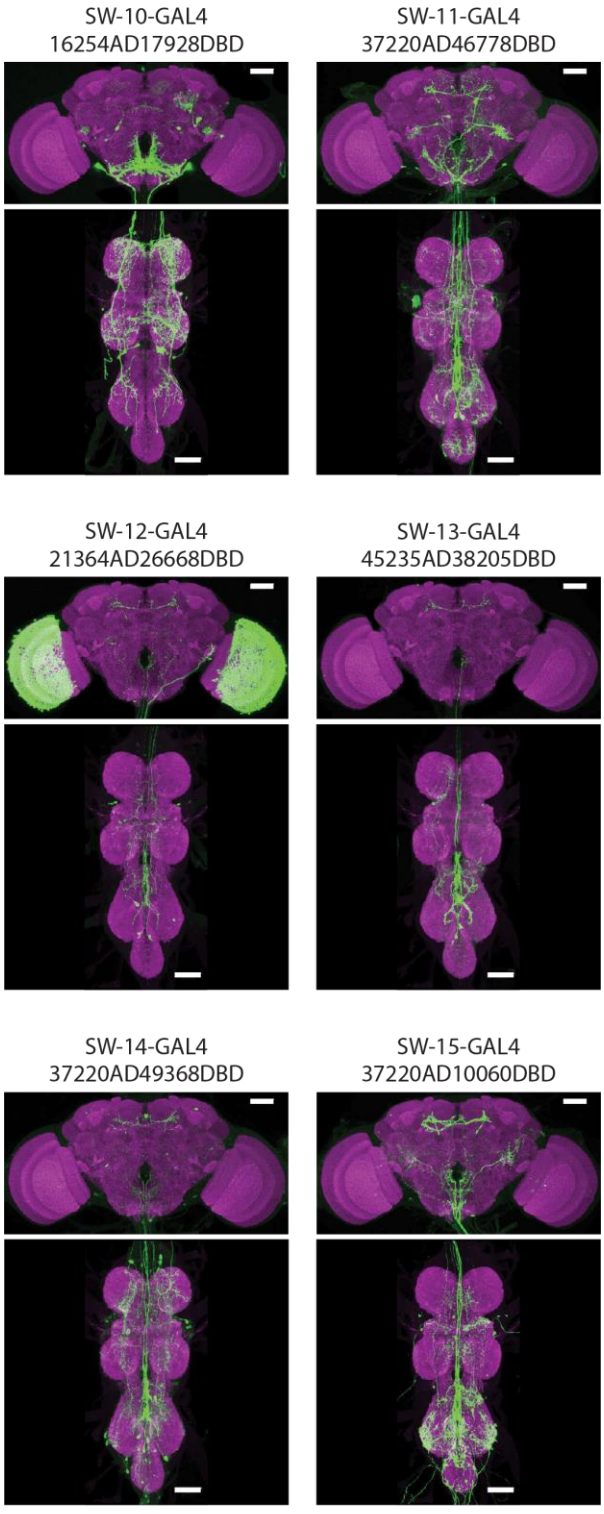

Figure 4. Expression patterns of representative SillyWalker neurons from Cluster 2
Expression patterns of representative hits from Cluster 2. Staining and analysis are performed as in Figure 3. Scale bar, 50 μ. See also Table S1.

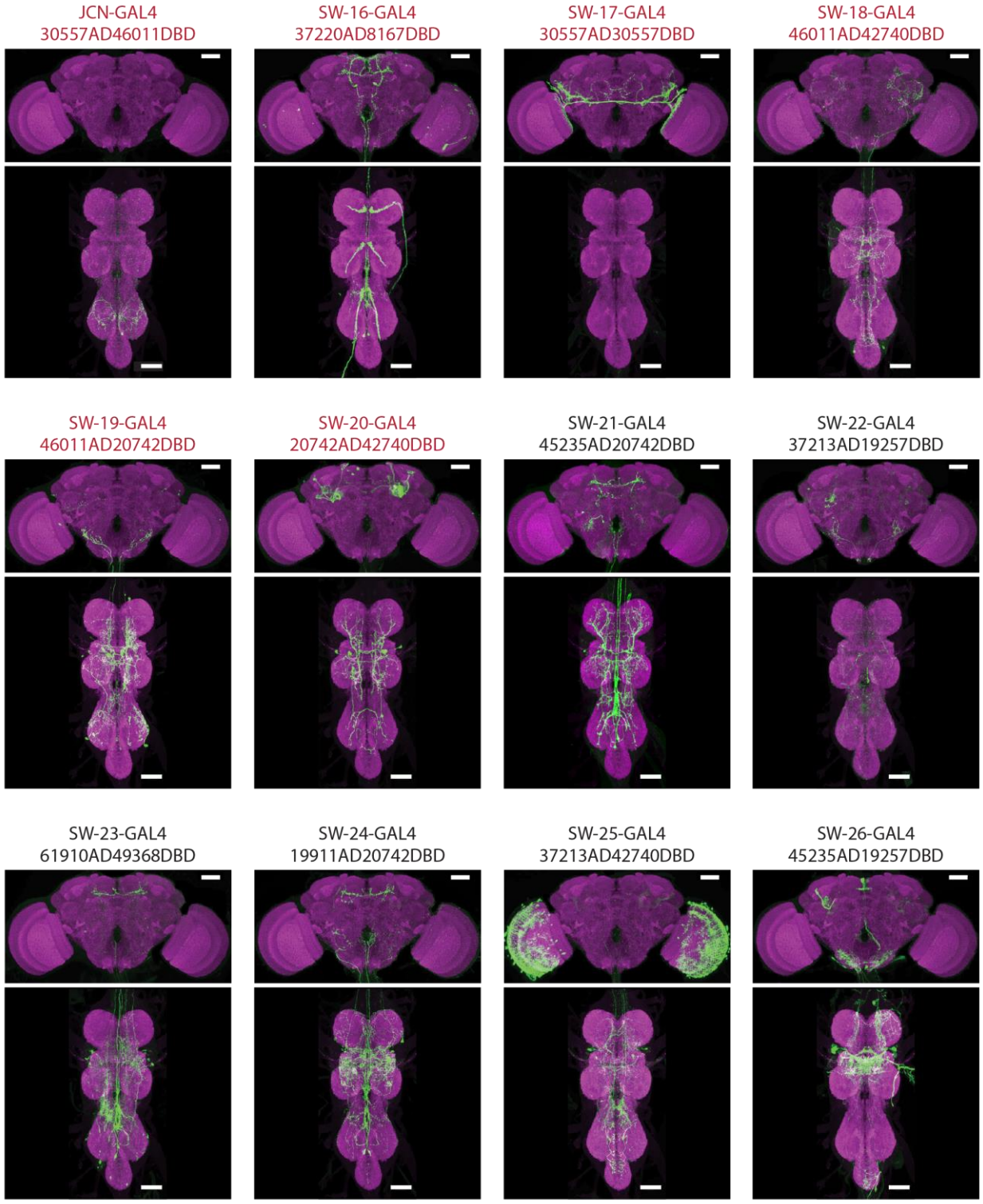

Figure 5. Expression patterns of representative SillyWalker neurons from Cluster 3
Expression patterns of representative hits from Cluster 3. Staining and analysis are performed as in Figure 3. Lines marked in red are further tested for general locomotion defects in the ring assay. Scale bar, 50 μ. See also Figure S6 and Table S1.

We checked the expression patterns of a subset of hits from each cluster (Figures 3, 4 and 5; Tables S1 and S3) and found a considerable enrichment for expression in the ventral nerve cord (VNC). We mainly focused on Clusters 1 and 3, since they represented strong and specific backward walking defects. Out of 16 hits stained from Cluster 1, 11 hits were moderately restricted (Figure 3) and included 2 new reagents labeling MDNs and 2 hits (SW-05-GAL4 and SW-06-GAL4) that appeared to label the same interneurons in the VNC. Out of 24 hits stained in Cluster 3, 12 hits were moderately restricted (Figure 5), and included 2 split-GAL4 combinations (SW-20-GAL4 and SW-21-GAL4) that labeled the identical pairs of intersegmental neurons in the VNC. In addition to intersegmental VNC neurons (Cluster 1, SW-04-GAL4, SW-05-GAL4, SW-06-GAL4; Cluster 3, SW-20-GAL4 and SW-21-GAL4), cell-types labeled by Cluster 1 and 3 included ascending neurons (Cluster 1, SW-01-GAL4, SW-04-GAL4, SW-05-GAL4, SW-06-GAL4), sparse populations of local interneurons (Cluster 1, SW-01-GAL4, SW-03-GAL4, SW-07-GAL4; Cluster 3, John Cleese Neuron (JCN)-1-GAL4, SW-19-GAL4), central neurons restricted to the brain (Cluster 3; SW-17-GAL4) and putative mechanosensory neurons with cell bodies in the periphery and axonal bundles in the VNC (Cluster 1, SW-02-GAL4; Cluster 3, SW-16-GAL4). We stained 9 lines from Cluster 2 (Figure 4); 7 of these were moderately labeled and included descending neurons and interneurons in the VNC.

3.4.4 JCNs, a cluster of T3 local interneurons, are necessary for backward locomotion and control hindleg extension

Owing to its interesting anatomy, we chose to study John Cleese Neurons (JCNs) from Cluster 3 in greater detail. JCNs are two pairs of local interneurons in the T3 neuromere of the VNC. *JCN-1-GAL4* reproducibly labeled these neurons; however, on occasion only one of the two pairs was labeled. Each cell arborizes on the ventral side of T3 and extends its processes to the ipsilateral leg neuropil on the dorsal side of T3 (Figure 6; Movie M1). To further characterize the anatomy of JCNs, we used *JCN-1-GAL4* to drive the expression of the membrane marker *myr-tdTomato* (membrane targeted red fluorescent protein) [37] along with the pre-synaptic marker *syt-GFP* (GFP tagged with the synaptic vesicle protein, synaptotagmin) [39]. We predominantly observed pre-synaptic sites (indicated by colocalizations of synaptotagmin and the cell membrane) in the anterior (upper) branches of JCNs with none or few in the posterior (lower) branches (Figure 6B). Owing to the absence of synaptotagmin localizations in the lower branches of JCNs, we

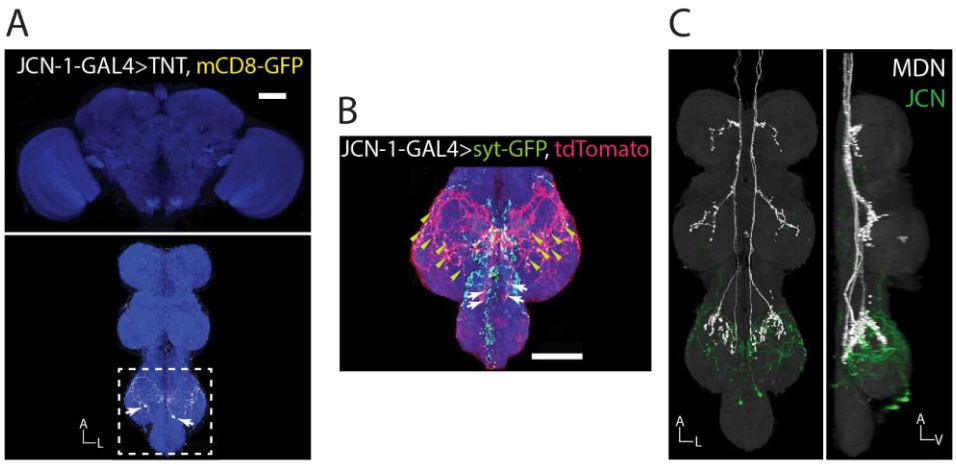

Figure 6. Anatomy of a representative SillyWalker neuron: John Cleese Neuron (JCN)
(A) Brain and VNC of a male carrying *JCN-1-GAL4* split combination driving the expression of *UAS-mCD8-GFP* and *UAS-TNT*, stained with anti-GFP (yellow) and nc82 counterstain (blue). Scale bar, 50 µ. Boxed region is expanded in (B).
(B) The metathoracic and abdominal segments of a *JCN-1-GAL4 UAS-syt-GFP UAS-tdTomato* male, stained with anti-dsRed (magenta), anti-GFP (green) and nc82 (blue). Yellow arrowheads indicate regions of synaptotagmin (*UAS-syt-GFP*) localization, and thus represent the likely sites of presynaptic specializations. White arrowheads indicate the soma of JCN. Scale bar, 50 µ.
(C) Segmented MDN axons and JCN registered and overlaid onto a common reference VNC template. MDN is in white and JCN in green. Potential overlap of arborizations is seen in the metathoracic segments of the VNC.

inferred that these branches are post-synaptic. The latter are anatomically close to outputs of MDNs (Figure 6C), suggesting that JCNs might receive inputs from MDNs. Functionally imaging calcium activity in JCNs upon optogenetic activation of MDNs would further establish if JCNs indeed receive inputs from MDNs.

Silencing the activity of JCNs in the linear assay dramatically impaired backward locomotion in flies (Figures 2, S4, 7A; Movie M2). The reduction in the extent of backward walking in JCN-silenced flies was indistinguishable from our positive controls in which MDNs were inactivated (Figure 7A), suggesting that JCNs are necessary for execution of backward locomotion. Distances covered in forward walking state were indistinguishable between JCN-silenced flies and controls (Figure 7B; Movie M3), suggesting that JCNs specifically control aspects of backward locomotion.

When we acutely depolarized JCNs with CsChrimson in freely walking flies, we failed to observe any locomotion phenotype (data not shown). This observation, along with the knowledge of the anatomy of JCNs, lead us to propose that, rather than triggering coordinated backward locomotion, JCNs could instead control subsets of limb movements unique to backward locomotion. In order to uncover such unique limb movements, we decapitated *JCN-1-GAL4 UAS-CsChrimson* flies to eliminate forward-walking signals from the brain to the VNC, and optogenetically activated JCNs in this semi-intact VNC preparation. We now observed robust and reliable, albeit transient, extensions of both hindlegs, irrespective of whether the headless flies were standing on the ground or lying upside-down (Figure 7C; Movie M4). Importantly, the extensions involved at least the femur-tibia joints and were restricted to only the hindlimbs. Upright headless flies expressing CsChrimson in MDNs, on the other hand, robustly walked backwards upon optogenetic activation (Figure 7C; Movie M5). As previously observed, their phase and sequence of leg movements were switched [24], likely due to a critical flip in the premotor circuits in the VNC. When taped upside-down on their thoraces, decapitated flies with optogenetically activated MDNs actively extended their hindlegs with considerably less movements in the other legs (Movie M5). The large-amplitude hindleg extensions were interspersed with rhythmic twitches of low-amplitude flexions that, we interpret, should otherwise have triggered a touch-down of the tarsi to the ground in a walking fly. Control headless flies, where an empty driver was used to drive the expression of *CsChrimson*, showed no movement, whether upright or supine (Figure C; Movie M6).

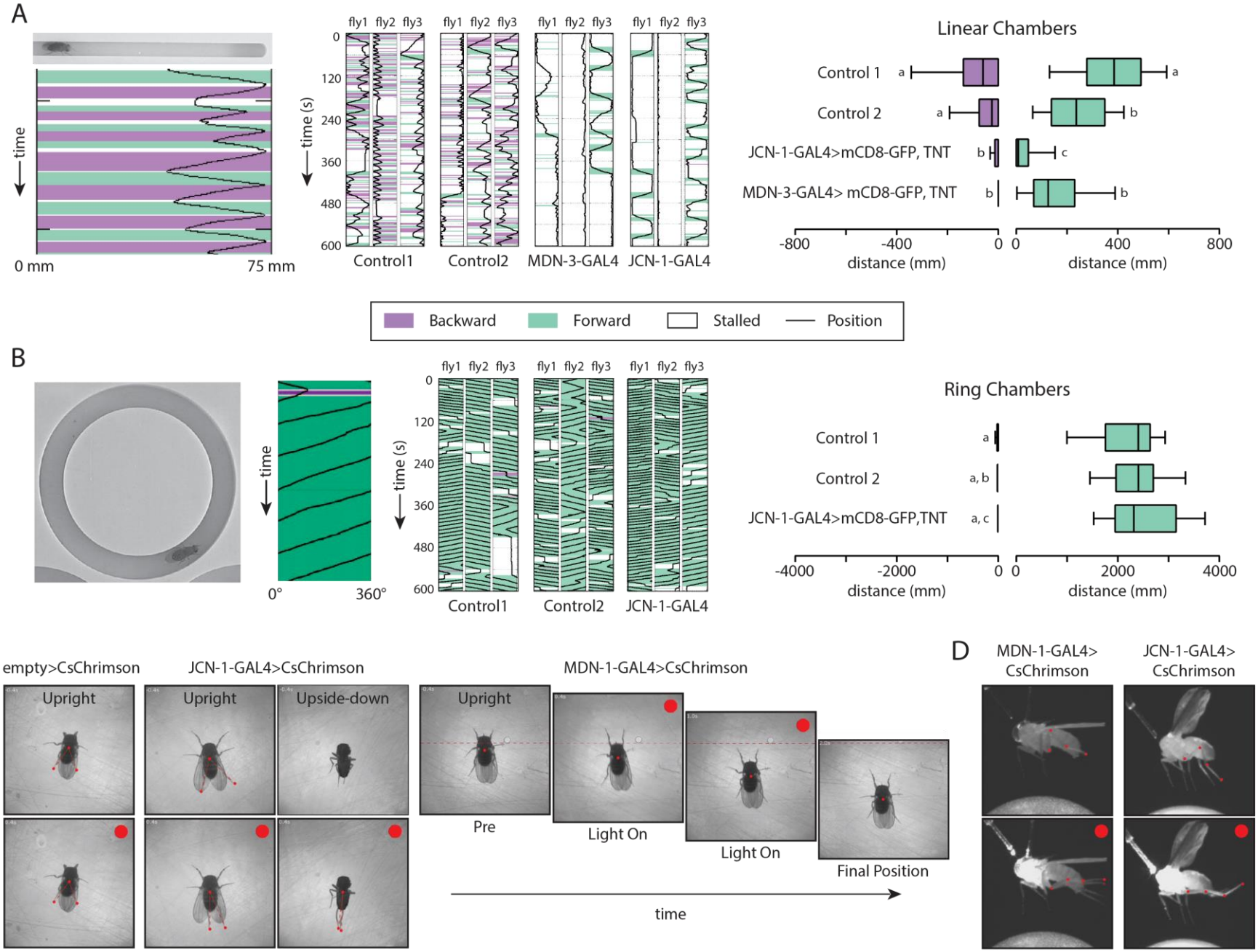
A
time
0 mm
75 mm
fly1 fly2 fly3
time (s)
0
120
240
360
480
600
Control1
Control2
MDN-3-GAL4
JCN-1-GAL4
Linear Chambers
Control 1
Control 2
JCN-1-GAL4>mCD8-GFP, TNT
MDN-3-GAL4> mCD8-GFP, TNT
-800
-400
0
400
800
distance (mm)
Backward
Forward
Stalled
Position
B
time
0°
360°
Ring Chambers
-4000
-2000
2000
4000
C
empty>CsChrimson
JCN-1-GAL4>CsChrimson
MDN-1-GAL4>CsChrimson
Upright
Upside-down
Pre
Light On
Final Position
time
D
MDN-1-GAL4> CsChrimson
JCN-1-GAL4> CsChrimson

Figure 7. JCN interneurons are necessary for backward locomotion and trigger hindleg extension in flies

(A) Left: Example tracking data of a single male fly in the linear assay. Middle: 10-minute motion plots of males carrying the indicated driver along with *UAS-TNT UAS-mCD8-GFP*. Three representative plots are shown for each genotype. See also Table S1 for detailed genotypes. Right: Total walking distance in a 10-min assay in linear chambers (n = 40-112 flies; Control-1 *30557-p65AD*, n = 72; Control-2 *46011-GAL4DBD UAS-TNT UAS-mCD8-GFP*, n = 78; *MDN-3-GAL4 UAS-TNT UAS-mCD8-GFP*, n = 40; *JCN-1-GAL4 UAS-TNT UAS-mCD8-GFP*, n = 112). Box-and-whisker plots in this and other panels represent 10^{th}, 25^{th}, 50^{th}, 75^{th}, and 90^{th} percentiles. Statistical significance was assessed using Kruskal-Wallis test ($p < 0.0001$ for both panels), followed by Dunn's post-hoc test. Results of statistical analyses in this and other panels are represented as letter codes such that groups that are not statistically significant from each other have the same letter code. When a group has more than one letter code, the given group is not significantly different from other groups that have any of its letter codes.

(B) Left: Ring assay for forward walking and representative motion plot of a single male fly walking predominantly anti-clockwise. Middle: 10-minute motion plots of males carrying the indicated driver along with *UAS-TNT UAS-mCD8-GFP*. Three representative plots are shown for each genotype. See also Table S1 for detailed genotypes. Right: Total walking distance in a 10-min assay in ring chambers (n = 42-47 flies; Control-1 *30557-p65AD*, n = 45; Control-2 *46011-GAL4DBD UAS-TNT UAS-mCD8-GFP* n = 42; *JCN-1-GAL4 UAS-TNT UAS-mCD8-GFP*, n = 47).

(C) Movie stills from optogenetic activation of decapitated flies carrying the indicated split-GAL4 drivers along with *UAS-CsChrimson.* The center of fly and the tip of two hindlegs are marked with red dots. Red circles, light on.

(D) Movie stills of air-stepping upon optogenetic activation of tethered decapitated flies carrying MDN-1- and JCN-GAL4 split combinations along with *UAS-CsChrimson.* Four joints in left hindleg are indicated with red dots. Red circles, light on.

We next sought to understand the role of hindleg extensions in the context of backward locomotion. We recorded high-resolution videos of tethered *MDN-1-GAL4 UAS-CsChrimson* flies as they walked on an air-suspended polypropylene ball. We allowed flies to first walk forwards (Movie M7) and then acutely stimulated MDN activity with a red laser of wavelength ~617 nm, pointed towards the center of the fly-head (Movie M8). We observed that when a forward-walking hindleg was in contact with the substrate, it extended and retracted (moved backwards) to propel the animal forwards (power stroke/stance phase). At the end of this phase, it was lifted up, and flexed and protracted in the air (carried forwards) before being placed again on the ground to restart the step cycle (return stroke/swing phase). A backward-walking hindleg, on the other hand (Movie M8), flexed and protracted (moved forwards) on contact with substrate, and extended and retracted (moved backwards) in the air during its return stroke. We also observed that backward translation was initiated by hindleg movements. Headless flies with activated MDNs walked slower in this tethered preparation but were still coordinated, and showed identical sequence of joint movements in individual legs as intact flies with activated MDNs (Movie M9).

Are JCNs transiently recruited by MDNs during the swing phase of backward locomotion? As a first step to address this, we asked if JCN- and MDN-triggered hindleg extensions looked similar in a fly in absence of ground contact (Note that this manipulation also eliminated 'load', or the force exerted by the weight of the body on the fly's legs during stance phase). We eliminated ground contact by tethering headless flies and holding them suspended in the air. As in JCN activation in supine decapitated flies, activation of JCN in tethered decapitated flies likewise resulted in hindleg extension (Movie M11). Remarkably, in the absence of ground-contact, headless flies with MDNs activated also extended and moved their hindlegs backwards in the air (Movie M10). Qualitatively, the initiations of hindleg extensions in flies with activated MDNs appeared similar to those triggered upon JCN-activation. Nonetheless, some small differences could be seen: specifically, the extensions in MDNs persisted through most of the stimulation window, while those resulting from JCN activation were more transient (compare Movie M10 and Movie M11).

We also noted that the hindleg extensions in headless moonwalkers were accompanied with rhythmic depressions and low-amplitude flexions – the hindleg appeared as if it was searching for a substrate (Movie M10). These searching movements were not present upon JCN activation. We interpret that these depression and flexions are used to reestablish ground contact at the end of swing phase, a step that might be independent of JCN activity. More directly, upon MDN activation in suspended flies, the mechanosensors in the tarsi could

never signal ground contact and load sensors in the leg still signaled an ‘unloaded’ leg, causing the leg to be stuck in an endless loop of rhythmic extensions, depressions and lower-amplitude flexions. Presumably other neurons – separate from JCNs – allow this rhythmic cycle to be maintained independent of ground contact.

3.5 Discussion

GAL4 and follow-up split-GAL4 neuronal silencing screens

Unbiased neuronal silencing and activating screens have proved to be remarkably powerful in identifying specific neurons involved in Drosophila melanogaster behavior. These screens rely on large collections of randomly generated enhancer elements that allow reproducible genetically-controlled expression in subsets of neurons. Using a strategy derived from these large collections of genetic elements [36,37,34] we identified neurons that are involved in backward locomotion.

Previously described unbiased neuronal silencing or activation screens [24,40–45] have mainly used GAL4 lines to target and manipulate random populations of neurons in the nervous system. In most instances the hits from such GAL4 screens are broadly expressed and require further experiments to narrow down the neurons linked to the behavior from unlinked neurons. The usual follow-up approach has been to either 1) stochastically label and manipulate subsets of cells from the original GAL4 expression patterns, correlating the presence of a neuron with a behavior; 2) or to identify shared cells among the expression patterns of numerous hits which give a common behavior. In the second category, the split-GAL4 intersectional strategy has proved to be a useful technique to narrow down to a causative neuron that can be linked to the behavior being studied [24,41,42].

We conducted a two-stage behavioral screen: first, a GAL4 neuronal silencing screen to narrow our list of potential GAL4 drivers; and second, a split-GAL4 screen, using the shortened list of GAL4 drivers from our first stage, to narrow down on specific neurons. In the first stage, we obtained an initial pool of candidates with strong backward walking defects. In the second stage we generated split-GAL4 derivatives from our primary GAL4 hits. The split-GAL4 screen allowed us to bypass the labor intensive steps of either manually searching for shared neurons among the expression patterns of our hits or using stochastic labeling techniques to parse the relevant cells. The split-GAL4 screen identified multiple neurons spanning different areas of the fly central nervous system. Interestingly, a large number of our hits identified neurons located in the VNC. These results suggest a large, and

previously unappreciated, number of premotor circuits in the VNC that may be unique for the execution of backward locomotion.

Models for the premotor switch during backward locomotion

What is the nature of the premotor switch in the VNC that triggers a complete reversal of walking direction in all six legs when MDNs are active? There are 4 MDN cells, 2 on each hemisphere, with axonal projections that extend to the contralateral side of the VNC to all 3 leg neuropils [24]. MDNs are the command neurons that initiate, and likely maintain, backward locomotion. One can imagine two broad scenarios for the neurons in the VNC downstream of MDNs: either 1) MDNs act on CPGs that are specific for backward locomotion or 2) MDNs act on local VNC circuits, which in turn reverse the timing of CPGs that are common to forward and backward locomotion. While we have no definitive proof for which of these models is correct, we can speculate on their likelihood, both from the evidence from other organisms and our silencing screen results.

It has been suggested that in humans the neuronal networks involved in motor pattern generation during forward and backward walking are largely non-overlapping and independently adaptable [28] (challenging a previous study [30] that argued a common locomotor CPG in humans). On the other hand, in stick insects the switch from forward to backward walking can be explained by a state dependent switch in the effect of sensory feedback on the timing and sequence of the motor rhythms generated by a common locomotor CPG [17,46]. A neuromechanical model in stick insects [46] has suggested that a layer of premotor interneurons between locomotor CPGs and motor neurons may play an instrumental role in maintaining directional walking. These interneurons would need to simultaneously receive inputs from 1) forward/backward state-specific circuit components 2) and CPG elements, such that, based on whether the forward or backward specific neurons are active, they can exchange the functional connections of the CPGs to different motorneurons. Alternatively, parallel pathways processing sensory information can be selectively inhibited or enhanced depending on walking direction [47]. Further evidence for CPGs that are shared between forward and backward locomotion comes from lamprey. Specifically, the direction of the rostrocaudal undulatory wave that underlies forward swimming can be reversed to a caudorostral wave during backward swimming by increasing the relative excitability of the spinal circuits in the caudal segments of spinal lampreys [9–12]. These observations are consistent with a common CPG for forward and backward locomotion in both stick insects and lamprey.

Functional evidence to distinguish between common and distinct CPGs would provide important insights on the neuronal control of walking direction. Our data do not conclusively demonstrate which of the two models is correct. Indeed, neither previously published work nor our screen have unambiguously defined locomotor CPGs in Drosophila. However, as the function of the neurons identified in our screen starts to be uncovered, we can use the two models to inform us as to where to look for additional circuit components. As a hypothetical example, if specialized CPGs exist for backward locomotion, these neurons would be found in the groups from hierarchical clustering analysis with a specific decrement in backward locomotion (for example cluster 1 and subsets of cluster 3). CPG elements can often be identified due to their ability to generate rhythmic activity upon tonic activation. We predict that we can readily initiate such CPGs by activating MDNs in a dissected nervous system 'in a dish', which is free of any sensory feedback. Once identified, we can refer back to our clustering analysis to search for additional CPG components. In the hypothetical example above, the CPGs would be found to cluster with other hits with a specific decrease in backward locomotion. By contrast, if forward and backward locomotion share common CPGs, silencing components of these CPGs would result in general locomotion defects. Our hits include neurons that affect general locomotion (for example cluster 2 and subset of cluster 3). Hence, the identification of a candidate CPG in cluster 2 would lead to a directed search for additional CPG components sharing the characteristic of a general locomotion deficit. In this second hypothetical example, the hits that showed specific backward locomotion might represent higher-order neurons that initiate and maintain a switch in the processing of sensory feedback in the VNC. In this case, we predict that activation of these higher-order VNC neurons would recapitulate aspects of limb movements observed during backward locomotion, due to an artificial reversal of thoracic reflexes.

Distinct limb movements during backward locomotion?

In order to determine whether common or distinct CPGs underlie Drosophila locomotion we must also ask the question of whether backward locomotion includes distinct limb movements not observed during forward locomotion. While the timing of joint movements in individual legs appears to be essentially reversed, we observed additional differences in hindleg movements between forward and backward walking. Hindlegs are observed to extend during the swing phase of backward locomotion targeting the tarsae to the ground to restart the next step cycle. During forward locomotion, hindleg extensions are instead observed during the stance phase, but are noted to be much less elaborate (at least qualitatively). This

raises the possibility that backward walking may require additional neurons that are dispensable for forward walking. Our screen has uncovered a set of neurons that fit this description. Our detailed behavioral analysis with JCNs show that activation of JCNs specifically triggers hind leg extensions, while silencing its activity results in a specific impairment in backward locomotion. Optogenetic activation of MDNs in the absence of ground contact (i.e, in suspended flies) also triggers hindleg extensions, albeit interspersed with lower amplitude flexions, depressions and levations. Based on these observations, we infer that JCNs control the unique joint movements that are required during the swing phase of a backward-stepping hindleg. Given the similarity between JCN-triggered and MDN-triggered limb extensions upon optogenetic activation in suspended flies, we hypothesize that JCNs could be transiently recruited by MDNs during the swing phase of backward locomotion in the hindlegs. We predict that silencing JCN activity in a backward walking fly or a fly where MDNs are activated would impair the swing phase of a backward-stepping hindleg. Given that backward walking is initiated by hindleg movements, an inability to execute the swing phase in the hindlegs would impair initiation of backward locomotion in flies. Further behavioral and functional studies are required to test these hypotheses and determine the role of JCNs in backward locomotion. Also, it remains to be determined whether the JCNs are at all recruited during the stance phase of forward locomotion where the hindlegs extend as well. We did not observe any obvious impairment in forward locomotion upon silencing JCN activity when the flies were allowed to walk forwards in the ring assay. This observation favors a hypothesis that the JCNs are indeed specific for the elaborate hindleg extensions necessary for the swing phase of backward locomotion, and that the relatively low-amplitude extensions of hindlegs during the stance phase of forward locomotion rely on separate or redundant circuit components. Hence it is possible that in *Drosophila* the pattern-generators used in forward and backward walking have partially non-overlapping neurons, or have additional connections to motor neurons that are selectively enhanced during backward locomotion to control the distinct limb movements observed in the latter. The VNC circuit downstream MDNs could exist in two (or more) states of stable network activity – corresponding to forward and backward walking states. MDNs might switch the bias of this bi-stable (or multi-stable) circuit to backward walking mode. The unique limb movements during backward locomotion could be an emerging property of the stable VNC network activity during this MDN-triggered backward walking mode.

Inter-leg coordination during backward locomotion

We identified several intersegmental neurons from our silencing screen that are specific for backward locomotion. These neurons could be important for coordinating the 6 legs during backward walking in Drosophila. The importance of proprioceptive feedback for inter-limb coordination in Drosophila is clearly seen in our experiments. Specifically, we observed a dramatic difference in leg movements during backward locomotion triggered in suspended versus non-suspended flies. Optogenetic activation of MDNs triggers coordinated backward locomotion in flies even when they are decapitated (Figure 7; Movies M5 and M9), but the coordination among legs is severely impaired (Figure 7; Movie M10) in the absence of ground contact (when load signals are presumably also absent). Based on the understanding of inter-leg coordination in stick insects [48,49], we postulate that intersegmental interneurons in the VNC might play a critical role in the inter-leg sensory feedback during backward locomotion. It has been shown in stick insects that during forward walking, sensory feedback from an intact forward-stepping foreleg entrains the activity of the CPGs in mid- and hindlegs [49]. A backward-stepping hindleg, similarly, can entrain the activity of CPGs on the other legs in backward walking mode by intersegmental coordination signals. Hits identified in our silencing screen could provide such signals, and a careful analysis of gait upon silencing these interneurons in a backward walking fly would give us important insights on their specific roles in coordinating backward locomotion.

Concluding remarks

In future, a high-resolution analysis of joint movements in both backward and forward walking flies would shed some light on the similarities and differences in leg kinematics during the two modes of locomotion and their underlying neuronal basis. Careful phenotypic analysis of limb movements in flies where our VNC hits are silenced will shed light on their contribution to limb movements during backward locomotion. In addition, silencing the same VNC neurons during forward locomotion will serve to identify common and unique attributes of our hits with regards to limb movement. Since flies seldom walk backwards, understanding the contributions of our VNC hits to backward locomotion will likely involve neuronal epistasis experiments where MDNs are used to trigger backward locomotion. Together, these experiments will determine if hits like the JCNs are common or whether neurons with unique features in controlling backward locomotion are rare.

While specific models for the execution of backward locomotion in the VNC will have to await further characterization of the underlying circuits, our screen has given us a vital first

step: an extensive list of candidate neurons. Importantly, these neurons show a wealth of different behaviors when silenced. This observation tells us that we are likely to have covered many different circuit components of the VNC – from putative CPG components to somatosensory feedback neurons. Additionally, our detailed clustering analysis can guide us towards hits that may contain common circuit components between forward and backward locomotion. Further, the existing models for CPGs and their control will guide our search for specific circuit elements within the larger circuits for directed locomotion.

3.6 Author contributions

RS and BJD conceived the project and designed the experiments. RS conducted the split-GAL4 silencing screen and the behavioral experiments, and analyzed all data. MD and TB engineered the rig for ball assay. TB contributed to data acquired from the ball assay. SB supervised and led the primary GAL4 silencing screen. AB and BJD supervised the project. RS wrote the manuscript.

3.7 Acknowledgements

We thank Kai Feng for valuable discussions, Hideo Otsuna and Ryo Minegishi for the registration of the confocal stacks of stained fly nervous systems to a common template, and the Project Technical Resources and Instrument Design and Fabrication teams in Janelia Research Campus for technical assistance. This work was supported by Boehringer Ingelheim GmbH and the Howard Hughes Medical Institute.

3.8 References

1. Brown, T.G. (1911). The intrinsic factors in the act of progression in the mammal. Proc. R. Soc. Lond. B Biol. Sci. 84, 308–319.

2. Büschges, A., Schmitz, J., and Bässler, U. (1995). Rhythmic patterns in the thoracic nerve cord of the stick insect induced by pilocarpine. J. Exp. Biol. *198*, 435–456.

3. Chrachri, A., and Clarac, F. (1987). Induction of rhythmic activity in motoneurons of crayfish thoracic ganglia by cholinergic agonists. Neurosci. Lett. *77*, 49–54.

4. Grillner, S. (2006). Biological pattern generation: the cellular and computational logic of networks in motion. Neuron *52*, 751–766.

5. Kiehn, O. (2006). Locomotor circuits in the mammalian spinal cord. Annu. Rev. Neurosci. *29*, 279–306.

6. Pearson, K.G. (1972). Central programming and reflex control of walking in the cockroach. J. Exp. Biol. *56*, 173–193.

7. Chalfie, M., Sulston, J.E., White, J.G., Southgate, E., Thomson, J.N., and Brenner, S. (1985). The neural circuit for touch sensitivity in *Caenorhabditis elegans*. J. Neurosci. *5*, 956–964.

8. Wicks, S.R., Roehrig, C.J., and Rankin, C.H. (1996). A dynamic network simulation of the nematode tap withdrawal circuit: predictions concerning synaptic function using behavioral criteria. J. Neurosci. *16*, 4017–4031.

9. Islam, S.S., Zelenin, P.V., Orlovsky, G.N., Grillner, S., and Deliagina, T.G. (2006). Pattern of motor coordination underlying backward swimming in the lamprey. J. Neurophysiol. *96*, 451–460.

10. Kotaleski, J.H., Grillner, S., and Lansner, A. (1999). Neural mechanisms potentially contributing to the intersegmental phase lag in lamprey. Biol. Cybern. *81*, 317–330.

11. Matsushima, T., and Grillner, S. (1992). Neural mechanisms of intersegmental coordination in lamprey: local excitability changes modify the phase coupling along the spinal cord. J. Neurophysiol. *67*, 373–388.

12. Wadden, T., Hellgren, J., Lansner, A., and Grillner, S. (1997). Intersegmental coordination in the lamprey: simulations using a network model without segmental boundaries. Biol. Cybern. *76*, 1–9.

13. Grillner, S. (1974). On the generation of locomotion in the spinal dogfish. Exp. Brain Res. *20*, 459–470.

14. Ayers, J.L., and Davis, W.J. (1977). Neuronal control of locomotion in the lobster, Homarus americanus. J. Comp. Physiol. *115*, 1–27.

15. Chasserat, C., and Clarac, F. (1980). Interlimb coordinating factors during driven walking in Crustacea. J. Comp. Physiol. *139*, 293–306.

16. Bowerman, R.F. (1981). Arachnid Locomotion. In Locomotion and Energetics in Arthropods (Springer, Boston, MA), pp. 73–102.

17. Akay, T., Ludwar, B.C., Göritz, M.L., Schmitz, J., and Büschges, A. (2007). Segment specificity of load signal processing depends on walking direction in the stick insect leg muscle control system. J. Neurosci. *27*, 3285–3294.

18. Graham, D., and Epstein, S. (1985). Behaviour and motor output for an insect walking on a slippery surface: II. backward walking. J. Exp. Biol. *118*, 287–296.

19. Rosenbaum, P., Wosnitza, A., Büschges, A., and Gruhn, M. (2010). Activity patterns and timing of muscle activity in the Forward walking and backward walking stick insect Carausius morosus. J. Neurophysiol. *104*, 1681–1695.

20. Ardin, P.B., Mangan, M., and Webb, B. (2016). Ant homing ability is not diminished when traveling backwards. Front. Behav. Neurosci. *10*.

21. Pfeffer, S.E., Wahl, V.L., and Wittlinger, M. (2016). How to find home backwards? Locomotion and inter-leg coordination during rearward walking of Cataglyphis fortis desert ants. J. Exp. Biol. *219*, 2110–2118.

22. Pfeffer, S.E., and Wittlinger, M. (2016). How to find home backwards? Navigation during rearward homing of Cataglyphis fortis desert ants. J. Exp. Biol. *219*, 2119–2126.

23. Schwarz, S., Mangan, M., Zeil, J., Webb, B., and Wystrach, A. (2017). How ants use vision when homing backward. Curr. Biol. *27*, 401–407.

24. Bidaye, S.S., Machacek, C., Wu, Y., and Dickson, B.J. (2014). Neuronal control of *Drosophila* walking direction. Science *344*, 97–101.

25. Parigi, A., Porter, C., Cermak, M., Pitchers, W.R., and Dworkin, I. (2014). How predator hunting-modes affect prey behaviour: capture deterrence in *Drosophila* melanogaster. bioRxiv, 10330. doi: https://doi.org/10.1101/010330.

26. Sen, R., Wu, M., Branson, K., Robie, A., Rubin, G.M., and Dickson, B.J. (2017). Moonwalker descending neurons mediate visually evoked retreat in *Drosophila*. Curr. Biol. *27*, 766–771.

27. Wu, M., Nern, A., Williamson, W.R., Morimoto, M.M., Reiser, M.B., Card, G.M., and Rubin, G.M. (2016). Visual projection neurons in the *Drosophila* lobula link feature detection to distinct behavioral programs. eLife *5*, e21022.

28. Choi, J.T., and Bastian, A.J. (2007). Adaptation reveals independent control networks for human walking. Nat. Neurosci. *10*, 1055–1062.

29. Grasso, R., Bianchi, L., and Lacquaniti, F. (1998). Motor patterns for human gait: abckward versus forward Locomotion. J. Neurophysiol. *80*, 1868–1885.

30. Lamb, T., and Yang, J.F. (2000). Could different directions of infant stepping be controlled by the same locomotor central pattern generator? J. Neurophysiol. *83*, 2814–2824.

31. Mu, L., and Ritzmann, R.E. (2008). Interaction between descending input and thoracic reflexes for joint coordination in cockroach: I. descending influence on thoracic sensory reflexes. J. Comp. Physiol. A *194*, 283–298.

32. Mu, L., and Ritzmann, R.E. (2008). Interaction between descending input and thoracic reflexes for joint coordination in cockroach. II. comparative studies on tethered turning and searching. J. Comp. Physiol. A *194*, 299–312.

33. Berendes, V., Zill, S.N., Büschges, A., and Bockemühl, T. (2016). Speed-dependent interplay between local pattern-generating activity and sensory signals during walking in *Drosophila.* J. Exp. Biol. *219*, 3781–3793.

34. Tirian, L., and Dickson, B. (2017). The VT GAL4, LexA, and split-GAL4 driver line collections for targeted expression in the *Drosophila* nervous system. bioRxiv, 198648. https://www.biorxiv.org/content/early/2017/10/05/198648

35. Sweeney, S.T., Broadie, K., Keane, J., Niemann, H., and O'Kane, C.J. (1995). Targeted expression of tetanus toxin light chain in *Drosophila* specifically eliminates synaptic transmission and causes behavioral defects. Neuron *14*, 341–351.

36. Luan, H., Peabody, N.C., Vinson, C.R., and White, B.H. (2006). Refined spatial manipulation of neuronal function by combinatorial restriction of transgene expression. Neuron *52*, 425–436.

37. Pfeiffer, B.D., Ngo, T.-T.B., Hibbard, K.L., Murphy, C., Jenett, A., Truman, J.W., and Rubin, G.M. (2010). Refinement of tools for targeted gene expression in *Drosophila*. Genetics *186*, 735–755.

38. Klapoetke, N.C., Murata, Y., Kim, S.S., Pulver, S.R., Birdsey-Benson, A., Cho, Y.K., Morimoto, T.K., Chuong, A.S., Carpenter, E.J., Tian, Z., *et al.* (2014). Independent optical excitation of distinct neural populations. Nat. Methods *11*, 338–346.

39. Zhang, Y.Q., Rodesch, C.K., and Broadie, K. (2002). Living synaptic vesicle marker: synaptotagmin-GFP. Genesis *34*, 142–145.

40. Robie, A.A., Hirokawa, J., Edwards, A.W., Umayam, L.A., Lee, A., Phillips, M.L., Card, G.M., Korff, W., Rubin, G.M., Simpson, J.H., et al. Mapping the neural substrates of behavior. Cell *170*, 393–406.e28.

41. Feng, K., Palfreyman, M.T., Häsemeyer, M., Talsma, A., and Dickson, B.J. (2014). Ascending SAG neurons control sexual receptivity of Drosophila females. Neuron *83*, 135–148.

42. Hampel, S., Franconville, R., Simpson, J.H., and Seeds, A.M. (2015). A neural command circuit for grooming movement control. eLife *4*, e08758.

43. Häsemeyer, M., Yapici, N., Heberlein, U., and Dickson, B.J. (2009). Sensory neurons in the *Drosophila* genital tract regulate female reproductive behavior. Neuron 6*1*, 511–518.

44. von Philipsborn, A.C., Liu, T., Yu, J.Y., Masser, C., Bidaye, S.S., and Dickson, B.J. (2011). Neuronal control of *Drosophila* courtship song. Neuron *69*, 509–522.

45. Yapici, N., Cohn, R., Schusterreiter, C., Ruta, V., and Vosshall, L.B. (2016). A taste circuit that regulates ingestion by integrating food and hunger Signals. Cell *165*, 715–729.

46. Toth, T.I., Knops, S., and Daun-Gruhn, S. (2012). A neuromechanical model explaining forward and backward stepping in the stick insect. J. Neurophysiol. *107*, 3267–3280.

47. Zill, S., Schmitz, J., and Büschges, A. (2004). Load sensing and control of posture and locomotion. Arthropod Struct. Dev. *33*, 273–286.

48. Daun-Gruhn, S. (2011). A mathematical modeling study of inter-segmental coordination during stick insect walking. J. Comput. Neurosci. *30*, 255–278.

49. Borgmann, A., Hooper, S.L., and Büschges, A. (2009). Sensory feedback induced by front-leg stepping entrains the activity of central pattern generators in caudal segments of the stick insect walking system. J. Neurosci. *29*, 2972–2983.

3.9 Supplemental Materials

3.9.1 Supplemental Figures and Tables

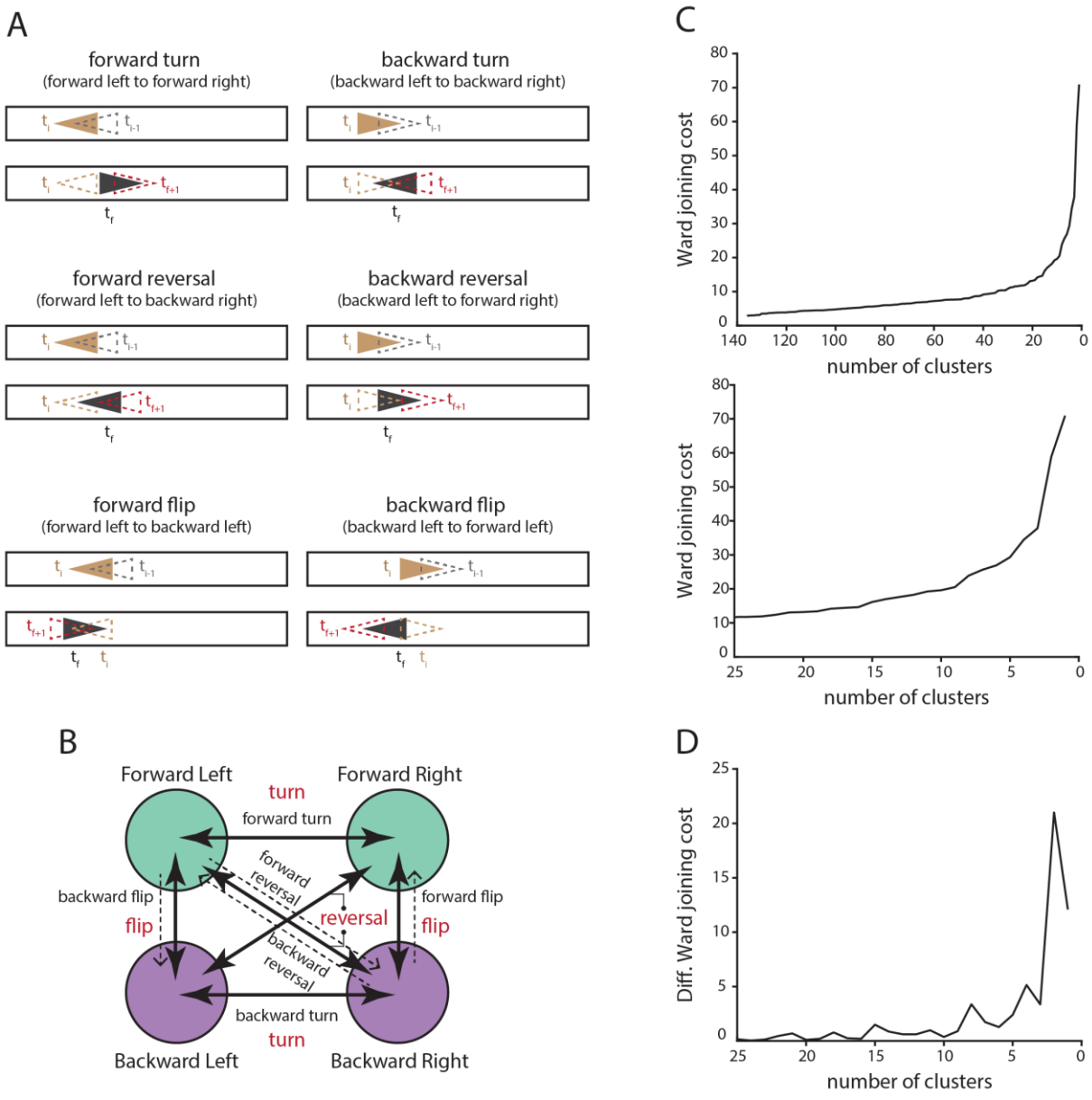

Figure S1. Hierarchical agglomerative clustering identifies distinct categories of backward walking defects. Related to Figures 2, S2, S3 and S4.

(A) Schematic examples of three major transitions between walking modes in the linear assay. Top: Example of forward and backward turns. Middle: Example of forward and backward reversals. Bottom: Example of forward and backward flips.

(B) Schematic explaining all possible ways transitions can occur between walking modes in the linear assay.

(C) Top: Ward's joining cost for agglomerative hierarchical clustering versus number of clusters. Bottom: A zoom-in of the plot above, in the interesting range of 1 - 25 clusters where Ward's linkage cost increases significantly.

(D) Differential of Ward's joining caost in the interesting range of number of clusters. Joining cost rises significantly if the dataset is grouped into less than 3 clusters. Also note that local minima exist at 6 and 10 clusters.

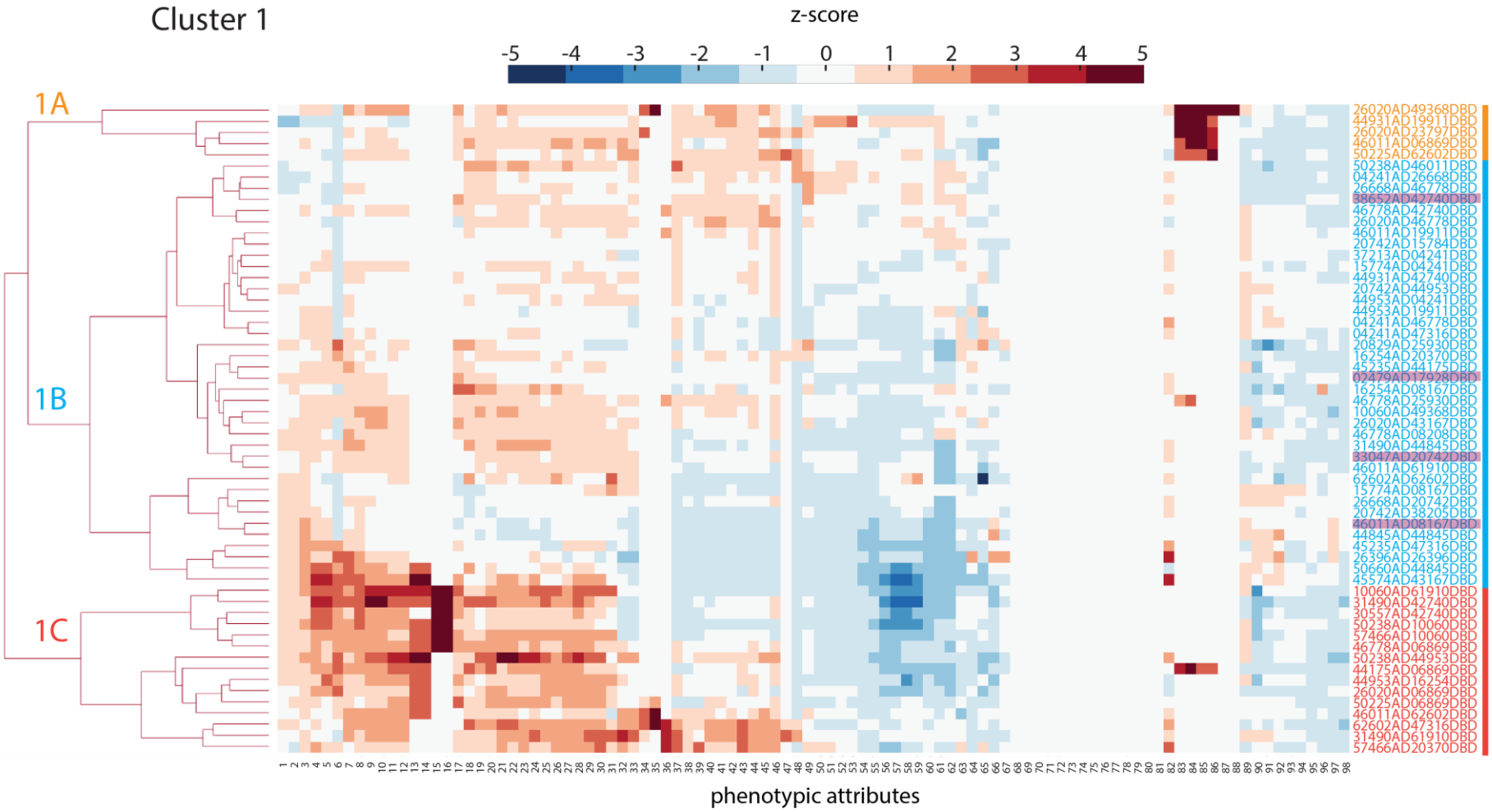

Figure S2. An enlarged view of Cluster 1 from agglomerative hierarchical clustering. Related to Figures 2 and 3.
Cluster 1 further separated into 3 sub-clusters using a threshold of linkage cost to obtain 6 clusters from the entire 137 X 98 phenotype matrix. Clustered data is shown as a heatmap where values range from -5 z-score (pure blue) to +5 z-score (pure red). Colors and numbers on the dendogram demarcate neighboring sub-clusters. Highlighted split-combinations correspond to lines marked in red in Figure 3. 1-98 phenotypic attributes are in same order as in Figure 2. See also Table S1.

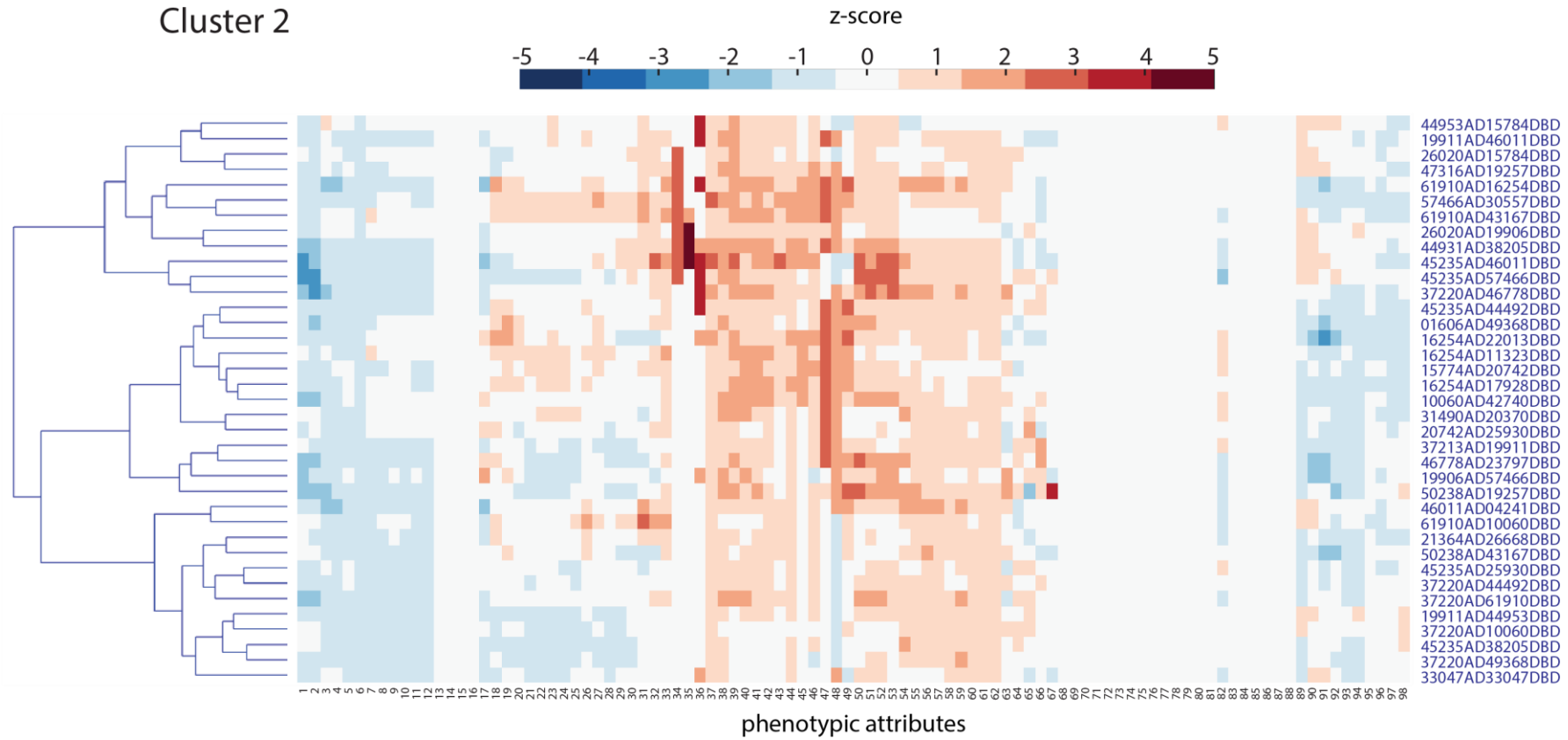

Figure S3. An enlarged view of Cluster 2 from agglomerative hierarchical clustering. Related to Figure 2.
Clustered data is shown as a heatmap where values range from -5 z-score (pure blue) to +5 z-score (pure red). 1-98 phenotypic attributes are in same order as in Figure 2. See also Table S1.

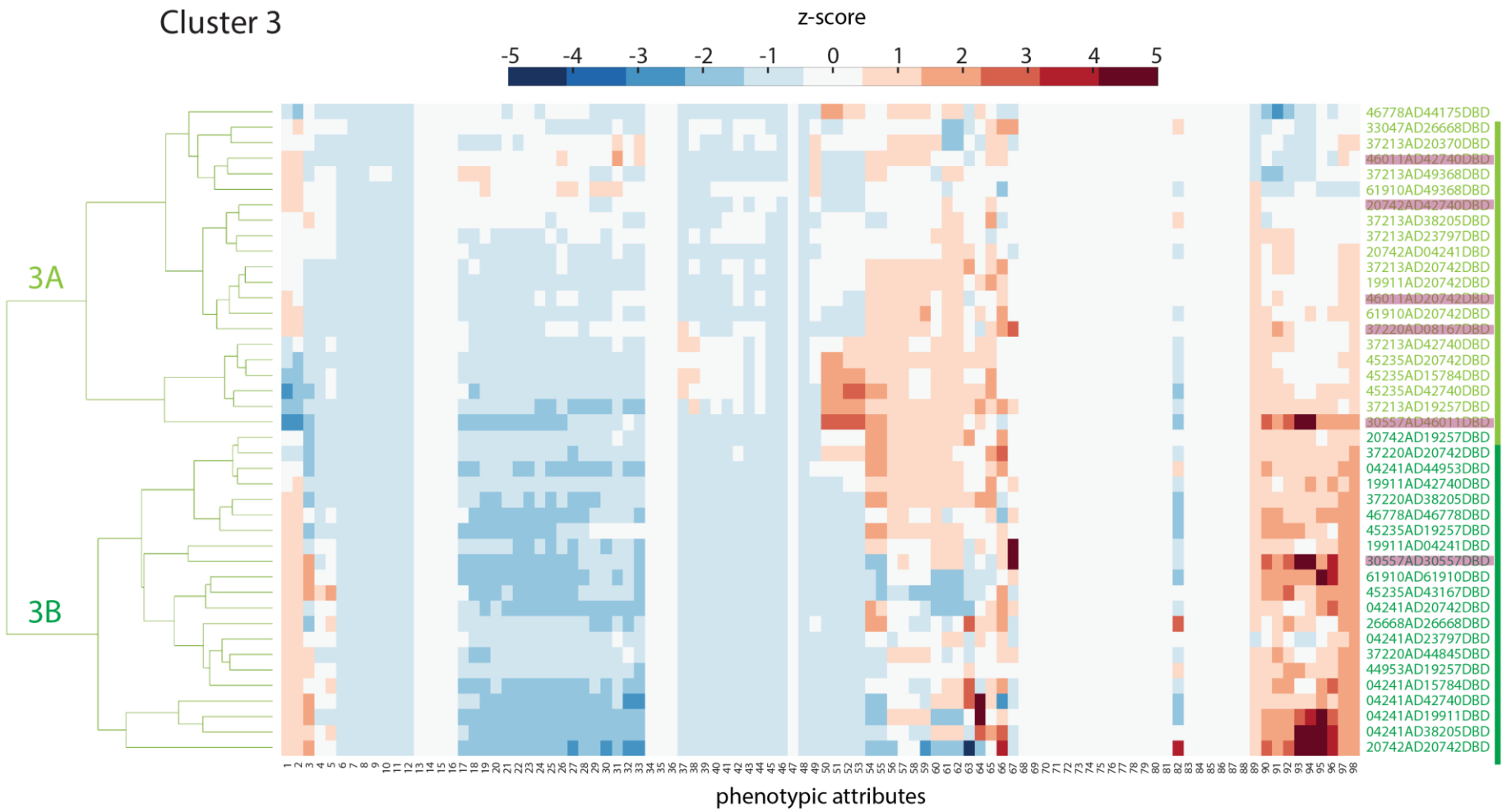

Figure S4. An enlarged view of Cluster 3 from agglomerative hierarchical clustering. Related to Figures 2 and 5.
Cluster 3 further separated into 2 sub-clusters using a threshold of linkage cost to obtain 6 clusters from the entire 137 X 98 phenotype matrix. Clustered data is shown as a heatmap where values range from -5 z-score (pure blue) to +5 z-score (pure red). Colors and numbers on the dendogram demarcate neighboring sub-clusters. Highlighted split-combinations correspond to lines marked in red in Figure 5. 1-98 phenotypic attributes are in same order as in Figure 2. See also Table S1.

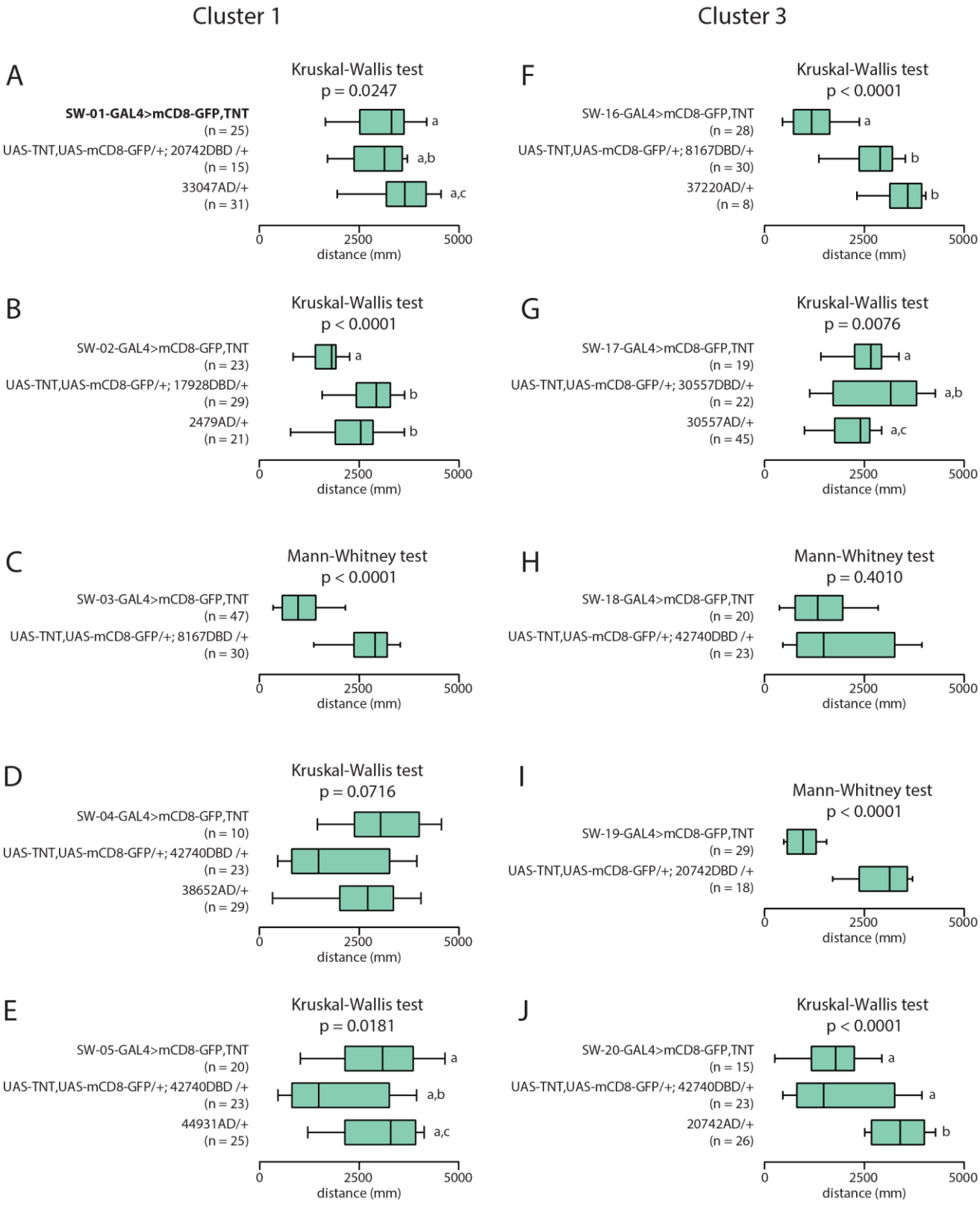

Figures S5. Quantification of forward locomotion of representative SillyWalkers in ring assay. Related to Figures 2, 3 and 5.

Total walking distance of representative SillyWalkers from Cluster 1 (A-E) and Cluster 3 (F-J) in a 10-min assay in ring chambers. Sample numbers (n), tests used to assess statistical significance and corresponding p values are indicated. See also Table S1.

Table S1. List of Genotypes

Figure	Genotype	Driver(s)/Cluster #
Figure 1C	w-; UAS-TNT-E, UAS-mCD8-GFP (VIE-19a)/X-p65ADZp (attP40); Y-ZpGAL4DBD (attP2)/+	X-p65ADZp ∩ Y-ZpGAL4DBD 1741 split-combinations
	w-; UAS-TNT-E, UAS-mCD8-GFP (VIE-19a)/37220-p65ADZp (attP40); 44845-ZpGAL4DBD (attP2)/+	Positive control 1 or MDN-2 [1]
	w-; UAS-TNT-E, UAS-mCD8-GFP (VIE-19a)/44845-p65ADZp (attP40); 44845-ZpGAL4DBD (attP2)/+	Positive control 2
	w-; UAS-TNT-E, UAS-mCD8-GFP (VIE-19a)/50660-p65ADZp (attP40); 44845-ZpGAL4DBD (attP2)/+	Positive control 3 or MDN-3 [1]
	w-; UAS-TNT-E, UAS-mCD8-GFP (VIE-19a)/+; 61910-ZpGAL4DBD (attP2)/+	Negative control 4
	w-; UAS-TNT-E, UAS-mCD8-GFP (VIE-19a)/+; 46011-ZpGAL4DBD (attP2)/+	Negative control 5
	w-; UAS-TNT-E, UAS-mCD8-GFP (VIE-19a)/+; 44845-ZpGAL4DBD (attP2)/+	Negative control 6
	w-; UAS-TNT-E, UAS-mCD8-GFP (VIE-19a)/+; 10060-ZpGAL4DBD (attP2)/+	Negative control 7
	w-; UAS-TNT-E, UAS-mCD8-GFP (VIE-19a)/+; 44845-ZpGAL4DBD (attP2)/+	Negative control 8
	w-;57466-p65ADZp/+	Negative control 9
	w-;10060-p65ADZp/+	Negative control 10
	w-;44953-p65ADZp/+	Negative control 11
	w-;50238-p65ADZp/+	Negative control 12
	w-;61910-p65ADZp/+	Negative control 13
Figure 2	Refer to Figure S2 for Cluster 1, Figure S3 for Cluster 2, and Figure S4 for Cluster 3	Clusters 1-3
Figure 3	w-; UAS-TNT-E, UAS-mCD8-GFP (VIE-19a)/33047-p65ADZp (attP40); 20742-ZpGAL4DBD (attP2)/+	SW-01-GAL4
	w-; UAS-TNT-E, UAS-mCD8-GFP (VIE-19a)/02479-p65ADZp (attP40); 17928-ZpGAL4DBD (attP2)/+	SW-02-GAL4
	w-; UAS-TNT-E, UAS-mCD8-GFP (VIE-19a)/46011-p65ADZp (attP40); 08167-ZpGAL4DBD (attP2)/+	SW-03-GAL4
	w-; UAS-TNT-E, UAS-mCD8-GFP (VIE-19a)/38652-p65ADZp (attP40); 42740-ZpGAL4DBD (attP2)/+	SW-04-GAL4
	w-; UAS-TNT-E, UAS-mCD8-GFP (VIE-19a)/44931-p65ADZp (attP40); 42740-ZpGAL4DBD (attP2)/+	SW-05-GAL4
Figure 3	w-; UAS-TNT-E, UAS-mCD8-GFP (VIE-19a)/46778-p65ADZp (attP40); 42740-ZpGAL4DBD (attP2)/+	SW-06-GAL4
	w-; UAS-TNT-E, UAS-mCD8-GFP (VIE-19a)/46778-p65ADZp (attP40); 06869-ZpGAL4DBD (attP2)/+	SW-07-GAL4
	w-; UAS-TNT-E, UAS-mCD8-GFP (VIE-19a)/44175-p65ADZp (attP40); 06869-ZpGAL4DBD (attP2)/+	SW-08-GAL4

	w-; UAS-TNT-E, UAS-mCD8-GFP (VIE-19a)/50238-p65ADZp (attP40); 46011-ZpGAL4DBD (attP2)/+	SW-09-GAL4
Figure 4	w-; UAS-TNT-E, UAS-mCD8-GFP (VIE-19a)/16254-p65ADZp (attP40); 17928-ZpGAL4DBD (attP2)/+	SW-10-GAL4
	w-; UAS-TNT-E, UAS-mCD8-GFP (VIE-19a)/37220-p65ADZp (attP40);46778-ZpGAL4DBD (attP2)/+	SW-11-GAL4
	w-; UAS-TNT-E, UAS-mCD8-GFP (VIE-19a)/21364-p65ADZp (attP40); 26668-ZpGAL4DBD (attP2)/+	SW-12-GAL4
	w-; UAS-TNT-E, UAS-mCD8-GFP (VIE-19a)/45235-p65ADZp (attP40); 38205-ZpGAL4DBD (attP2)/+	SW-13-GAL4
	w-; UAS-TNT-E, UAS-mCD8-GFP (VIE-19a)/37220-p65ADZp (attP40); 49368-ZpGAL4DBD (attP2)/+	SW-14-GAL4
	w-; UAS-TNT-E, UAS-mCD8-GFP (VIE-19a)/37220-p65ADZp (attP40); 10060-ZpGAL4DBD (attP2)/+	SW-15-GAL4
Figure 5	w-; UAS-TNT-E, UAS-mCD8-GFP (VIE-19a)/30557-p65ADZp (attP40); 46011-ZpGAL4DBD (attP2)/+	JCN-GAL4
	w-; UAS-TNT-E, UAS-mCD8-GFP (VIE-19a)/37220-p65ADZp (attP40); 08167-ZpGAL4DBD (attP2)/+	SW-16-GAL4
	w-; UAS-TNT-E, UAS-mCD8-GFP (VIE-19a)/30557-p65ADZp (attP40); 30557-ZpGAL4DBD (attP2)/+	SW-17-GAL4
	w-; UAS-TNT-E, UAS-mCD8-GFP (VIE-19a)/46011-p65ADZp (attP40); 42740-ZpGAL4DBD (attP2)/+	SW-18-GAL4
	w-; UAS-TNT-E, UAS-mCD8-GFP (VIE-19a)/46011-p65ADZp (attP40); 20742-ZpGAL4DBD (attP2)/+	SW-19-GAL4
	w-; UAS-TNT-E, UAS-mCD8-GFP (VIE-19a)/20742-p65ADZp (attP40); 42740-ZpGAL4DBD (attP2)/+	SW-20-GAL4
	w-; UAS-TNT-E, UAS-mCD8-GFP (VIE-19a)/45235-p65ADZp (attP40); 20742-ZpGAL4DBD (attP2)/+	SW-21-GAL4
	w-; UAS-TNT-E, UAS-mCD8-GFP (VIE-19a)/37213-p65ADZp (attP40); 19257-ZpGAL4DBD (attP2)/+	SW-22-GAL4
	w-; UAS-TNT-E, UAS-mCD8-GFP (VIE-19a)/61910-p65ADZp (attP40); 49368-ZpGAL4DBD (attP2)/+	SW-23-GAL4
	w-; UAS-TNT-E, UAS-mCD8-GFP (VIE-19a)/19911-p65ADZp (attP40); 20742-ZpGAL4DBD (attP2)/+	SW-24-GAL4
	w-; UAS-TNT-E, UAS-mCD8-GFP (VIE-19a)/37213-p65ADZp (attP40); 42740-ZpGAL4DBD (attP2)/+	SW-25-GAL4
Figure 5	w-; UAS-TNT-E, UAS-mCD8-GFP (VIE-19a)/45235-p65ADZp (attP40); 19257-ZpGAL4DBD (attP2)/+	SW-26-GAL4
Figure 6A	w-; UAS-TNT-E, UAS-mCD8-GFP (VIE-19a)/30557-p65ADZp (attP40); 46011-ZpGAL4DBD (attP2)/+	JCN-GAL4
Figure 6B	UAS-syt-GFP/30557-p65ADZp (attP40); pJFRC22-10XUAS-IVS-myr::tdTomato (attP2)/ 46011-ZpGAL4DBD (attP2)	JCN-GAL4
Figure 7A-B	w-; 30557-p65ADZp/+	Control-1
	w-; UAS-TNT-E, UAS-mCD8-GFP (VIE-19a)/+; 46011-ZpGAL4DBD (attP2)/+	Control-2

	w-; UAS-TNT-E, UAS-mCD8-GFP (VIE-19a)/30557-p65ADZp (attP40); 46011-ZpGAL4DBD (attP2)/+	JCN-GAL4
	w-; UAS-TNT-E, UAS-mCD8-GFP (VIE-19a)/50660-p65ADZp (attP40); 44845-ZpGAL4DBD (attP2)/+	MDN-3-GAL4
Figure 7C-D	20XUAS-CsChrimson-mVenus (attP18); 30557-p65ADZp (attP40)/+; 46011-ZpGAL4DBD (attP2)/+	JCN-GAL4
	20XUAS-CsChrimson-mVenus (attP18); 44845-ZpGAL4DBD (attP40)/+; 50660- p65ADZp (attP2)/+	MDN-1-GAL4
	20XUAS-CsChrimson-mVenus (attP18); +/+; pBDPGAL4/+	empty
Figure S2	w-; UAS-TNT-E, UAS-mCD8-GFP (VIE-19a)/26020-p65ADZp (attP40); 49368-ZpGAL4DBD (attP2)/+	Cluster 1A
	w-; UAS-TNT-E, UAS-mCD8-GFP (VIE-19a)/44931-p65ADZp (attP40); 19911-ZpGAL4DBD (attP2)/+	Cluster 1A
	w-; UAS-TNT-E, UAS-mCD8-GFP (VIE-19a)/26020-p65ADZp (attP40); 23797-ZpGAL4DBD (attP2)/+	Cluster 1A
	w-; UAS-TNT-E, UAS-mCD8-GFP (VIE-19a)/46011-p65ADZp (attP40); 06869-ZpGAL4DBD (attP2)/+	Cluster 1A
	w-; UAS-TNT-E, UAS-mCD8-GFP (VIE-19a)/50225-p65ADZp (attP40); 62602-ZpGAL4DBD (attP2)/+	Cluster 1A
	w-; UAS-TNT-E, UAS-mCD8-GFP (VIE-19a)/50238-p65ADZp (attP40); 46011-ZpGAL4DBD (attP2)/+	Cluster 1B
	w-; UAS-TNT-E, UAS-mCD8-GFP (VIE-19a)/04241-p65ADZp (attP40); 26668-ZpGAL4DBD (attP2)/+	Cluster 1B
	w-; UAS-TNT-E, UAS-mCD8-GFP (VIE-19a)/26668-p65ADZp (attP40); 46778-ZpGAL4DBD (attP2)/+	Cluster 1B
	w-; UAS-TNT-E, UAS-mCD8-GFP (VIE-19a)/38652-p65ADZp (attP40); 42740-ZpGAL4DBD (attP2)/+	Cluster 1B
	w-; UAS-TNT-E, UAS-mCD8-GFP (VIE-19a)/46778-p65ADZp (attP40); 42740-ZpGAL4DBD (attP2)/+	Cluster 1B
	w-; UAS-TNT-E, UAS-mCD8-GFP (VIE-19a)/26020-p65ADZp (attP40); 46778-ZpGAL4DBD (attP2)/+	Cluster 1B
Figure S2	w-; UAS-TNT-E, UAS-mCD8-GFP (VIE-19a)/46011-p65ADZp (attP40); 19911-ZpGAL4DBD (attP2)/+	Cluster 1B
	w-; UAS-TNT-E, UAS-mCD8-GFP (VIE-19a)/20742-p65ADZp (attP40); 15784-ZpGAL4DBD (attP2)/+	Cluster 1B
	w-; UAS-TNT-E, UAS-mCD8-GFP (VIE-19a)/37213-p65ADZp (attP40); 04241-ZpGAL4DBD (attP2)/+	Cluster 1B
	w-; UAS-TNT-E, UAS-mCD8-GFP (VIE-19a)/15774-p65ADZp (attP40); 04241-ZpGAL4DBD (attP2)/+	Cluster 1B
	w-; UAS-TNT-E, UAS-mCD8-GFP (VIE-19a)/44931-p65ADZp (attP40); 42740-ZpGAL4DBD (attP2)/+	Cluster 1B
	w-; UAS-TNT-E, UAS-mCD8-GFP (VIE-19a)/20742-p65ADZp (attP40); 44953-ZpGAL4DBD (attP2)/+	Cluster 1B
	w-; UAS-TNT-E, UAS-mCD8-GFP (VIE-19a)/44953-p65ADZp (attP40); 04241-ZpGAL4DBD (attP2)/+	Cluster 1B

	w-; UAS-TNT-E, UAS-mCD8-GFP (VIE-19a)/44953-p65ADZp (attP40); 19911-ZpGAL4DBD (attP2)/+	Cluster 1B
	w-; UAS-TNT-E, UAS-mCD8-GFP (VIE-19a)/04241-p65ADZp (attP40); 46778-ZpGAL4DBD (attP2)/+	Cluster 1B
	w-; UAS-TNT-E, UAS-mCD8-GFP (VIE-19a)/04241-p65ADZp (attP40); 47316-ZpGAL4DBD (attP2)/+	Cluster 1B
	w-; UAS-TNT-E, UAS-mCD8-GFP (VIE-19a)/20829-p65ADZp (attP40); 25930-ZpGAL4DBD (attP2)/+	Cluster 1B
	w-; UAS-TNT-E, UAS-mCD8-GFP (VIE-19a)/16254-p65ADZp (attP40); 20370-ZpGAL4DBD (attP2)/+	Cluster 1B
	w-; UAS-TNT-E, UAS-mCD8-GFP (VIE-19a)/45235-p65ADZp (attP40); 44175-ZpGAL4DBD (attP2)/+	Cluster 1B
	w-; UAS-TNT-E, UAS-mCD8-GFP (VIE-19a)/02479-p65ADZp (attP40); 17928-ZpGAL4DBD (attP2)/+	Cluster 1B
	w-; UAS-TNT-E, UAS-mCD8-GFP (VIE-19a)/16254-p65ADZp (attP40); 08167-ZpGAL4DBD (attP2)/+	Cluster 1B
	w-; UAS-TNT-E, UAS-mCD8-GFP (VIE-19a)/46778-p65ADZp (attP40); 25930-ZpGAL4DBD (attP2)/+	Cluster 1B
	w-; UAS-TNT-E, UAS-mCD8-GFP (VIE-19a)/10060-p65ADZp (attP40); 49368-ZpGAL4DBD (attP2)/+	Cluster 1B
	w-; UAS-TNT-E, UAS-mCD8-GFP (VIE-19a)/26020-p65ADZp (attP40); 43167-ZpGAL4DBD (attP2)/+	Cluster 1B
	w-; UAS-TNT-E, UAS-mCD8-GFP (VIE-19a)/46778-p65ADZp (attP40); 08208-ZpGAL4DBD (attP2)/+	Cluster 1B
	w-; UAS-TNT-E, UAS-mCD8-GFP (VIE-19a)/31490-p65ADZp (attP40); 44845-ZpGAL4DBD (attP2)/+	Cluster 1B
	w-; UAS-TNT-E, UAS-mCD8-GFP (VIE-19a)/33047-p65ADZp (attP40); 20742-ZpGAL4DBD (attP2)/+	Cluster 1B
Figure S2	w-; UAS-TNT-E, UAS-mCD8-GFP (VIE-19a)/46011-p65ADZp (attP40); 61910-ZpGAL4DBD (attP2)/+	Cluster 1B
	w-; UAS-TNT-E, UAS-mCD8-GFP (VIE-19a)/62602-p65ADZp (attP40); 62602-ZpGAL4DBD (attP2)/+	Cluster 1B
	w-; UAS-TNT-E, UAS-mCD8-GFP (VIE-19a)/15774-p65ADZp (attP40); 08167-ZpGAL4DBD (attP2)/+	Cluster 1B
	w-; UAS-TNT-E, UAS-mCD8-GFP (VIE-19a)/26668-p65ADZp (attP40); 20742-ZpGAL4DBD (attP2)/+	Cluster 1B
	w-; UAS-TNT-E, UAS-mCD8-GFP (VIE-19a)/20742-p65ADZp (attP40); 38205-ZpGAL4DBD (attP2)/+	Cluster 1B
	w-; UAS-TNT-E, UAS-mCD8-GFP (VIE-19a)/46011-p65ADZp (attP40); 08167-ZpGAL4DBD (attP2)/+	Cluster 1B
	w-; UAS-TNT-E, UAS-mCD8-GFP (VIE-19a)/44845-p65ADZp (attP40); 44845-ZpGAL4DBD (attP2)/+	Cluster 1B
	w-; UAS-TNT-E, UAS-mCD8-GFP (VIE-19a)/45235-p65ADZp (attP40); 47316-ZpGAL4DBD (attP2)/+	Cluster 1B

	w-; UAS-TNT-E, UAS-mCD8-GFP (VIE-19a)/26396-p65ADZp (attP40); 26396-ZpGAL4DBD (attP2)/+	Cluster 1B
	w-; UAS-TNT-E, UAS-mCD8-GFP (VIE-19a)/50660-p65ADZp (attP40); 44845-ZpGAL4DBD (attP2)/+	Cluster 1B
	w-; UAS-TNT-E, UAS-mCD8-GFP (VIE-19a)/45574-p65ADZp (attP40); 43167-ZpGAL4DBD (attP2)/+	Cluster 1B
	w-; UAS-TNT-E, UAS-mCD8-GFP (VIE-19a)/10060-p65ADZp (attP40); 61910-ZpGAL4DBD (attP2)/+	Cluster 1C
	w-; UAS-TNT-E, UAS-mCD8-GFP (VIE-19a)/31490-p65ADZp (attP40); 42740-ZpGAL4DBD (attP2)/+	Cluster 1C
	w-; UAS-TNT-E, UAS-mCD8-GFP (VIE-19a)/30557-p65ADZp (attP40); 42740-ZpGAL4DBD (attP2)/+	Cluster 1C
	w-; UAS-TNT-E, UAS-mCD8-GFP (VIE-19a)/50238-p65ADZp (attP40); 10060-ZpGAL4DBD (attP2)/+	Cluster 1C
	w-; UAS-TNT-E, UAS-mCD8-GFP (VIE-19a)/57466-p65ADZp (attP40); 10060-ZpGAL4DBD (attP2)/+	Cluster 1C
	w-; UAS-TNT-E, UAS-mCD8-GFP (VIE-19a)/46778-p65ADZp (attP40); 06869-ZpGAL4DBD (attP2)/+	Cluster 1C
	w-; UAS-TNT-E, UAS-mCD8-GFP (VIE-19a)/50238-p65ADZp (attP40); 44953-ZpGAL4DBD (attP2)/+	Cluster 1C
	w-; UAS-TNT-E, UAS-mCD8-GFP (VIE-19a)/44175-p65ADZp (attP40); 06869-ZpGAL4DBD (attP2)/+	Cluster 1C
	w-; UAS-TNT-E, UAS-mCD8-GFP (VIE-19a)/44953-p65ADZp (attP40); 16254-ZpGAL4DBD (attP2)/+	Cluster 1C
	w-; UAS-TNT-E, UAS-mCD8-GFP (VIE-19a)/26020-p65ADZp (attP40); 06869-ZpGAL4DBD (attP2)/+	Cluster 1C
Figure S2	w-; UAS-TNT-E, UAS-mCD8-GFP (VIE-19a)/50225-p65ADZp (attP40); 06869-ZpGAL4DBD (attP2)/+	Cluster 1C
	w-; UAS-TNT-E, UAS-mCD8-GFP (VIE-19a)/46011-p65ADZp (attP40); 62602-ZpGAL4DBD (attP2)/+	Cluster 1C
	w-; UAS-TNT-E, UAS-mCD8-GFP (VIE-19a)/62602-p65ADZp (attP40); 47316-ZpGAL4DBD (attP2)/+	Cluster 1C
	w-; UAS-TNT-E, UAS-mCD8-GFP (VIE-19a)/31490-p65ADZp (attP40); 61910-ZpGAL4DBD (attP2)/+	Cluster 1C
	w-; UAS-TNT-E, UAS-mCD8-GFP (VIE-19a)/57466-p65ADZp (attP40); 20370-ZpGAL4DBD (attP2)/+	Cluster 1C
Figure S3	w-; UAS-TNT-E, UAS-mCD8-GFP (VIE-19a)/44953-p65ADZp (attP40); 15784-ZpGAL4DBD (attP2)/+	Cluster 2
	w-; UAS-TNT-E, UAS-mCD8-GFP (VIE-19a)/19911-p65ADZp (attP40); 46011-ZpGAL4DBD (attP2)/+	Cluster 2
	w-; UAS-TNT-E, UAS-mCD8-GFP (VIE-19a)/26020-p65ADZp (attP40); 15784-ZpGAL4DBD (attP2)/+	Cluster 2
	w-; UAS-TNT-E, UAS-mCD8-GFP (VIE-19a)/47316-p65ADZp (attP40); 19257-ZpGAL4DBD (attP2)/+	Cluster 2

	w-; UAS-TNT-E, UAS-mCD8-GFP (VIE-19a)/61910-p65ADZp (attP40); 16254-ZpGAL4DBD (attP2)/+	Cluster 2
	w-; UAS-TNT-E, UAS-mCD8-GFP (VIE-19a)/57466-p65ADZp (attP40); 30557-ZpGAL4DBD (attP2)/+	Cluster 2
	w-; UAS-TNT-E, UAS-mCD8-GFP (VIE-19a)/61910-p65ADZp (attP40); 43167-ZpGAL4DBD (attP2)/+	Cluster 2
	w-; UAS-TNT-E, UAS-mCD8-GFP (VIE-19a)/26020-p65ADZp (attP40); 19906-ZpGAL4DBD (attP2)/+	Cluster 2
	w-; UAS-TNT-E, UAS-mCD8-GFP (VIE-19a)/44931-p65ADZp (attP40); 38205-ZpGAL4DBD (attP2)/+	Cluster 2
	w-; UAS-TNT-E, UAS-mCD8-GFP (VIE-19a)/45235-p65ADZp (attP40); 46011-ZpGAL4DBD (attP2)/+	Cluster 2
	w-; UAS-TNT-E, UAS-mCD8-GFP (VIE-19a)/45235-p65ADZp (attP40); 57466-ZpGAL4DBD (attP2)/+	Cluster 2
	w-; UAS-TNT-E, UAS-mCD8-GFP (VIE-19a)/37220-p65ADZp (attP40); 46778-ZpGAL4DBD (attP2)/+	Cluster 2
	w-; UAS-TNT-E, UAS-mCD8-GFP (VIE-19a)/45235-p65ADZp (attP40); 44492-ZpGAL4DBD (attP2)/+	Cluster 2
	w-; UAS-TNT-E, UAS-mCD8-GFP (VIE-19a)/01606-p65ADZp (attP40); 49368-ZpGAL4DBD (attP2)/+	Cluster 2
	w-; UAS-TNT-E, UAS-mCD8-GFP (VIE-19a)/16254-p65ADZp (attP40); 22013-ZpGAL4DBD (attP2)/+	Cluster 2
	w-; UAS-TNT-E, UAS-mCD8-GFP (VIE-19a)/16254-p65ADZp (attP40); 11323-ZpGAL4DBD (attP2)/+	Cluster 2
Figure S3	w-; UAS-TNT-E, UAS-mCD8-GFP (VIE-19a)/15774-p65ADZp (attP40); 20742-ZpGAL4DBD (attP2)/+	Cluster 2
	w-; UAS-TNT-E, UAS-mCD8-GFP (VIE-19a)/16254-p65ADZp (attP40); 17928-ZpGAL4DBD (attP2)/+	Cluster 2
	w-; UAS-TNT-E, UAS-mCD8-GFP (VIE-19a)/10060-p65ADZp (attP40); 42740-ZpGAL4DBD (attP2)/+	Cluster 2
	w-; UAS-TNT-E, UAS-mCD8-GFP (VIE-19a)/31490-p65ADZp (attP40); 20370-ZpGAL4DBD (attP2)/+	Cluster 2
	w-; UAS-TNT-E, UAS-mCD8-GFP (VIE-19a)/20742-p65ADZp (attP40); 25930-ZpGAL4DBD (attP2)/+	Cluster 2
	w-; UAS-TNT-E, UAS-mCD8-GFP (VIE-19a)/37213-p65ADZp (attP40); 19911-ZpGAL4DBD (attP2)/+	Cluster 2
	w-; UAS-TNT-E, UAS-mCD8-GFP (VIE-19a)/46778-p65ADZp (attP40); 23797-ZpGAL4DBD (attP2)/+	Cluster 2
	w-; UAS-TNT-E, UAS-mCD8-GFP (VIE-19a)/19906-p65ADZp (attP40); 57466-ZpGAL4DBD (attP2)/+	Cluster 2
	w-; UAS-TNT-E, UAS-mCD8-GFP (VIE-19a)/50238-p65ADZp (attP40); 19257-ZpGAL4DBD (attP2)/+	Cluster 2
	w-; UAS-TNT-E, UAS-mCD8-GFP (VIE-19a)/46011-p65ADZp (attP40); 04241-ZpGAL4DBD (attP2)/+	Cluster 2

	w-; UAS-TNT-E, UAS-mCD8-GFP (VIE-19a)/61910-p65ADZp (attP40); 10060-ZpGAL4DBD (attP2)/+	Cluster 2
	w-; UAS-TNT-E, UAS-mCD8-GFP (VIE-19a)/21364-p65ADZp (attP40); 26668-ZpGAL4DBD (attP2)/+	Cluster 2
	w-; UAS-TNT-E, UAS-mCD8-GFP (VIE-19a)/50238-p65ADZp (attP40); 43167-ZpGAL4DBD (attP2)/+	Cluster 2
	w-; UAS-TNT-E, UAS-mCD8-GFP (VIE-19a)/45235-p65ADZp (attP40); 25930-ZpGAL4DBD (attP2)/+	Cluster 2
	w-; UAS-TNT-E, UAS-mCD8-GFP (VIE-19a)/37220-p65ADZp (attP40); 44492-ZpGAL4DBD (attP2)/+	Cluster 2
	w-; UAS-TNT-E, UAS-mCD8-GFP (VIE-19a)/37220-p65ADZp (attP40); 61910-ZpGAL4DBD (attP2)/+	Cluster 2
	w-; UAS-TNT-E, UAS-mCD8-GFP (VIE-19a)/19911-p65ADZp (attP40); 44953-ZpGAL4DBD (attP2)/+	Cluster 2
	w-; UAS-TNT-E, UAS-mCD8-GFP (VIE-19a)/37220-p65ADZp (attP40); 10060-ZpGAL4DBD (attP2)/+	Cluster 2
	w-; UAS-TNT-E, UAS-mCD8-GFP (VIE-19a)/45235-p65ADZp (attP40); 38205-ZpGAL4DBD (attP2)/+	Cluster 2
	w-; UAS-TNT-E, UAS-mCD8-GFP (VIE-19a)/37220-p65ADZp (attP40); 49368-ZpGAL4DBD (attP2)/+	Cluster 2
	w-; UAS-TNT-E, UAS-mCD8-GFP (VIE-19a)/33047-p65ADZp (attP40); 33047-ZpGAL4DBD (attP2)/+	Cluster 2
Figure S4	w-; UAS-TNT-E, UAS-mCD8-GFP (VIE-19a)/46778-p65ADZp (attP40); 44175-ZpGAL4DBD (attP2)/+	Cluster 3A
	w-; UAS-TNT-E, UAS-mCD8-GFP (VIE-19a)/33047-p65ADZp (attP40); 26668-ZpGAL4DBD (attP2)/+	Cluster 3A
	w-; UAS-TNT-E, UAS-mCD8-GFP (VIE-19a)/37213-p65ADZp (attP40); 20370-ZpGAL4DBD (attP2)/+	Cluster 3A
	w-; UAS-TNT-E, UAS-mCD8-GFP (VIE-19a)/46011-p65ADZp (attP40); 42740-ZpGAL4DBD (attP2)/+	Cluster 3A
	w-; UAS-TNT-E, UAS-mCD8-GFP (VIE-19a)/37213-p65ADZp (attP40); 49368-ZpGAL4DBD (attP2)/+	Cluster 3A
	w-; UAS-TNT-E, UAS-mCD8-GFP (VIE-19a)/61910-p65ADZp (attP40); 49368-ZpGAL4DBD (attP2)/+	Cluster 3A
	w-; UAS-TNT-E, UAS-mCD8-GFP (VIE-19a)/20742-p65ADZp (attP40); 42740-ZpGAL4DBD (attP2)/+	Cluster 3A
	w-; UAS-TNT-E, UAS-mCD8-GFP (VIE-19a)/37213-p65ADZp (attP40); 38205-ZpGAL4DBD (attP2)/+	Cluster 3A
	w-; UAS-TNT-E, UAS-mCD8-GFP (VIE-19a)/37213-p65ADZp (attP40); 23797-ZpGAL4DBD (attP2)/+	Cluster 3A
	w-; UAS-TNT-E, UAS-mCD8-GFP (VIE-19a)/20742-p65ADZp (attP40); 04241-ZpGAL4DBD (attP2)/+	Cluster 3A
	w-; UAS-TNT-E, UAS-mCD8-GFP (VIE-19a)/37213-p65ADZp (attP40); 20742-ZpGAL4DBD (attP2)/+	Cluster 3A

	w-; UAS-TNT-E, UAS-mCD8-GFP (VIE-19a)/19911-p65ADZp (attP40); 20742-ZpGAL4DBD (attP2)/+	Cluster 3A
	w-; UAS-TNT-E, UAS-mCD8-GFP (VIE-19a)/46011-p65ADZp (attP40); 20742-ZpGAL4DBD (attP2)/+	Cluster 3A
	w-; UAS-TNT-E, UAS-mCD8-GFP (VIE-19a)/61910-p65ADZp (attP40); 20742-ZpGAL4DBD (attP2)/+	Cluster 3A
	w-; UAS-TNT-E, UAS-mCD8-GFP (VIE-19a)/37220-p65ADZp (attP40); 08167-ZpGAL4DBD (attP2)/+	Cluster 3A
	w-; UAS-TNT-E, UAS-mCD8-GFP (VIE-19a)/37213-p65ADZp (attP40); 42740-ZpGAL4DBD (attP2)/+	Cluster 3A
	w-; UAS-TNT-E, UAS-mCD8-GFP (VIE-19a)/45235-p65ADZp (attP40); 20742-ZpGAL4DBD (attP2)/+	Cluster 3A
	w-; UAS-TNT-E, UAS-mCD8-GFP (VIE-19a)/45235-p65ADZp (attP40); 15784-ZpGAL4DBD (attP2)/+	Cluster 3A
	w-; UAS-TNT-E, UAS-mCD8-GFP (VIE-19a)/45235-p65ADZp (attP40); 42740-ZpGAL4DBD (attP2)/+	Cluster 3A
	w-; UAS-TNT-E, UAS-mCD8-GFP (VIE-19a)/37213-p65ADZp (attP40); 19257-ZpGAL4DBD (attP2)/+	Cluster 3A
	w-; UAS-TNT-E, UAS-mCD8-GFP (VIE-19a)/30557-p65ADZp (attP40); 46011-ZpGAL4DBD (attP2)/+	Cluster 3A
Figure S4	w-; UAS-TNT-E, UAS-mCD8-GFP (VIE-19a)/20742-p65ADZp (attP40); 19257-ZpGAL4DBD (attP2)/+	Cluster 3B
	w-; UAS-TNT-E, UAS-mCD8-GFP (VIE-19a)/37220-p65ADZp (attP40); 20742-ZpGAL4DBD (attP2)/+	Cluster 3B
	w-; UAS-TNT-E, UAS-mCD8-GFP (VIE-19a)/04241-p65ADZp (attP40); 44953-ZpGAL4DBD (attP2)/+	Cluster 3B
	w-; UAS-TNT-E, UAS-mCD8-GFP (VIE-19a)/19911-p65ADZp (attP40); 42740-ZpGAL4DBD (attP2)/+	Cluster 3B
	w-; UAS-TNT-E, UAS-mCD8-GFP (VIE-19a)/37220-p65ADZp (attP40); 38205-ZpGAL4DBD (attP2)/+	Cluster 3B
	w-; UAS-TNT-E, UAS-mCD8-GFP (VIE-19a)/46778-p65ADZp (attP40); 46778-ZpGAL4DBD (attP2)/+	Cluster 3B
	w-; UAS-TNT-E, UAS-mCD8-GFP (VIE-19a)/45235-p65ADZp (attP40); 19257-ZpGAL4DBD (attP2)/+	Cluster 3B
	w-; UAS-TNT-E, UAS-mCD8-GFP (VIE-19a)/19911-p65ADZp (attP40); 04241-ZpGAL4DBD (attP2)/+	Cluster 3B
	w-; UAS-TNT-E, UAS-mCD8-GFP (VIE-19a)/30557-p65ADZp (attP40); 30557-ZpGAL4DBD (attP2)/+	Cluster 3B
	w-; UAS-TNT-E, UAS-mCD8-GFP (VIE-19a)/61910-p65ADZp (attP40); 61910-ZpGAL4DBD (attP2)/+	Cluster 3B
	w-; UAS-TNT-E, UAS-mCD8-GFP (VIE-19a)/45235-p65ADZp (attP40); 43167-ZpGAL4DBD (attP2)/+	Cluster 3B
	w-; UAS-TNT-E, UAS-mCD8-GFP (VIE-19a)/04241-p65ADZp (attP40); 20742-ZpGAL4DBD (attP2)/+	Cluster 3B

	w-; UAS-TNT-E, UAS-mCD8-GFP (VIE-19a)/26668-p65ADZp (attP40); 26668-ZpGAL4DBD (attP2)/+	Cluster 3B
	w-; UAS-TNT-E, UAS-mCD8-GFP (VIE-19a)/04241-p65ADZp (attP40); 23797-ZpGAL4DBD (attP2)/+	Cluster 3B
	w-; UAS-TNT-E, UAS-mCD8-GFP (VIE-19a)/37220-p65ADZp (attP40); 44845-ZpGAL4DBD (attP2)/+	Cluster 3B
	w-; UAS-TNT-E, UAS-mCD8-GFP (VIE-19a)/44953-p65ADZp (attP40); 19257-ZpGAL4DBD (attP2)/+	Cluster 3B
	w-; UAS-TNT-E, UAS-mCD8-GFP (VIE-19a)/04241-p65ADZp (attP40); 15784-ZpGAL4DBD (attP2)/+	Cluster 3B
	w-; UAS-TNT-E, UAS-mCD8-GFP (VIE-19a)/04241-p65ADZp (attP40); 42740-ZpGAL4DBD (attP2)/+	Cluster 3B
	w-; UAS-TNT-E, UAS-mCD8-GFP (VIE-19a)/04241-p65ADZp (attP40); 19911-ZpGAL4DBD (attP2)/+	Cluster 3B
	w-; UAS-TNT-E, UAS-mCD8-GFP (VIE-19a)/04241-p65ADZp (attP40); 38205-ZpGAL4DBD (attP2)/+	Cluster 3B
	w-; UAS-TNT-E, UAS-mCD8-GFP (VIE-19a)/20742-p65ADZp (attP40); 20742-ZpGAL4DBD (attP2)/+	Cluster 3B
Figure S5A	w-; UAS-TNT-E, UAS-mCD8-GFP (VIE-19a)/33047-p65ADZp (attP40); 20742-ZpGAL4DBD (attP2)/+	SW-01-GAL4
Figure S5A	w-; UAS-TNT-E, UAS-mCD8-GFP (VIE-19a)/+; 20742-ZpGAL4DBD (attP2)/+	
	w-; 33047-p65ADZp (attP40)/+	
Figure S5B	w-; UAS-TNT-E, UAS-mCD8-GFP (VIE-19a)/02479-p65ADZp (attP40); 17928-ZpGAL4DBD (attP2)/+	SW-02-GAL4
	w-; UAS-TNT-E, UAS-mCD8-GFP (VIE-19a)/+; 17928-ZpGAL4DBD (attP2)/+	
	w-; 02479-p65ADZp (attP40)/+	
Figure S5C	w-; UAS-TNT-E, UAS-mCD8-GFP (VIE-19a)/46011-p65ADZp (attP40); 08167-ZpGAL4DBD (attP2)/+	SW-03-GAL4
	w-; UAS-TNT-E, UAS-mCD8-GFP (VIE-19a)/+; 08167-ZpGAL4DBD (attP2)/+	
Figure S5D	w-; UAS-TNT-E, UAS-mCD8-GFP (VIE-19a)/38652-p65ADZp (attP40); 42740-ZpGAL4DBD (attP2)/+	SW-04-GAL4
	w-; UAS-TNT-E, UAS-mCD8-GFP (VIE-19a)/+; 42740-ZpGAL4DBD (attP2)/+	
	w-; 38652-p65ADZp (attP40)/+	
Figure S5E	w-; UAS-TNT-E, UAS-mCD8-GFP (VIE-19a)/44931-p65ADZp (attP40); 42740-ZpGAL4DBD (attP2)/+	SW-05-GAL4
	w-; UAS-TNT-E, UAS-mCD8-GFP (VIE-19a)/+; 42740-ZpGAL4DBD (attP2)/+	
	w-; 44931-p65ADZp (attP40)/+	
Figure S5F	w-; UAS-TNT-E, UAS-mCD8-GFP (VIE-19a)/37220-p65ADZp (attP40); 08167-ZpGAL4DBD (attP2)/+	SW-16-GAL4

	w-; UAS-TNT-E, UAS-mCD8-GFP (VIE-19a)/+; 08167-ZpGAL4DBD (attP2)/+	
	w-; 37220-p65ADZp (attP40)/+	
Figure S5G	w-; UAS-TNT-E, UAS-mCD8-GFP (VIE-19a)/30557-p65ADZp (attP40); 30557-ZpGAL4DBD (attP2)/+	SW-17-GAL4
	w-; UAS-TNT-E, UAS-mCD8-GFP (VIE-19a)/+; 30557-ZpGAL4DBD (attP2)/+	
	w-; 30557-p65ADZp (attP40)/+	
Figure S5H	w-; UAS-TNT-E, UAS-mCD8-GFP (VIE-19a)/46011-p65ADZp (attP40); 42740-ZpGAL4DBD (attP2)/+	SW-18-GAL4
	w-; UAS-TNT-E, UAS-mCD8-GFP (VIE-19a)/+; 42740-ZpGAL4DBD (attP2)/+	
Figure S5I	w-; UAS-TNT-E, UAS-mCD8-GFP (VIE-19a)/46011-p65ADZp (attP40); 20742-ZpGAL4DBD (attP2)/+	SW-19-GAL4
	w-; UAS-TNT-E, UAS-mCD8-GFP (VIE-19a)/+; 20742-ZpGAL4DBD (attP2)/+	
Figure S5J	w-; UAS-TNT-E, UAS-mCD8-GFP (VIE-19a)/20742-p65ADZp (attP40); 42740-ZpGAL4DBD (attP2)/+	SW-20-GAL4
	w-; UAS-TNT-E, UAS-mCD8-GFP (VIE-19a)/+; 42740-ZpGAL4DBD (attP2)/+	
	w-; 20742-p65ADZp (attP40)/+	

Table S2. Definitions of linear assay tracking parameters

	Attribute	Definition
1	distance backwards	Distance covered in backward walking state, as defined previously in [1]. In brief, a variant of Viterbi algorithm is used to assign a walking or stalled state to a given fly in a given frame. Each state has a velocity threshold, and erratic transitions between the different states are penalized. Velocity threshold for backward walking state, < -0.2 mm/s. Unit, mm.
2	distance forwards	Distance covered in forward walking state as defined previously in [1]. Velocity threshold for forward walking state, >1 mm/s. Unit, mm.
3	distance forwards + backwards	Total distance covered in forward and backward walking states. Unit, mm.
4	distance backwards/(distance forwards+ backwards)	Ratio of total distance covered in backward walking state/ total distance covered in forward and backward walking states.
5	distance forwards/(distance forwards + backwards)	Ratio of total distance covered in backward walking state / total distance covered in forward and backward walking states.
6	distance backwards/distance forwards	Ratio of total distance covered in backward walking state/ total distance covered in forward walking state.
7	time backwards	Time spent in backward walking state. Unit, s.
8	time forwards	Time spent in forward walking state. Unit, s.
9	time forwards + backwards	Total time spent in forward and backward walking states. Unit, s.
10	time backwards/(time backwards+ forwards)	Ratio of total time spent in backward walking state / total time spent in forward and backward walking states.
11	time forwards/(time forwards + backwards)	Ratio of total time spent in forward walking state / total time spent in forward and backward walking states.
12	time backwards/time forwards	Ratio of total time spent in backward walking state / total time spent in forward walking state.
13	total movement	Total translation i.e., total distance covered without assigning velocity thresholds for forward or backward movement. Unit, mm.

14	total movement in center	Total translation in the center of the linear chamber without considering any velocity threshold. 'Center' is defined as the region spanning the center ½ of the chamber, i.e., ¼ of the chamber-length from the mid-point to either direction. Unit, mm.
15	total movement in periphery	Total translation in the peripheral ends of the linear chamber without considering any velocity threshold. 'Periphery' is defined as ¼ left + ¼ right distal ends of the linear chamber. Unit, mm.
16	total backward movement	Total backward translation. Unit, mm.
17	total backward movement in center	Total backward translation in 'center'. Unit, mm.
18	total backward movement in periphery	Total backward translation in 'periphery'. Unit, mm.
19	total forward movement	Total forward translation. Unit, mm.
20	total forward movement in center	Total backward translation in 'center'. Unit, mm.
21	total forward movement in periphery	Total backward translation in 'periphery'. Unit, mm.
22	backward/total movement	Ratio of backward to total translation.
23	backward/total movement in center	Ratio of backward to total translation in 'center'.
24	backward/total movement in periphery	Ratio of backward to total translation in 'periphery'.
25	forward/total movement	Ratio of forward to total translation.
26	forward/total movement in center	Ratio of forward to total translation in 'center'.
27	forward/total movement in periphery	Ratio of forward to total translation in 'periphery'.
28	backward/forward movement	Ratio of backward to forward translation.
29	backward/forward movement in center	Ratio of backward to forward translation in 'center'.
30	backward/forward movement in periphery	Ratio of backward to forward translation in 'periphery'.
31	mean body size	Mean area of the ellipse fitted to the fly over the 10-minute assay. Unit, mm^2. (A frequently turning fly has relatively low mean body size over a 10-minute video).
32	#backward bouts	Number of continuous forward walking states.
33	#forward bouts	Number of continuous backward walking states.
34	mean backward bout duration	Time in backward walking state/#backward bouts.

35	mean forward bout duration	Time in forward walking state/#forward bouts.
36	#heading changes	Number of instances of changes in the orientation of fly.
37	#turns	Number of turns as defined in Figure S1.
38	#turns forced	Number of turns with the fly's head facing the end of the linear chamber. Any 'forced' transition is defined as a transition where the fly body-centroid is <3 mm from the boundary of the chamber.
39	#turns in center	Number of turns in 'center'.
40	#turns in periphery	Number of turns in 'periphery'.
41	#backward turns	Number of backward turns (Figure S1).
42	#backward turns forced	Number of backward turns 'forced'.
43	#backward turns in center	Number of backward turns in 'center'.
44	#backward turns in periphery	Number of backward turns in 'periphery'.
45	#forward turns	Number of forward turns (Figure S1).
46	#forward turns forced	Number of forward turns 'forced'.
47	#forward turns in center	Number of forward turns in 'center'.
48	#forwards turns in periphery	Number of forward turns in 'periphery'.
49	total turn duration	Total duration for all turns. Unit, s.
50	mean turn duration	Total duration for all turns/#turns.
51	#flips	Number of flips (Figure S1).
52	#flips forced	Number of flips 'forced'.
53	#flips in center	Number of flips in 'center'.
54	#flips in periphery	Number of flips in 'periphery'.
55	#backward flips	Number of backward flips (Figure S1).
56	#backward flips forced	Number of backward flips 'forced'.
57	#backward flips in center	Number of backward flips in 'center'.
58	#backward flips in periphery	Number of backward flips in 'periphery'.
59	#forward flips	Number of forward flips (Figure S1).
60	#forward flips forced	Number of forward flips 'forced'.

61	#forward flips in center	Number of forward flips in ‘center’.
62	#forward flips in periphery	Number of forward flips in ‘periphery’.
63	total flip duration	Total duration for all flips. Unit, s.
64	mean flip duration	Total duration for all flips/#flips.
65	#reversals	Number of total reversals (Figure S1).
66	#reversals forced	Number of reversals ‘forced’.
67	#reversals in center	Number of reversals in ‘center’.
68	#reversals in periphery	Number of reversals in ‘periphery’.
69	#backward reversals	Number of backward reversals (Figure S1).
70	#backward reversals forced	Number of backward reversals ‘forced’.
71	#backward reversals in center	Number of backward reversals in ‘center’.
72	#backward reversals in periphery	Number of backward reversals in ‘periphery’.
73	#forward reversals	Number of forward reversals (Figure S1).
74	#forward reversals forced	Number of forward reversals ‘forced’.
75	#forward reversals in center	Number of forward reversals in ‘center’.
76	#forward reversals in periphery	Number of forward reversals in ‘periphery’.
77	total reversal duration	Total duration for all reversals. Unit, s.
78	mean reversal duration	Total duration for all reversals/#reversals.
79	#stalls	Number of stalls. ‘Stalled’ state is determined as in [1]. Velocity threshold, <1.5 mm/s.
80	#stalls forced	Number of stalls ‘forced’.
81	#stalls in center	Number of stalls in ‘center’.
82	#stalls in periphery	Number of stalls in ‘periphery’.
83	#stalls forced/#stalls	Ratio of forced stalls to total number of stalls.
84	total stall duration	Total time spent in stalled state.
85	total forced stall duration	Total time spent in stalls that are ‘forced’.
86	mean stall duration	Time spent in stalled state/#stalls.
87	mean forced stall duration	Total time spent in ‘forced’ stalls/#stalls forced.

88	Stuckness	Measure of the fly's affinity to the chamber-ends, such that ±1 signifies a totally 'stuck' fly and 0 signifies a fly that spends the entire assay time in the middle of the chamber. Calculated as the mean, averaged over all frames, of the following: ((fractional distance between the current position of the fly and the chamber-center in the given frame) x 2) x heading-direction) (heading direction is negative for leftward movement, positive for rightward movement).
89	time in periphery	Time spent in 'periphery'. Unit, s.
90	time in outer periphery	Time spent in 'outer periphery'. 'Outer periphery' is defined as 1/10 left + 1/10 right distal ends of the linear chamber. Unit, s.
91	#turns/#transitions	Ratio of number of turns to total number of transitions.
92	#flips/#transitions	Ratio of number of flips to total number of transitions.
93	#reversals/#transitions	Ratio of number of reversals to total number of transitions.
94	#stalls/#transitions	Ratio of number of stalls to total number of transitions.
95	(#turns forced + #flips forced)/#transitions forced	Ratio of the sum of number of 'forced' turns and flips to total number of 'forced' transitions.
96	#reversals/(#turns + #reversals)	Ratio of number of reversals to sum of total number of reversals and turns. (The most common choice at the end of the linear chamber is either a reversal or a turn).
97	#reversals forced / (#turns forced + #reversals forced)	Ratio of number of 'forced' reversals to sum of total number of 'forced' reversals and 'forced' turns.
98	#reversals forced / (#turns forced + #reversals forced + #flips forced)	Ratio of number of 'forced' reversals to sum of total number of 'forced' reversals, turns and flips.

Table S3. Notes on expression patterns of other stained hits

	Genotype	Expression strength/ sparseness/ labels MDNs	Cluster
1	w-; UAS-TNT-E, UAS-mCD8-GFP (VIE-19a)/45235-p65ADZp (attP40); 47316-ZpGAL4DBD (attP2)/+	labels MDNs	1B
2	w-; UAS-TNT-E, UAS-mCD8-GFP (VIE-19a)/31490-p65ADZp (attP40); 44845-ZpGAL4DBD (attP2)/+	labels MDNs	1B
3	w-; UAS-TNT-E, UAS-mCD8-GFP (VIE-19a)/15774-p65ADZp (attP40); 04241-ZpGAL4DBD (attP2)/+	weak	1B
4	w-; UAS-TNT-E, UAS-mCD8-GFP (VIE-19a)/15774-p65ADZp (attP40); 08167-ZpGAL4DBD (attP2)/+	weak	1B
5	w-; UAS-TNT-E, UAS-mCD8-GFP (VIE-19a)/26020-p65ADZp (attP40); 43167-ZpGAL4DBD (attP2)/+	weak	1B
7	w-; UAS-TNT-E, UAS-mCD8-GFP (VIE-19a)/30557-p65ADZp (attP40); 42740-ZpGAL4DBD (attP2)/+	weak	1C
8	w-; UAS-TNT-E, UAS-mCD8-GFP (VIE-19a)/19911-p65ADZp (attP40); 46011-ZpGAL4DBD (attP2)/+	broad	2
9	w-; UAS-TNT-E, UAS-mCD8-GFP (VIE-19a)/45235-p65ADZp (attP40); 46011-ZpGAL4DBD (attP2)/+	moderate	2
10	w-; UAS-TNT-E, UAS-mCD8-GFP (VIE-19a)/46011-p65ADZp (attP40); 04241-ZpGAL4DBD (attP2)/+	weak	2
11	w-; UAS-TNT-E, UAS-mCD8-GFP (VIE-19a)/19911-p65ADZp (attP40); 44953-ZpGAL4DBD (attP2)/+	weak	2
12	w-; UAS-TNT-E, UAS-mCD8-GFP (VIE-19a)/45235-p65ADZp (attP40); 25930-ZpGAL4DBD (attP2)/+	weak	2
13	w-; UAS-TNT-E, UAS-mCD8-GFP (VIE-19a)/37213-p65ADZp (attP40); 49368-ZpGAL4DBD (attP2)/+	broad	3A
14	w-; UAS-TNT-E, UAS-mCD8-GFP (VIE-19a)/37213-p65ADZp (attP40); 49368-ZpGAL4DBD (attP2)/+	broad	3A
16	w-; UAS-TNT-E, UAS-mCD8-GFP (VIE-19a)/20742-p65ADZp (attP40); 04241-ZpGAL4DBD (attP2)/+	weak	3A
17	w-; UAS-TNT-E, UAS-mCD8-GFP (VIE-19a)/33047-p65ADZp (attP40); 26668-ZpGAL4DBD (attP2)/+	weak	3A
18	w-; UAS-TNT-E, UAS-mCD8-GFP (VIE-19a)/45235-p65ADZp (attP40); 15784-ZpGAL4DBD (attP2)/+	weak	3A
15	w-; UAS-TNT-E, UAS-mCD8-GFP (VIE-19a)/19911-p65ADZp (attP40); 42740-ZpGAL4DBD (attP2)/+	moderate	3B
19	w-; UAS-TNT-E, UAS-mCD8-GFP (VIE-19a)/45235-p65ADZp (attP40); 19257-ZpGAL4DBD (attP2)/+	broad	3B
20	w-; UAS-TNT-E, UAS-mCD8-GFP (VIE-19a)/61910-p65ADZp (attP40); 20742-ZpGAL4DBD (attP2)/+	broad	3B
21	w-; UAS-TNT-E, UAS-mCD8-GFP (VIE-19a)/04241-p65ADZp (attP40); 15784-ZpGAL4DBD (attP2)/+	weak	3B
22	w-; UAS-TNT-E, UAS-mCD8-GFP (VIE-19a)/04241-p65ADZp (attP40); 38205-ZpGAL4DBD (attP2)/+	weak	3B

23	w-; UAS-TNT-E, UAS-mCD8-GFP (VIE-19a)/04241-p65ADZp (attP40); 44953-ZpGAL4DBD (attP2)/+	weak	3B
24	w-; UAS-TNT-E, UAS-mCD8-GFP (VIE-19a)/19911-p65ADZp (attP40); 04241-ZpGAL4DBD (attP2)/+	weak	3B

3.9.2 Supplemental Movie Legends

Movies are available in the accompanying CD.

Movie M1. JCNs and MDNs are anatomically close to each other. Related to Figure 6.

Overlaid segmentations of JCNs (green) and MDNs (gray) onto common reference template, following non-rigid registration.

Movie M2 A-D. Silencing JCN significantly impairs backward locomotion in flies. Related to Figure 7A.

Representative flies in the groove assay carrying *JCN-GAL4* (A), *MDN-1-GAL4* (B), *46011-ZpGAL4DBD* (C) or *30557-p65ADZp* (D) drivers in combination with the effectors *UAS-TNT-E and UAS-mCD8-GFP*.

Movie M3 A-C. Forward locomotion is unaffected in flies with JCNs silenced. Related to Figure 7B.

Representative flies in the ring assay carrying *JCN-GAL4* (A), *46011-ZpGAL4DBD* (B) or *30557-p65ADZp* (C) drivers in combination with the effectors *UAS-TNT-E and UAS-mCD8-GFP*.

Movie M4 A-B. Optogenetic activation of JCNs in decapitated flies causes transient hindleg extension in upright and supine positions. Related to Figure 7C.

Optogenetic stimulation of upright (A) and supine (B) decapitated flies carrying the *JCN-GAL4* in combination with *UAS-CsChrimson*. Red dots, LED indicator.

Movie M5 A-B. Optogenetic activation of MDNs in decapitated flies causes coordinated backward locomotion when upright and prominent hindleg movements, when supine (B). Related to Figure 7C.

Optogenetic stimulation of upright (A) and supine (B) decapitated flies carrying *MDN-1-GAL4* in combination with *UAS-CsChrimson*, positions. Red dots, LED indicator.

Movie M6 A-B. Optogenetic activation of control decapitated flies causes no movement. Related to Figure 7C.

Optogenetic stimulation of upright (A) and supine (B) decapitated flies carrying the empty control vector in combination with *UAS-CsChrimson*. Red dots, LED indicator.

Movie M7. Tethered forward walking in ball assay. Related to Figure 7D.

Forward locomotion by a tethered fly carrying *MDN-1-GAL4* in combination with *UAS-CsChrimson* in the absence of red light stimulation in the ball assay; topview

Movie M8. Optogenetic activation of MDNs in tethered intact flies triggers coordinated backward locomotion in the ball assay. Related to Figure 7D.

Optogenetic activation of a tethered fly carrying *MDN-1-GAL4* in combination with *UAS-CsChrimson* in the ball assay; topview.

Movie 9. Optogenetic activation of MDNs in tethered decapitated flies triggers coordinated backward locomotion in the ball assay. Related to Figure 7D.

Optogenetic activation of a tethered decapitated fly carrying *MDN-1-GAL4* in combination with *UAS-CsChrimson* in the ball assay; topview.

Movie M10. Optogenetic activation of MDNs in tethered decapitated flies causes elaborate hindleg movements when lifted off the substrate. Related to Figure 7D.

Optogenetic stimulation of tethered decapitated flies carrying *MDN-1-GAL4* in combination with *UAS-CsChrimson* when lifted off the ball, sideview. Red dots, LED indicator.

Movie M11. Optogenetic activation of JCNs in tethered decapitated flies causes transient hindleg extension when lifted off the substrate. Related to Figure 7D.

Optogenetic stimulation of tethered decapitated flies carrying *JCN-1-GAL4* in combination with *UAS-CsChrimson* when lifted off the ball; sideview. Red dots, LED indicator.

3.9.3 Supplemental Experimental Procedures

3.9.3.1 Fly genetics

Split-GAL4 derivatives of the relevant VT enhancer-GAL4 lines were generated using the same strategy as [2,3], and inserted into either attP2 or attP40 [4] landing sites by phiC31-mediated recombination. Other stocks used were *UAS-TNT-E* [5]; *20XUAS-CsChrimson-mVenus* (attP18) [6,7]; *UAS-mCD8-GFP* (VIE-19a) [8]; UAS-syt-GFP [9] (Bloomington #6925); pJFRC22-10XUAS-IVS-myr::tdTomato (attP2) [3] (Bloomington #32221); and *Canton S.*

All experiments were done on adult male *Drosophila*, raised at 25^0 C and 50% relative humidity.

For silencing with TNT, flies were reared in a 12hr:12hr dark:light cycle on semidefined medium, collected in groups of 12-15 at eclosion, and then aged for 4-6 days prior to experiments. For optogenetic activation using CsChrimson, flies were reared in the dark on cornmeal-molasses food supplemented with all-trans retinal (0.2 mM prior to eclosion and 0.4 mM post-eclosion), collected in groups of 20-25 at eclosion, and aged for 5-6 days prior to experiments.

3.9.3.2 Behavioral assays and analysis

Linear and ring assays

All silencing experiments were conducted either in the morning or early evening, Zeitgeber time. The fly chambers used in the assays were same as described previously [1]. Linear chambers were 1.5 mm high and wide (just larger than a 4-day old adult male raised at 25^0 C) and 75 mm long. A behavioral assay plate comprised 12 such linear grooves covered by transparent plastic. Ring chambers were 2.5 mm in height and width and 16 mm in diameter, with 11 chambers per plate covered with transparent plastic. A single male fly was loaded into each groove or each ring chamber. Behavior from both the linear and ring assays were recorded for 10 minutes using a camera from above (JVC GZ-HD10E) at 25 frames per second (fps) and 1920X1080 pixel resolution. Videos were processed in an automated fashion using a previously described computer-vision software [1] that tracked the orientation and velocity of flies at every frame of a given video.

Optogenetic assay with intact and decapitated flies

Both male and female flies were cold anesthesized at 4°C for a few minutes. For assays with decapitated flies, their heads were rapidly chopped off with a surgical scissor. A healthy decapitated preparation was identified as one where the upright headless fly had a strong grip on the substrate and displayed grooming when touched with a brush. In Figure 7C, flies either stood upright on substrate or were positioned on a double-sided tape, facing upwards. Optogenetic stimulation was provided with a red laser of wavelength 635 nm (DA-635-1-3 (16X5); Picotronic). For the ball assays, intact or decapitated flies were placed inside a groove in a cooled aluminum block under a light microscope. Using a 3D micromanipulator, the tip of a copper wire (.15 mm diameter) was tethered to the dorsal side of the fly's thorax with a light-curable dental glue, that was cured with light of ~470 nm wavelength. The wire was clamped into a holder, which in turn was inserted into a 3D micromanipulator. Using the manipulator, the fly was placed on an air-suspended polypropylene ball (~6mm diameter). . The fly was filmed from the side using a CMOS camera with an industrial lens of 25 mm focal length (AVT Marlin F131B; resolution, used resolution, 640X480 pixels; speed 50 Hz), and from above using a high-speed camera VC-2MC-M340 (Vieworks, Korea; used resolution, 1200X500 pixels; speed, 300 Hz) with telecentric lens TEL-M55 (Computar,

USA). The video stream acquired from the latter was transmitted to a frame grabber interface (Solios eV-CLF, Matrox, Canada). Two additional sideviews of the walking fly was acquired by the high-speed camera by placing two mirrors 10° off from the vertical orientation of the ball. For optogenetic stimulation, a laser was adjusted to point to the thorax of the fly with the help of a 3D micromanipulator. Optogenetic stimulation was provided with high intensity red light of wavelength ~617 nm.

3.9.3.3 Agglomerative hierarchical clustering

The agglomerative hierarchical clustering of the 137X98 phenotype matrix was done in Matlab 2016b using the 'clustergram' function. The analysis for Ward linkage cost was done as in [11,12] using the 'linkage' function with 'Euclidean' as the distance parameter and 'ward' as the linkage method. In this method, every genotype (i.e., the row vector of normalized attribute values in the phenotype matrix) is first assigned to be an independent cluster. The algorithm then searches the entire matrix to identify two clusters that produce the smallest joining costs, merges them into one cluster, and repeats this process iteratively until all the genotypes are grouped into one cluster. Specifically, the algorithm first calculates the variance of each cluster (defined as the sum of the squared Euclidean distances between each component vector in a given cluster and the centroid of that cluster), and then searches for the two clusters that would provide the least increase in variance when merged. The color scale of all 'clustergrams' (Figures 2, S2, S3 and S4) was adjusted to be in the same range for comparison across all clustering outputs.

3.9.3.4 Immunohistochemistry and imaging

Immunohistochemistry was done on the dissected central nervous systems of 5-7 days old adult male flies. Flies expressing *UAS-mCD8-GFP UAS-TNT* were stained using the protocol described in https://www.janelia.org/sites/default/files/Project%20Teams/Fly%20Light/FL%20Protocol%20-%20Adult%20IHC%20-%20Anti-GFP.pdf. Antibodies used were rabbit anti-GFP (1:500, Invitrogen), mouse mAb nc82 (1:50, Hybridoma Bank) and secondary Alexa Fluor (AF) 488 anti-rabbit and AF568 anti-mouse antibodies (1:300, Life Technologies). Flies expressing *UAS-syt-GFP pJFRC22-10XUAS-IVS-myr::tdTomato* were stained using the protocol described in https://www.janelia.org/sites/default/files/FL%20Protocol%20-%20Adult%20IHC%20-%20Polarity%20Sequential.pdf with the modifications that we used chicken anti-GFP (1:1500, Abcam), rabbit anti-dsRed (1:1000, Clontech Laboratories), and secondary AF488 anti-chicken (1:800, Thermo Fisher Scientific), Cy3 anti-rabbit (1:1000, Jackson ImmunoResearch), and Cy5 anti-mouse (1:1000, Jackson ImmunoResearch) antibodies. Confocal stacks of stained nervous systems were taken using LSM 710 with a 20X air objective. For Figures 3, 4, 5, and S5, confocal stacks of brains and VNCs were registered onto a common reference template and each image is a maximum intensity projection generated from the registered volumes. For Figure 6, maximum intensity projections were obtained with ImageJ (http://fiji.sc). Additionally, we used Fiji and Illustrator to remove debris outside the sample area and rotate the images for alignment. Movies showing overlaid segmentations of MDNs and JCN onto a reference ventral nerve cord template were generated using Fluorender [10], an image-rendering software.

3.9.4 Supplemental References

1. Bidaye, S.S., Machacek, C., Wu, Y., and Dickson, B.J. (2014). Neuronal control of drosophila walking direction. Science *344*, 97–101.

2. Luan, H., Peabody, N.C., Vinson, C.R., and White, B.H. (2006). Refined spatial manipulation of neuronal function by combinatorial restriction of transgene expression. Neuron *52*, 425–436.

3. Pfeiffer, B.D., Ngo, T.-T.B., Hibbard, K.L., Murphy, C., Jenett, A., Truman, J.W., and Rubin, G.M. (2010). Refinement of tools for targeted gene expression in Drosophila. Genetics *186*, 735–755.

4. Groth, A.C., Fish, M., Nusse, R., and Calos, M.P. (2004). Construction of transgenic Drosophila by using the site-specific integrase from phage φC31. Genetics *166*, 1775–1782.

5. Sweeney, S.T., Broadie, K., Keane, J., Niemann, H., and O'Kane, C.J. (1995). Targeted expression of tetanus toxin light chain in Drosophila specifically eliminates synaptic transmission and causes behavioral defects. Neuron *14*, 341–351.

6. Sen, R., Wu, M., Branson, K., Robie, A., Rubin, G.M., and Dickson, B.J. (2017). Moonwalker descending neurons mediate visually evoked retreat in Drosophila. Curr. Biol. *27*, 766–771.

7. Klapoetke, N.C., Murata, Y., Kim, S.S., Pulver, S.R., Birdsey-Benson, A., Cho, Y.K., Morimoto, T.K., Chuong, A.S., Carpenter, E.J., Tian, Z., *et al.* (2014). Independent optical excitation of distinct neural populations. Nat. Methods *11*, 338–346.

8. Yu, J.Y., Kanai, M.I., Demir, E., Jefferis, G.S.X.E., and Dickson, B.J. (2010). Cellular organization of the neural circuit that drives Drosophila courtship behavior. Curr. Biol. *20*, 1602–1614.

9. Zhang, Y.Q., Rodesch, C.K., and Broadie, K. (2002). Living synaptic vesicle marker: synaptotagmin-GFP. Genes. N. Y. N 2000 *34*, 142–145.

10. Braun, E., Geurten, B., and Egelhaaf, M. (2010). Identifying prototypical components in behaviour using clustering algorithms. PLoS ONE *5*, e9361.

11. Geurten, B.R.H., Kern, R., Braun, E., and Egelhaaf, M. (2010). A syntax of hoverfly flight prototypes. J. Exp. Biol. *213*, 2461–2475.

12. Wan, Y., Otsuna, H., Chien, C.-B., and Hansen, C. (2012). FluoRender: An application of 2D image space methods for 3D and 4D confocal microscopy data visualization in neurobiology research. IEEE Pac. Vis. Symp. Proc. IEEE Pac. Vis. Symp., 201.

Chapter 4

Twolumps Ascending Neurons Mediate Touch-Evoked Reversal Of Walking Direction in *Drosophila*

4.1 Highlights

- Silencing the activity of TLAs impairs backward but not general locomotion
- Optogenetic activation of TLAs triggers backward locomotion
- Both TLAs and MDNs mediate touch-evoked backing up
- Optogenetic activation of TLAs elicits calcium responses in MDNs

4.2 Summary

To flexibly walk through rugged terrains, animals heavily rely on closed-loop somatosensory feedback from internal and external mechanosensors (for reviews see [1–7]). Somatosensory feedback from limbs fine-tunes the magnitude and timing of the rhythmic motor outputs of leg-muscles during walking, enabling coordinated motion. Additionally, external mechanosensory stimuli act on ongoing motor outputs enabling a walking animal to flexibly maneuver around obstacles and extricate itself from dead-ends. Currently, we have only a limted understanding for how proprioceptive feedback and tactile stimuli are computed during active navigation. *Drosophila melanogaster* serves as a genetically tractable model to address this question. We previously identified a cluster of 4 descending neurons – the moonwalker descending neurons (MDNs) – the activity of which is necessary and sufficient to trigger backward locomotion in flies [8,9]. This discovery has served as a toehold for our inroads into understanding locomotor circuits in *Drosophila* [10]. Here, using intersectional genetics, neuronal silencing, in vivo optogenetics, and functional imaging experiments, we characterize a pair of ascending neurons – the Twolumps ascending neurons (TLAs).

Artificial activation of the TLAs is sufficient to trigger transient backward locomotion. Silencing of the TLAs decreases touch-evoked reversals during locomotion. Further, we show that MDNs receive excitatory inputs from TLAs; neuronal polarity markers indicate that this input takes place in the brain. Based on our findings, we hypothesize that TLAs either convey feedforward mechanosensory stimuli to transiently activate MDNs in response to anterior-body touch, or provide feedback signals to entrain MDN activity during backward locomotion.

4.3 Results and Discussions

Flies in which the activity of MDNs is silenced have a specific defect in backward locomotion with no impairment in forward locomotion [8]. To identify additional neurons involved in backward locomotion, we conducted a neuronal silencing screen using the split-GAL4 intersectional system [10,11] (refer to Chapter 3 for details of the screen). In our screen, we identified a sparsely labeled split-GAL4 combination of interest, henceforth referred to as Twolumps or *TL-1-GAL4*. Since flies seldom walk backwards, our screen was designed to force flies to walk in narrow linear grooves which restricted the majority of their lateral movement while still preserving forward and backward locomotion (Figure 1A; Movie M1). A computer vision software was used to detect forward and backward walking states in flies [8]. We found that inactivating neurons labeled in *TL-1-GAL4* with the chronic neuronal silencer tetanus toxin light chain (TNT) [12] impaired backward locomotion but left forward locomotion intact (Figure 1A). Total distances covered in the backward walking state in *TL-1-GAL4 UAS-TNT* flies were significantly reduced when compared to 2 independent controls – one carrying only the TNT effector and the other only the split-GAL4 driver. However, the reduction in backward locomotion in these flies was not as severe as when the activity of MDNs was silenced (Figure 1A; Movie M1), suggesting that neurons labeled in *TL-1-GAL4* are important but not necessary for the execution of backward locomotion. In an independent walking assay, where flies walked forwards in a ring-shaped chamber for 10 minutes, *TL-1-GAL4 UAS-TNT* flies showed no perceivable defect in general locomotion (Figure 1B; Movie M2), confirming that the relevant neurons specifically control aspects of backward locomotion. Moreover, optogenetic activation of neurons labeled in *TL-1-GAL4* with a red light activated cation channel CsChrimson [13] was sufficient to elicit transient backward locomotion in flies (Figures 1C and 1D; Movie M3). Thus, our results indicate that a subset

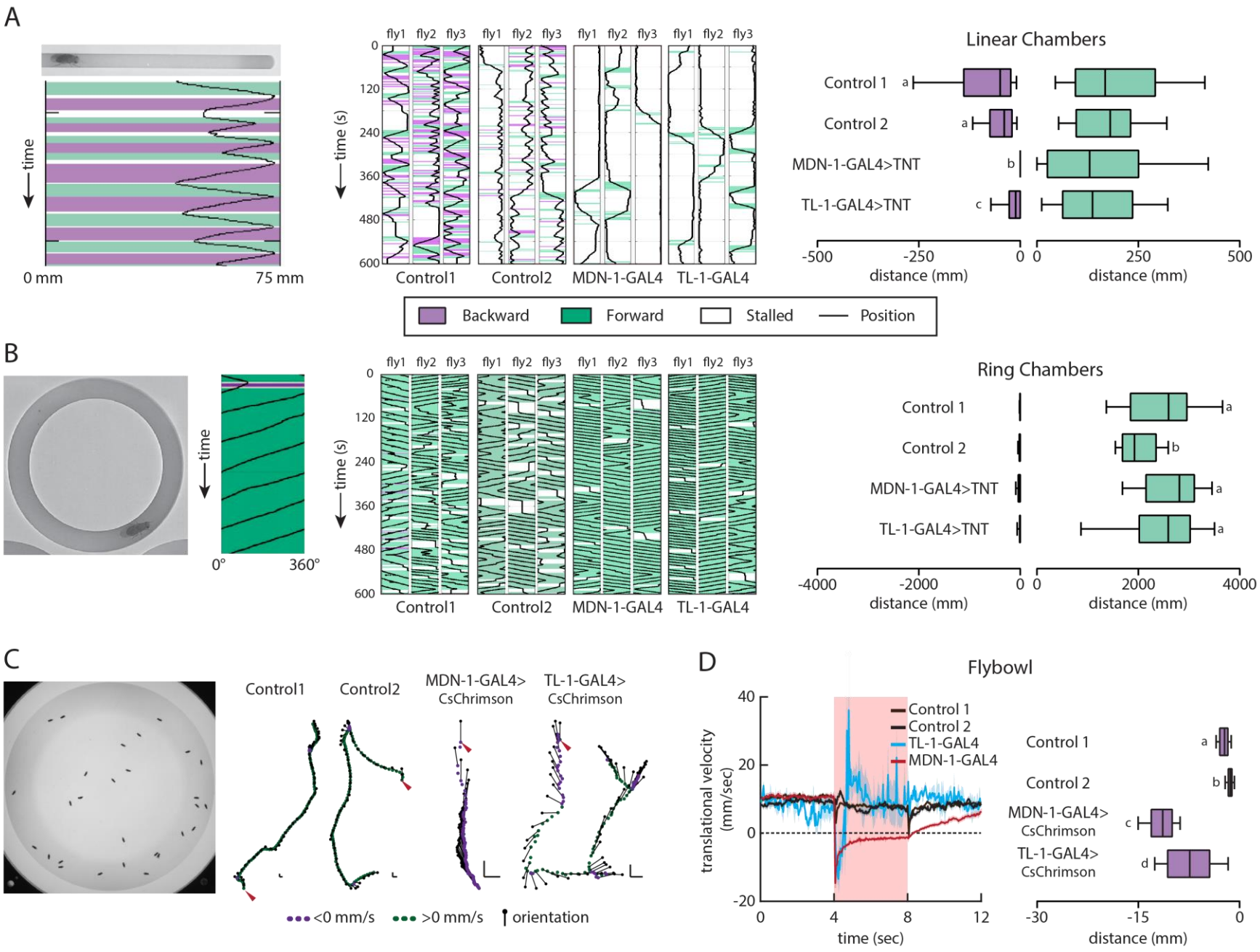
A
time
0 mm
75 mm
fly1 fly2 fly3
time (s)
0
120
240
360
480
600
Control1
Control2
MDN-1-GAL4
TL-1-GAL4
Linear Chambers
Control 1
Control 2
MDN-1-GAL4>TNT
TL-1-GAL4>TNT
distance (mm)
Backward
Forward
Stalled
Position
B
0°
360°
Ring Chambers
C
Control1
Control2
MDN-1-GAL4> CsChrimson
TL-1-GAL4> CsChrimson
<0 mm/s
>0 mm/s
orientation
D
Flybowl
translational velocity (mm/sec)
time (sec)

Figure 1. Neurons labeled in Twolumps (*TL-1-GAL4*) are important and sufficient for backward locomotion

(A) Left: A still-frame from the linear assay (top) and an example of the output from the automated tracker. Middle: 10-min motion plots of males carrying the indicated driver along with *UAS-TNT*. The plots from three representative animals are shown for each genotype (see Table S1 for detailed genotypes). Right: Total walking distance in a 10-min assay in linear chambers (Control-1 *UAS-TNT*, n = 100 flies; Control-2 *TL-1-GAL4*, n = 35 flies; *MDN-1-GAL4 UAS-TNT*, n = 48 flies; *TL-1-GAL4 UAS-TNT*, n = 93 flies). Box-and-whisker plots in this and other panels represent 10^{th}, 25^{th}, 50^{th}, 75^{th}, and 90^{th} percentiles. Statistical significance in this and other panels was assessed using Kruskal-Wallis test followed by Dunn's post-hoc test, unless otherwise mentioned. Results of statistical analyses in this and other panels are represented as letter codes such that groups that are not statistically significant from each other have the same letter code. When a group has more than one letter code, the given group is not significantly different from other groups that have any of its letter codes. Panels without letter codes represent conditions where no significant difference exists among groups.

(B) Left: Ring assay for forward walking and representative motion plot of a single male fly walking predominantly anti-clockwise. Middle: 10-min motion plots of males carrying the indicated driver along with *UAS-TNT*. Three representative plots are shown for each genotype. Right: Total walking distance in a 10-min assay in ring chambers (Control-1 *UAS-TNT*, n = 108 flies; Control-2 *TL-1-GAL4*, n = 29 flies; *MDN-GAL4 UAS-TNT*, n = 29 flies*; TL-1-GAL4 UAS-TNT*, n = 29 flies).

(C) Left: A still-frame from the flybowl optogenetic activation assay. Middle: Representative trajectories of flies carrying the indicated split-GAL4 drivers along with *UAS-CsChrimson*, color-coded for backward (<0 mm/s) or forward (>0 mm/s) translational velocity, during the 4-sec optogenetic stimulation window. Head positions are indicated by black dots and head-to-centroid orientations by black dashes. Arrowheads indicate position at the beginning of optogenetic stimulation. Scale bar, 1 mm x 1 mm.

(D) Left: Translational velocity versus time upon optogenetic stimulation. Dark traces indicate per-fly means over 5 trials and envelopes indicate ±standard error of mean (SEM). Right: Per-fly mean over 5 trials for total backward translation during the optogenetic stimulation window. (Control-1 *UAS-CsChrimson*, n = 96 flies; Control-2 *TL-1-GAL4*, n = 38 flies; *MDN-GAL4 UAS-CsChrimson*, n = 77 flies , *TL-1-GAL4 UAS-CsChrimson*, n = 67 flies).

of neurons in the expression pattern of *TL-1-GAL4* is sufficient and important for backward walking in *Drosophila*.

In order to identify the specific cells within the *TL-1-GAL4* expression pattern that are involved in backward locomotion, we used a genetic approach [9,14] to stochastically activate and label subsets of cells from the original split-GAL4 expression pattern. *TL-1-GAL4* reproducibly labels 7 clusters of neurons (Figure 2A). We used flies carrying the *TL-1-GAL4* combination along with the stop-cassette-effector *pJFRC300-20XUAS-FRT>-dSTOP-FRT>-CsChrimson::mVenus* [14]. The latter comprised a core promotor for GAL4-activated expression (*pJFRC300*), 20 copies of Upstream Activating Sequences (*20XUAS*), a transcriptional terminator (*dSTOP*) flanked by two Flp-recombinase target sites (*FRT*), and an *mVenus* tagged *CsChrimson* gene. By expressing Flp recombinase under a heat shock promoter, we could randomly excise the otherwise ubiquitously expressed transcriptional terminator dSTOP and allow the expression of CsChrimson tagged with mVenus in a random subset of the original split-GAL4 expression pattern. The presence of CsChrimson and mVenus in such dSTOP-free cells allowed us to both activate and visualize these neurons in the mosaic fly. Stochastically activated cells could thus be anatomically identified and correlated with individual fly's behavior.

We used two independent approaches to analyze the dataset from the stochastic labeling experiments: an approach using multiple linear regression and another using blinded manual scoring. For the multiple linear regression analysis, we used 1 and 0 as binary, independent variables that defined whether a given cell-type was labeled or not labeled in the sample. The dependent variable was the sample's average backward translation distance over all trials during optogenetic stimulation. Thus, a significant negative slope-coefficient for a given cluster corresponds to correlation between cell labeling and backward translation; a significant positive slope-coefficient corresponds to anti-correlation; and a slope-coefficient close to 0 corresponds to no correlation. In a complementary approach, we observed videos of individual flies and manually scored whether the fly walked backwards upon optogenetic activation. We calculated a 'backward score' for each of the 7 cell-types – defined as the fraction of samples in which activation of the cell-type elicited backward locomotion minus the fraction of samples where activation of the cell-type did not elicit backward locomotion. Hence, a backward score of +1 indicates perfect correlation between cell labeling and backward locomotion (all samples containing the cluster walk backwards); -1, perfect anti-

correlation, (none of the samples containing the cluster walks backwards); and 0, no correlation (half the samples containing the cluster walks backwards and half does not). For the manual scoring method, we chose to analyze flies with obvious phenotypes – that is, the ones that clearly walked backwards upon optogenetic stimulation and the ones that clearly did not (n = 141 flies) – we anticipated that this would reduce false positive and false negative rates. By contrast, for the linear regression analysis we included all samples tested (n = 213 flies). Both our analyses independently revealed that 2 distinct cell types in the expression pattern of *TL-1-GAL4* – Cluster 5 and Cluster 7 – are involved in backward locomotion (Figure 2B; Tables S2 and S3).

Cluster 5 is a single pair of ascending neurons with cell bodies in the mesothoracic ganglia, arborizations in the meso- and prothoracic ganglia of the ventral nerve cord (VNC), and axonal projections that ascend to the ipsilateral side of the central brain (Figures 2C and S1; Movie M4). Cluster 7 corresponds to two pairs of neurons located in the central brain (Figures 2C and S1; Movie M5). We pooled samples from our dataset that labeled Cluster 5 alone or Cluster 7 alone and found that either of these clusters could independently elicit backward locomotion upon optogenetic stimulation (Figure S1; Movie M6). However, backward walking upon activation of Cluster 5 was more robust; 28 out of 28 flies labeling Cluster 5 walked backwards when scored manually, whereas for Cluster 7, 61 out of 72 flies did so (Figure 2B). Furthermore, the estimated negative slope for Cluster 5 was larger than that for Cluster 7 in our multiple linear regression analysis (-3.60 for Cluster 5 versus -0.41 for Cluster 7) (Figure 2B; Table S2). Given the robustness of its activation phenotype, we chose to further investigate the function of Cluster 7, hereafter referred to as Twolumps Ascending Neurons (TLA).

In order to get reproducible and specific genetic access to TLA neurons, we searched the expression patterns of GAL4 lines in the image database of the VT- [15] and GMR- [16] GAL4 collections and identified 2 lines that target TLAs without targeting Cluster 7. We generated split-GAL4 derivatives of these GAL4 lines, intersected them with cognate hemidrivers from the original *TL-1-GAL4* split-combination and used the resultant split-combinations to drive the expression of *UAS-CsChrimson::mVenus.* We found 2 intersections (*TLA-1-GAL4* and *TLA-2-GAL4)* that labeled TLAs (Figure 2D). Importantly, both *TLA-1-GAL4* and *TLA-2-GAL4* recapitulated the optogenetic activation phenotype observed in *TL-1-GAL4 UAS-CsChrimson::mVenus* flies (Figures 2E and 2F; Movie M7). Of these two

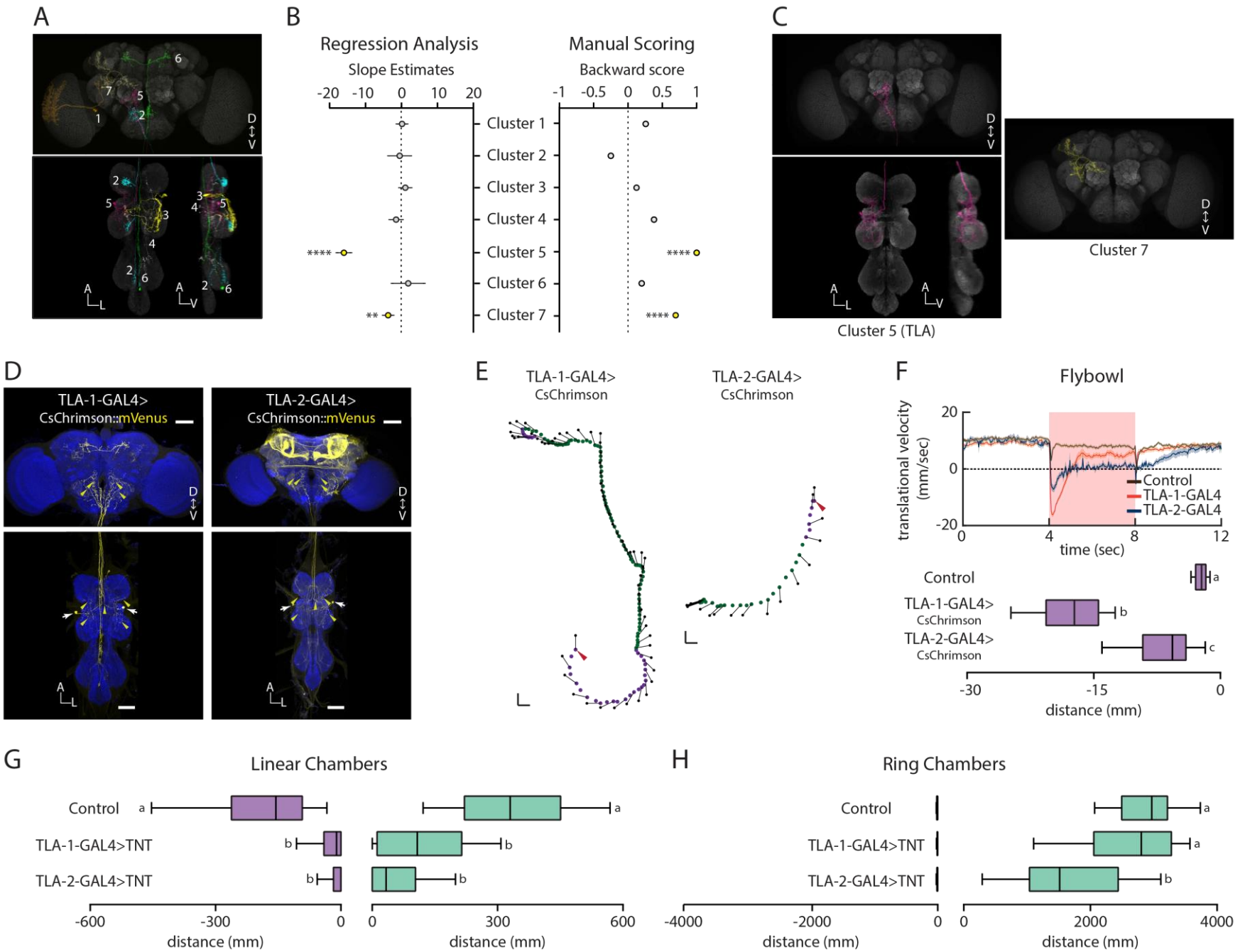
A
B
Regression Analysis
Slope Estimates
-20 -10 0 10 20
Manual Scoring
Backward score
-1 -0.5 0 0.5 1
Cluster 1
Cluster 2
Cluster 3
Cluster 4
Cluster 5
Cluster 6
Cluster 7
****
****
**
****
C
Cluster 7
Cluster 5 (TLA)
D
TLA-1-GAL4>
CsChrimson::mVenus
TLA-2-GAL4>
CsChrimson::mVenus
E
TLA-1-GAL4>
CsChrimson
TLA-2-GAL4>
CsChrimson
F
Flybowl
translational velocity (mm/sec)
20
0
-20
0
4
8
12
time (sec)
Control
TLA-1-GAL4
TLA-2-GAL4
Control
TLA-1-GAL4>
CsChrimson
TLA-2-GAL4>
CsChrimson
a
b
c
-30
-15
0
distance (mm)
G
Linear Chambers
Control
TLA-1-GAL4>TNT
TLA-2-GAL4>TNT
a
b
b
a
b
b
-600
-300
0
distance (mm)
0
300
600
distance (mm)
H
Ring Chambers
Control
TLA-1-GAL4>TNT
TLA-2-GAL4>TNT
a
a
b
-4000
-2000
0
distance (mm)
0
2000
4000
distance (mm)

Figure 2. Identification of Twolumps Ascending Neurons (TLA)

(A) The seven clusters of neurons that compose the expression pattern of *TL-1-GAL4* registered and overlaid onto a common brain and VNC reference template.

(B) Stochastic activation and labeling of *TL-1-GAL4*. Left: Slope estimates ± standard error (SE) obtained from multiple linear regression analysis (n = 213 flies). Right: Backward score for each cell cluster obtained from the blinded manual scoring method (n = 141 flies). Statistical significance was assessed using Fisher's exact test. ****$p < 0.0001$, **$p < 0.01$.

(C) A single Twolumps Ascending Neuron (TLA) (left) and a single clone from Cluster 7 (right) registered and overlaid onto a common reference template.

(D) Brain and VNC of a male carrying *TLA-1-GAL4* (left) and *TLA-2-GAL4* (right) split combination driving the expression of *UAS-CsChrimson::mVenus*, stained with anti-GFP (yellow) and nc82 counterstain (blue). Scale bar, 50 µ.

(E) Representative trajectories of flies upon optogenetic activation of TLA neurons, using *TLA-1* and *TLA-2* split-GAL4 drivers for driving the expression of *UAS-CsChrimson.* Traces include only the 4 sec stimulation window. Head positions are indicated by black dots and head-to-centroid orientations by black dashes. Arrowheads indicate position at the beginning of optogenetic stimulation. Scale bar, 1 mm x 1 mm.

(F) Top: Translational velocity versus time upon optogenetic stimulation. Dark traces indicate per-fly means over 5 trials and envelopes indicate ±SEM. Bottom: Per-fly mean over 5 trials for total distance backwards during the optogenetic stimulation window. (Control *UAS-CsChrimson*, n = 96 flies; *TLA-1-GAL4 UAS-CsChrimson*, n = 38 flies*; TLA-2-GAL4 UAS-CsChrimson*, n = 22 flies).

(G) Total walking distance in a 10-min assay in linear chambers (Control *UAS-TNT*, n = 36 flies; *TLA-1-GAL4 UAS-TNT*, n = 36 flies*; TLA-2-GAL4 UAS-TNT*, n = 36 flies).

(H) Total walking distance in a 10-min assay in ring chambers (Control *UAS-TNT*, n = 30 flies; *TLA-1-GAL4 UAS-TNT*, n = 30 flies, *TLA-2-GAL4 UAS-TNT*, n = 29 flies).

identified split-GAL4 combinations, *TLA-1-GAL4* specifically targeted TLAs while *TLA-2-GAL4* had expressions in additional neurons in the brain (Figure 2D). In linear assays, silencing the activity of TLA with TNT by using these 2 independent drivers significantly impaired backward locomotion (Figure 2G; Movie M8). Flies failed to initiate and execute backward locomotion and stalled more often, such that their overall forward locomotion also appeared impaired (Figure 2G). However, in the ring assay, where flies could walk forwards unimpeded, silencing the activity of *TLA* neurons with *TLA-1-GAL4* had no effect in forward locomotion when compared to controls (Figure 2H; Movie M9). By contrast, *TLA-2-GAL4 UAS-TNT* flies showed an additional reduction in total distance covered in forward walking state (Figure 2H; Movie M9). However, given that *TLA-1-GAL4* more specifically labeled TLAs (Figure 2D), had a stronger optogenetic activation phenotype than *TLA-2-GAL4* (Figure 2F; Movie M6), and recapitulated the initial behavioral phenotypes of *TL-1-GAL4*, we attributed the reduction in forward walking in *TLA-2-GAL4 UAS TNT* to the off-target neurons labeled in this driver.

Optogenetic activation of either MDNs or TLAs caused backward locomotion in our experiments; however, a closer look revealed intrinsic differences in the motor programs initiated by each cell-type. Bilateral activation of MDNs triggered straight backward locomotion that lasted throughout the optogenetic stimulation window (Figures 1C and 1D; Movie M3, [9]). Bilateral activation of TLAs, on the other hand, triggered backward locomotion that was transient, and had a strong turning component. Resumption of forward locomotion in flies where TLAs were activated occurred within the optogenetic stimulation window (Figures 1C, 1D, 2E, 2F; Movies M3 and M6). Interestingly, the activation phenotype of TLAs was similar to what we had previously observed upon activation of a population of visual projection neurons – the lobula columnar 16 cells (LC16) – that mediate visually-evoked backward-walking retreat in *Drosophila* by likely conveying sensory information of visual threats to MDNs [9].

What is the ethological context for TLA-mediated backward turning? To address this, we silenced the activity of TLAs in a setting where backward locomotion was more naturally triggered. Specifically, we had previously observed that flies backed up and steered away in response to head-on encounters with the wall in our circular arenas (Flybowl [9,17]) – a behavior that resembled the transient backward turning phenotype observed upon optogenetic TLA activation (compare trajectories in Figure 3A to Figures 1C and 2E). Anterior-touch

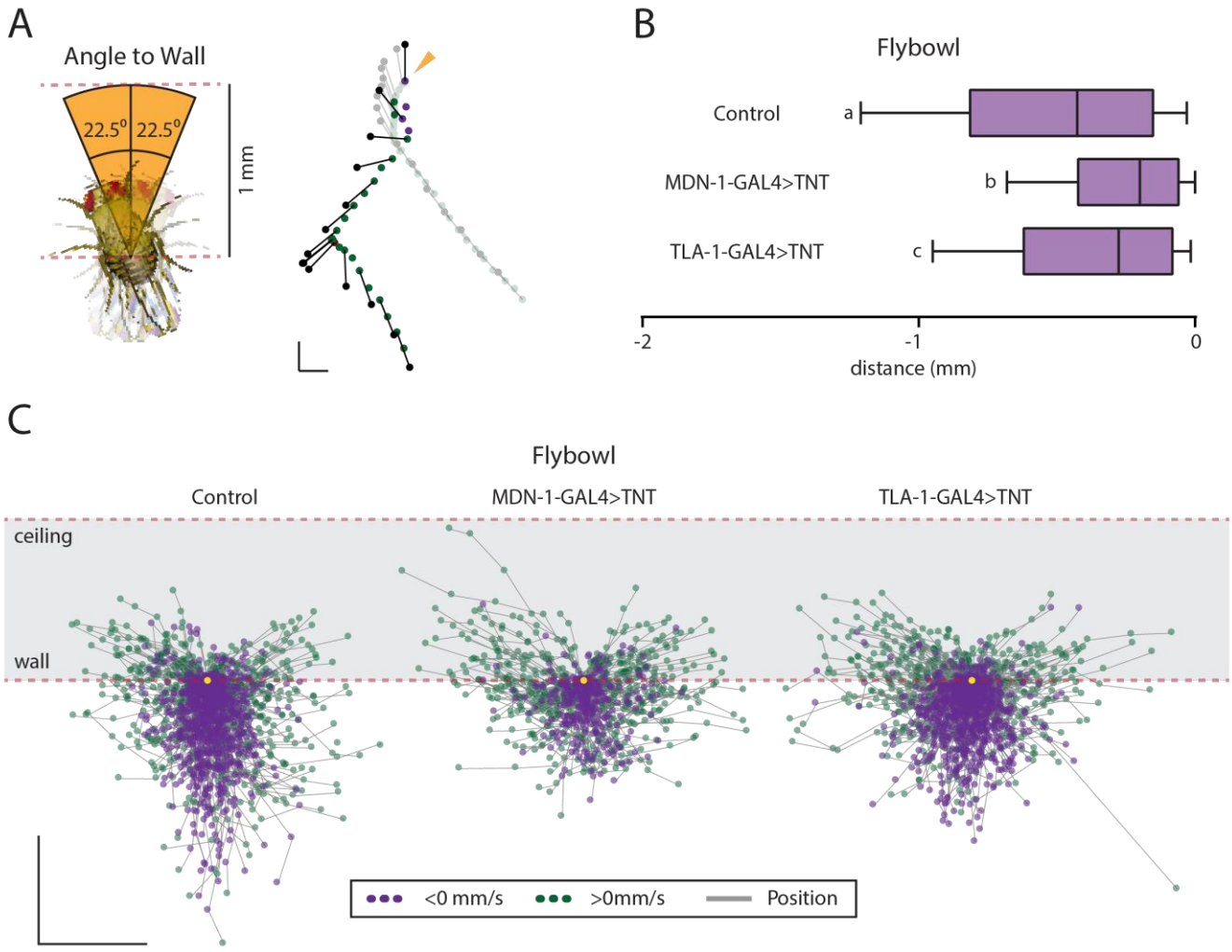

Figure 3. TLAs are involved in touch-triggered backing up

(A) Left: Orange denotes the range of angles relative to the fly's orientation during head-on collisions with the wall. Fly-wall encounters occur when the distance of the fly-centroid from the wall is <1 mm. Right: An example trajectory of fly 1 sec before (faded colors) and 1 sec during a wall-encounter.

(B) Total backward translation distances in the 200 ms period following a wall-touch (Control *BPZpGAL4DBD BPp65ADZp UAS-TNT*, n = 310 trajectories from 87 flies; *MDN-1-GAL4 UAS-TNT*, n = 185 trajectories from 70 flies, *TLA-1-GAL4 UAS-TNT*, n = 363 trajectories from 59 flies).

(C) Individual trajectories of all flies in the 200 ms period following a wall-touch. (Left: Control *BPZpGAL4DBD BPp65ADZp UAS-TNT*, n = 310 trajectories from 87 flies; Middle: *MDN-1-GAL4 UAS-TNT*, n = 185 trajectories from 70 flies; Right: *TLA-1-GAL4 UAS-TNT*, n = 363 trajectories from 59 flies). Yellow dots denote wall-touch. Boundaries for wall and ceiling are indicated. Trajectories between wall and ceiling boundaries represent instances when the flies climbed up the sloped wall. Scale bar, 1 mm x 1 mm.

triggered backing-up has also been reported in flies previously [18]. We asked whether silencing the activity of TLAs caused reductions in backward locomotion induced by head-on wall-encounters. We loaded groups of 20-30 flies in the Flybowl and allowed them to explore the arena freely in the dark, in the absence of any visual cue. We compared trajectories and backward translation distances of flies for the 180 ms following a head-on collision with the arena-wall (see Supplemental Methods), and found that silencing MDNs or TLAs significantly reduced wall-triggered reversals in walking direction when compared to controls (Figures 3B and 3C). Consistent with our observations described above, the reduction in backward translation distances was more pronounced upon silencing the activity of the MDNs compared to TLAs (Figure 3B and 3C).

Given the overall similarity in their silencing and activation phenotypes, we asked if TLA neurons and MDNs are functionally connected to each other. The MDNs are a cluster of 4 descending neurons, 2 on each side of the central nervous system. Each cell has extensive bilateral dendritic arborizations in the ventro-medial protocerebrum, an asymmetric arbor in the subesophageal ganglia (SEZ) and an axon that extends to the contralateral side of the VNC to all 3 leg neuropils [8]. To ascertain the polarity of TLA neurons, we used *TLA-1-GAL4* to drive the expression of myr-tdTomato (membrane targeted red fluorescent protein) [11] and syt-GFP (GFP tagged to the vesicle membrane protein synaptotagmin) [19]. We found co-localizations of membrane and synaptotagmin in the branches of TLAs in the brain, suggesting that the synaptic outputs of TLAs are located in the brain (Figure 4A). Owing to the absence of synaptotagmin localizations in the VNC arbors of TLAs, we inferred that the VNC branches were post-synaptic (Figure 4A). We next segmented the MDN and TLA neurons, aligned them to a common brain and VNC template following non-rigid registration, and observed that the output branches of TLAs were located in close proximity to the dendritic arbors of MDNs and the input branches of TLAs were anatomically close to the synaptic outputs of MDNs (Figure 4B and Movie M10). We combined *MDN-LexA* in double-labeling experiments with our *TLA-1-GAL4* and found that the arbors of MDNs and TLAs indeed come close to each other anatomically, but, do not obviously interdigitate (Figure 4C). Since the TLA output branches extensively followed the dendritic arborizations of the MDNs in the brain, we next asked if TLA neurons were functionally connected to MDNs in the brain. In preliminary experiments, we used our *TL-1-GAL4* split-GAL4 combination to drive the expression of CsChrimson and optogenetically activated TLAs by targeting the red light stimulation to the mesothoracic ganglia, while imaging for calcium responses in the dendritic

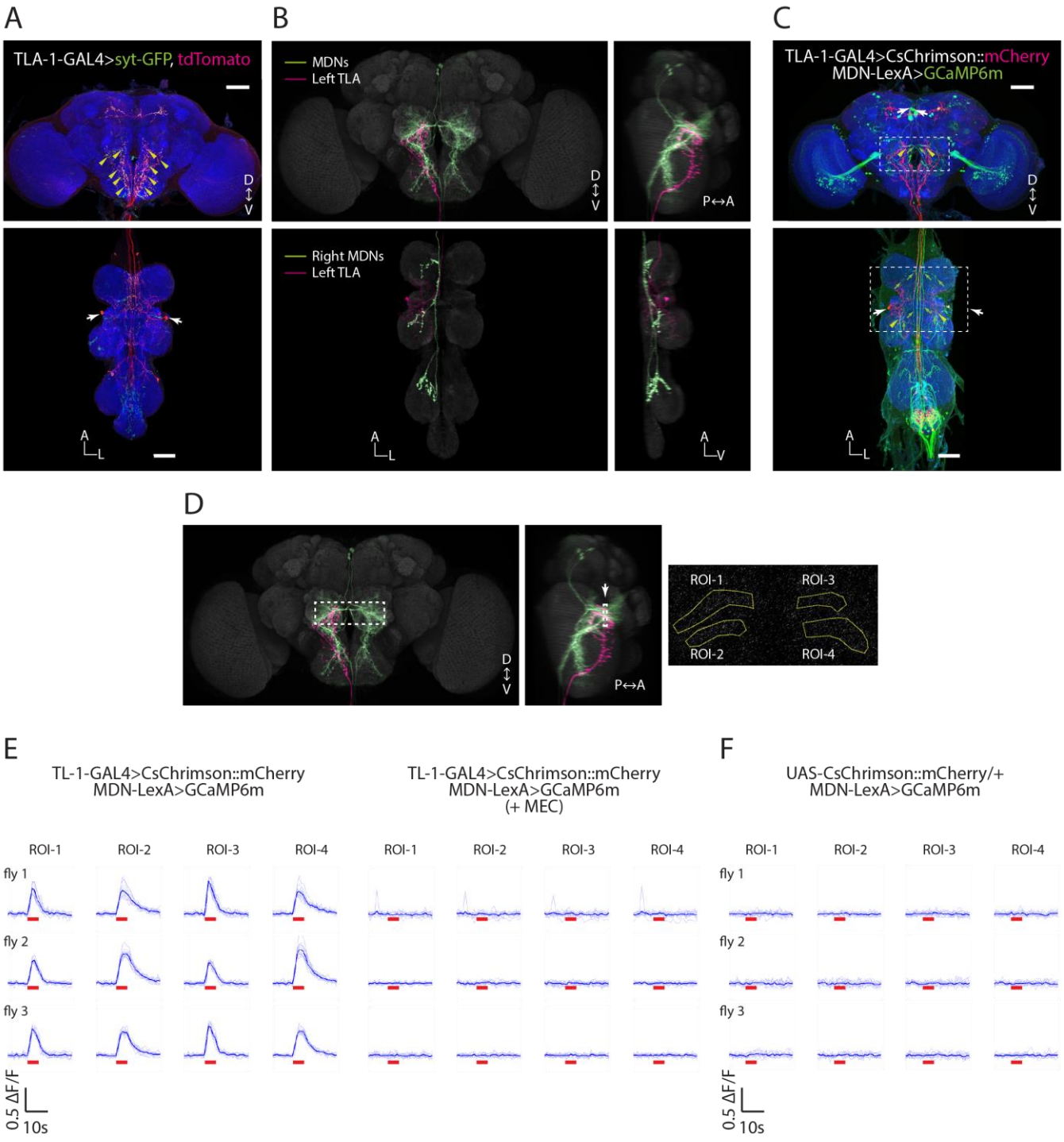
A
TLA-1-GAL4>syt-GFP, tdTomato
B
MDNs
Left TLA
Right MDNs
Left TLA
C
TLA-1-GAL4>CsChrimson::mCherry
MDN-LexA>GCaMP6m
D
ROI-1
ROI-2
ROI-3
ROI-4
E
TL-1-GAL4>CsChrimson::mCherry
MDN-LexA>GCaMP6m
TL-1-GAL4>CsChrimson::mCherry
MDN-LexA>GCaMP6m
(+ MEC)
F
UAS-CsChrimson::mCherry/+
MDN-LexA>GCaMP6m
fly 1
fly 2
fly 3
0.5 ΔF/F
10s

Figure 4. MDNs likely receive inputs from TLAs

(A) Brain and VNC of a *TLA-1-GAL4 UAS-syt-GFP UAS-tdTomato* male, stained with anti-dsRed (magenta), anti-GFP (green) and nc82 (blue). Yellow arrowheads indicate regions of synaptotagmin (*UAS-syt-GFP*) localization, and thus represent the likely sites of presynaptic specializations. White arrowheads indicate the soma of TLAs in the VNC. Scale bar, 50 µ.

(B) Segmented MDN and TLA neurons registered and overlaid onto a common reference brain and VNC template. MDNs are in green and TLAs in magenta. Areas of close proximity between MDN and TLA arborizations are observed in the central brain behind the antennal lobes, in the SEZ, and in the pro and mesothoracic segments of the VNC.

(C) Brain and VNC of a *TLA-1-GAL4 UAS-CsChrimson::mCherry MDN-LexA LexAop-GCaMP6m* male, stained with anti-dsRed (magenta), anti-GFP (green) and nc82 (blue). White arrowheads indicate the soma of MDNs in brain and TLAs in VNC. Green arrowheads indicate the branch points of MDN arbors in pro and mesothoracic ganglia. Yellow arrowheads within boxed regions indicate areas of close proximity between MDN and TLA arborizations. Scale bar, 50 µ.

(D) Left: Schematic of a brain showing MDNs and TLA neurons, with the boxed region indicating the area of interest in MDNs for calcium imaging. Right: Shapes of the 4 regions of interest (ROIs) analyzed in a typical sample.

(E) Optogenetic activation of TLA neurons elicits calcium responses in MDNs. $\Delta F/F_0$ versus time for each of the 4 ROIs from 3 flies. Each plot represents $\Delta F/F_0$ versus time plots for 12 trials of optogenetic simulation (faded blue lines), with the mean overlaid on top (dark blue line). Red dashes in each plot indicate the 5-sec stimulation window. The calcium responses in MDNs elicited by TLA activation are abolished upon application of mecamylamine. Each plot represents $\Delta F/F_0$ versus time plots for the same flies as in (E) but upon application of mecamylamine.

(F) $\Delta F/F_0$ versus time plots for each ROI upon red light stimulation in control flies.

arbors of MDNs using GCaMP6m [20] (Figure 4D). We observed calcium transients in the dendrites of MDNs in the brain (Figure 4E and 4F) in 3/3 flies tested and inferred that TLAs were likely responsible for this response. The responses were also abolished upon application of the cholinergic blocker mecamylamine (Figure 4E) and were not observed in control flies lacking any GAL4 driver (Figure 4F). Thus, our results suggest that TLAs likely provide cholinergic inputs to MDNs.

Based on our results, we propose two hypotheses for the function of TLAs – 1) they provide feedforward mechanosensory inputs to MDNs to trigger backward locomotion, or 2) they provide feedback signals to MDNs to entrain their activity upon initiation of backward locomotion.

If TLAs purely process external mechanosensory information for anterior touch, we predict that touching the head, forelegs or, more generally, the anterior end of the fly would elicit calcium responses in TLAs with a shorter latency than in MDNs, whereas touching the posterior end of the fly would elicit much weaker or no response in either of these cells. Noting that the defect in backward translation in response to wall-touch was less pronounced upon silencing the activity of TLAs compared to MDNs (Figure 3B), we infer that MDNs must also receive additional tactile information from other neurons. It is plausible that TLAs might be involved in more complex computations – they might, for example, integrate tactile stimuli with inputs from leg proprioceptors and actively modulate MDN activity based on context. Intersegmental ascending neurons that compare touch and proprioceptive signals in flies have been reported recently [21] and implicated to provide inputs to circuits that contextualize touch during self-triggered motion – for example, when a leg hits an obstruction during walking. Alternatively, it is plausible that TLAs receive feedback in the VNC from motor centers signaling that backward locomotion has been initiated, and loop back to MDNs to entrain their activity in the brain, thus sustaining or regulating backward locomotion once it is initiated. In the case that this is true, we predict that backward locomotion would elicit calcium transients in TLAs upon optogenetic activation of MDNs. Also, silencing the activity of TLAs in a background of sustained backward locomotion triggered by optogenetic activation of MDNs would impair important aspects of backward locomotion. If TLAs provide feedback signals to MDNs about the initiation of backward locomotion – the activity of TLAs would be important for backward locomotion triggered in multiple sensory contexts, including visual threats. If this is true, we predict that silencing

these neurons in visually evoked retreat (or upon optogenetic activation of LC16 visual projection neurons that artificially trigger the backward walking retreat) should have similar behavioral consequences as touch-triggered backing up.

While a definitive proof for either of these hypotheses awaits further experiments, here we have partaken a necessary first step: we have identified a vital pair of ascending neurons that interacts with MDNs and is important for naturally-triggered backward locomotion in *Drosophila*.

4.4 Author contributions

R.S. performed the behavioral experiments, the antibody staining and analyzed all related data. K.W. performed the calcium imaging experiments and analyzed all related data. R.S. and B.J.D. conceived the project and designed all experiments. R.S. wrote the manuscript.

4.5 Acknowledgements

We thank Scientific Computing, the Project Technical Resources, and Instrument Design and Fabrication teams in Janelia Research Campus for technical support. This work was supported by Howard Hughes Medical Institute.

4.6 References

1. Ayali, A., Couzin-Fuchs, E., David, I., Gal, O., Holmes, P., and Knebel, D. (2015). Sensory feedback in cockroach locomotion: current knowledge and open questions. J. Comp. Physiol. A *201*, 841–850.

2. Bässler, U., and Büschges, A. (1998). Pattern generation for stick insect walking movements—multisensory control of a locomotor program. Brain Res. Rev. *27*, 65–88.

3. Büschges, A., and Gruhn, M. (2007). Mechanosensory feedback in walking: from joint control to locomotor patterns. In Advances in Insect Physiology Insect Mechanics and Control., J. Casas and S. J. Simpson, eds. (Academic Press), pp. 193–230.

4. Buschmann, T., Ewald, A., Twickel, A. von, and Büschges, A. (2015). Controlling legs for locomotion—insights from robotics and neurobiology. Bioinspir. Biomim. *10*, 041001.

5. Dickinson, M.H., Farley, C.T., Full, R.J., Koehl, M. a. R., Kram, R., and Lehman, S. (2000). How animals move: an integrative view. Science *288*, 100–106.

6. Tuthill, J.C., and Wilson, R.I. (2016). Mechanosensation and adaptive motor control in insects. Curr. Biol. *26*, R1022–R1038.

7. Zill, S., Schmitz, J., and Büschges, A. (2004). Load sensing and control of posture and locomotion. Arthropod Struct. Dev. *33*, 273–286.

8. Bidaye, S.S., Machacek, C., Wu, Y., and Dickson, B.J. (2014). Neuronal control of *Drosophila* walking direction. Science *344*, 97–101.

9. Sen, R., Wu, M., Branson, K., Robie, A., Rubin, G.M., and Dickson, B.J. (2017). Moonwalker descending neurons mediate visually evoked retreat in *Drosophila*. Curr. Biol. *27*, 766–771.

10. Luan, H., Peabody, N.C., Vinson, C.R., and White, B.H. (2006). Refined spatial manipulation of neuronal function by combinatorial restriction of transgene expression. Neuron *52*, 425–436.

11. Pfeiffer, B.D., Ngo, T.-T.B., Hibbard, K.L., Murphy, C., Jenett, A., Truman, J.W., and Rubin, G.M. (2010). Refinement of tools for targeted gene expression in *Drosophila*. Genetics *186*, 735–755.

12. Sweeney, S.T., Broadie, K., Keane, J., Niemann, H., and O'Kane, C.J. (1995). Targeted expression of tetanus toxin light chain in *Drosophila* specifically eliminates synaptic transmission and causes behavioral defects. Neuron *14*, 341–351.

13. Klapoetke, N.C., Murata, Y., Kim, S.S., Pulver, S.R., Birdsey-Benson, A., Cho, Y.K., Morimoto, T.K., Chuong, A.S., Carpenter, E.J., Tian, Z., *et al.* (2014). Independent optical excitation of distinct neural populations. Nat. Methods *11*, 338–346.

14. Wu, M., Nern, A., Williamson, W.R., Morimoto, M.M., Reiser, M.B., Card, G.M., and Rubin, G.M. (2016). Visual projection neurons in the *Drosophila* lobula link feature detection to distinct behavioral programs. eLife *5*, e21022.

15. Tirian, L., and Dickson, B. (2017). The VT GAL4, LexA, and split-GAL4 driver line collections for targeted expression in the *Drosophila* nervous system. bioRxiv, 198648.

16. Jenett, A., Rubin, G.M., Ngo, T.-T.B., Shepherd, D., Murphy, C., Dionne, H., Pfeiffer, B.D., Cavallaro, A., Hall, D., Jeter, J., *et al.* (2012). A GAL4-driver line resource for *Drosophila* neurobiology. Cell Rep. *2*, 991–1001.

17. Robie, A.A., Hirokawa, J., Edwards, A.W., Umayam, L.A., Lee, A., Phillips, M.L., Card, G.M., Korff, W., Rubin, G.M., Simpson, J.H., *et al.* (2017). Mapping the neural substrates of behavior. Cell *170*, 393–406.e28.

18. Ramdya, P., Lichocki, P., Cruchet, S., Frisch, L., Tse, W., Floreano, D., and Benton, R. (2014). Mechanosensory interactions drive collective behaviour in *Drosophila*. Nature *519*, 233–236.

19. Zhang, Y.Q., Rodesch, C.K., and Broadie, K. (2002). Living synaptic vesicle marker: synaptotagmin-GFP. genesis *34*, 142–145.

20. Chen, T.-W., Wardill, T.J., Sun, Y., Pulver, S.R., Renninger, S.L., Baohan, A., Schreiter, E.R., Kerr, R.A., Orger, M.B., Jayaraman, V., *et al.* (2013). Ultrasensitive fluorescent proteins for imaging neuronal activity. Nature *499*, 295–300.

21. Tuthill, J., and Wilson, R. (2016). Parallel transformation of tactile signals in central circuits of *Drosophila*. Cell *164*, 1046–1059.

4.7 Supplemental Materials

4.7.1 Supplemental Figures and Tables

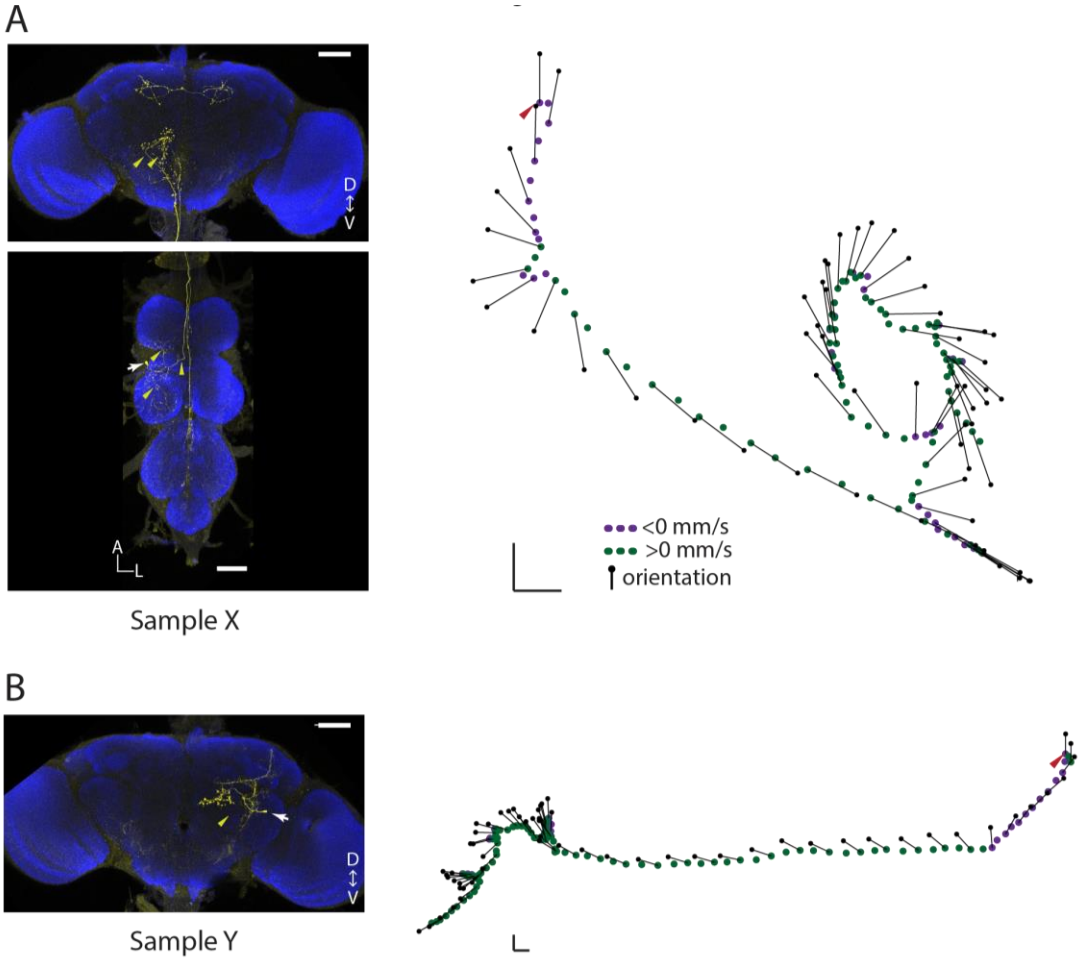
A
D
V
A
L
<0 mm/s
>0 mm/s
orientation
Sample X
B
D
V
Sample Y
C
Flybowl
None
TLA alone
Cluster 7 alone
a
b
b
-12
-6
0
distance (mm)

Figure S1

Figure S1. TLAs and Cluster 7 are independently sufficient to trigger backward locomotion upon optogenetic activation

(A) Left: Brain and VNC of a sample labeling a left TLA neuron from the stochastic labeling and activation experiments. White arrowheads indicate soma and yellow arrowheads indicate projections of the neurons. Scale bar, 50 µ. Right: Representative trajectory of the sample shown left during a 4-sec optogenetic stimulation window, color coded for backward (<0 mm/s) or forward (>0 mm/s) translational velocity. Head positions are indicated by black dots and head-to-centroid orientations by black dashes. Arrowheads indicate position at the beginning of optogenetic stimulation. Scale bar, 1 mm x 1 mm.

(B) Left: Brain of a sample labeling a single clone of TLB neuron from the stochastic labeling and activation experiments. White arrowheads indicate soma and yellow arrowheads indicate projections of the neurons. Right: Representative trajectory of the sample shown left during a 4-sec optogenetic stimulation window, color coded for backward (<0 mm/s) or forward (>0 mm/s) translational velocity. Head positions are indicated by black dots and head-to-centroid orientations by black dashes. Arrowheads indicate position at the beginning of optogenetic stimulation. Scale bar, 1 mm x 1 mm.

(C) Per-fly mean over 5 trials for backward translation distances for flies labeling with either only TLAs or only Cluster 7 activated. (None, n = 102 flies; TLAs, n =13 flies; Cluster 7, n = 80 flies).

Table S1. List of Genotypes

Figure	Genotype	Driver(s)
Figure 1A-B	w+; UAS-TNT-E/+; +/+	Control 1 [1]
	w+; 33047-p65ADZp (attP40)/+; 20742-ZpGAL4DBD (attP2)/+	Control 2
	w+; UAS-TNT-E/44845-ZpGAL4DBD (attP40); 50660-p65ADZp (attP2)/+	MDN-1-GAL4 [2]
	w+; UAS-TNT-E/33047-p65ADZp (attP40); 20742-ZpGAL4DBD (attP2)/+	TL-1-GAL4
Figure 1C	20XUAS-CsChrimson-mVenus (attP18); +/+; +/+	Control 1
	w+; 33047-p65ADZp (attP40)/+; 20742-ZpGAL4DBD (attP2)/+	Control 2
	20XUAS-CsChrimson-mVenus (attP18); 44845-ZpGAL4DBD (attP40)/+; 50660-p65ADZp (attP2)/+	MDN-1-GAL4 [2]
	20XUAS-CsChrimson-mVenus (attP18); 33047-p65ADZp (attP40)/+; 20742-ZpGAL4DBD (attP2)/+	TL-1-GAL4
Figure 2A-C	pJFRC300-20XUAS-FRT>dSTOP-FRT>-CsChrimson::mVenus (attP18), hs-FLP-PESTOpt (attP3)/+; 33047-p65ADZp (attP40)/+; 20742-ZpGAL4DBD (attP2)/+	TL-1-GAL4
Figure 2D-E	20XUAS-CsChrimson-mVenus (attP18); 125F10-p65ADZp (attP40)/+; 20742-ZpGAL4DBD (attP2)/+	TLA-1-GAL4
	20XUAS-CsChrimson-mVenus (attP18); 113C10-p65ADZp (attP40)/+; 20742-ZpGAL4DBD (attP2)/+	TLA-2-GAL4
Figure 2F	20XUAS-CsChrimson-mVenus (attP18); +/+; +/+	Control [3,4]
	20XUAS-CsChrimson-mVenus (attP18); 125F10-p65ADZp (attP40)/+; 20742-ZpGAL4DBD (attP2)/+	TLA-1-GAL4
	20XUAS-CsChrimson-mVenus (attP18); 113C10-p65ADZp (attP40)/+; 20742-ZpGAL4DBD (attP2)/+	TLA-2-GAL4
Figure 2G-H	w+; UAS-TNT-E/+; +/+	Control [1]
	w+; UAS-TNT-E/125F10-p65ADZp (attP40); 20742-ZpGAL4DBD (attP2)/+	TLA-1-GAL4
	w+; UAS-TNT-E/113C10-p65ADZp (attP40); 20742-ZpGAL4DBD (attP2)/+	TLA-2-GAL4
Figure 3B-C	w+; UAS-TNT-E/BPZpGAL4DBD (attP2); BPp65ADZp (attP40)/+	Control [1]
Figure 3B-C	w+; UAS-TNT-E/44845-ZpGAL4DBD (attP40); 50660-p65ADZp (attP2)/+	MDN-1-GAL4 [2]
	w+; UAS-TNT-E/125F10-p65ADZp (attP40); 20742-ZpGAL4DBD (attP2)/+	TLA-1-GAL4
Figure 4A	w-; UAS-syt-GFP/125F10-p65ADZp (attP40); pJFRC22-10XUAS-IVS-myr::tdTomato (attP2)/20742-ZpGAL4DBD (attP2)	TLA-1-GAL4

Figure 4C	w-; 5XUAS-CsChrimson::mCherry (su(Hw)attP5), 44845-LexAp65 (attP40)/125F10-p65ADZp (attP40); LexAop2-IVS-GCaMP6m-p10 (VK00005)/20742-ZpGAL4DBD (attP2)	TLA-1-GAL4, MDN-LexA
Figure 4E	w-; 5XUAS-CsChrimson::mCherry (su(Hw)attP5), 44845-LexAp65 (attP40)/33047-p65ADZp (attP40); LexAop2-IVS-GCaMP6m-p10 (VK00005)/20742-ZpGAL4DBD (attP2)	TL-1-GAL4, MDN-LexA
Figure 4F	w-; 5XUAS-CsChrimson::mCherry (su(Hw)attP5), 44845-LexAp65 (attP40)/+; LexAop2-IVS-GCaMP6m-p10 (VK00005)/+	Control [3]
Figure S1	pJFRC300-20XUAS-FRT>dSTOP-FRT>-CsChrimson::mVenus (attP18), hs-FLP-PESTOpt (attP3)/+; 33047-p65ADZp (attP40)/+; 20742-ZpGAL4DBD (attP2)/+	TLA-1-GAL4

Table S2. Multiple linear regression analysis for stochastic activation experiments. Related to Figure 2B.

Linear regression model: y ~ 1 + x1 + x2 + x3 + x4 + x5 + x6 + x7 (where y denotes the dependent variable and x(n) denotes the coefficient or slope estimate for the nth cluster)

	Slope estimate	Standard error (SE)	tStat	pValue
Intercept	-8.24	1.07	-7.69	0.00
x1 (Cluster 1)	0.24	1.38	0.18	0.86
x2 (Cluster 2)	-0.41	3.06	-0.14	0.89
x3 (Cluster 3)	1.15	1.60	0.72	0.48
x4 (Cluster 4)	-1.40	1.72	-0.81	0.42
x5 (Cluster 5)	-15.81	1.94	-8.15	0.00
x6 (Cluster 6)	1.95	4.45	0.44	0.66
x7 (Cluster 7)	-3.60	1.36	-2.64	0.01

Number of observations: 213; Error degrees of freedom: 205
Root Mean Squared Error: 9.39
R-squared: 0.295, Adjusted R-Squared: 0.271
F-statistic vs. constant model: 12.3, p-value = $4.33e^{-13}$

Table S3. Manual scoring for stochastic activation experiments. Related to Figure 2B.

	Cluster 1	Cluster 2	Cluster 3	Cluster 4	Cluster 5	Cluster 6	Cluster 7
Number of positives	39	3	18	20	28	3	61
Number of negatives	23	5	14	9	0	2	11
Total	62	8	32	29	28	5	72
Backward score: [(Number of Positives - Number of Negatives)/Total]	0.26	-0.25	0.13	0.38	1.00	0.20	0.69
pValue (Fisher's Test)	0.2047	1	0.8025	0.1821	< 0.0001	1	< 0.0001

4.7.2 Supplemental Movie Legends

Movies are available in the accompanying CD.

Movie M1 A-D. Silencing neurons labeled in *TL-1-GAL4* significantly impairs backward locomotion in flies. Related to Figure 1A.

Representative *UAS-TNT* (A), *TL-1-GAL4* (B), *MDN-1-GAL4 UAS-TNT* (C), *TL-1-GAL4 UAS-TNT* (D) flies in the linear assay.

Movie M2 A-D. Silencing neurons labeled in *TL-1-GAL4* does not impair forward walking. Related to Figure 1B.

Representative *UAS-TNT* (A), *TL-1-GAL4* (B), *MDN-1-GAL4 UAS-TNT* (C), *TL-1-GAL4 UAS-TNT* (D) flies in the ring assay.

Movie M3 A-D. Optogenetic activation of MDNs and neurons labeled in *TL-1-GAL4* elicit backward locomotion. Related to Figure 1C.

Optogenetic stimulation of *UAS-CsChrimson* (A), *TL-1-GAL4* (B) *UAS-CsChrimson MDN-1-GAL4* (C), *UAS-CsChrimson TL-1-GAL4* (D) flies in Flybowl. Red dots, LED indicator.

Movie M4. Anatomy of TLA neurons. Related to Figures 2B and S1.

A left TLA neuron registered to a common brain and VNC template. Related to Figures 2C and S1A.

Movie M5. Anatomy of Cluster 7. Related to Figure 2B and S1.

A single clone from Cluster 7 neurons registered to a common brain template. Related to Figures 2C and S1B.

Movie M6 A-B. Optogenetic activation of either TLA neurons alone or Cluster 7 alone can elicit backward locomotion flies in the Flybowl. Related to Figure S1.

Optogenetic stimulation of TLA alone (A), or Cluster 7 alone (B) in stochastic activation experiments. Red dots, LED indicator.

Movie M7 A-C. Optogenetic activation of TLA neurons elicits backward locomotion. Related to Figure 2E-F.

Optogenetic stimulation of *UAS-CsChrimson* (A), *UAS-CsChrimson TLA-1-GAL4* (B), and *UAS-CsChrimson TLA-2-GAL4* (C) flies in the Flybowl. Red dots, LED indicator.

Movie M8 A-C. Silencing the activity of TLA neurons significantly impairs backward locomotion in flies. Related to Figure 2G.

Representative *UAS-TNT* (A), *TLA-1-GAL4 UAS-TNT* (C), *TLA-2-GAL4 UAS-TNT* (D) flies in the linear assay.

Movie M9 A-C. Forward locomotion in *TLA-1-GAL4 UAS-TNT* and *TLA-2-GAL4 UAS-TNT* flies in the ring assay. Related to Figure 2H.

Representative *UAS-TNT* (A), *TLA-1-GAL4 UAS-TNT* (C), *TLA-2-GAL4 UAS-TNT* (D) flies in the ring assay.

Movie M10. TLA neurons and MDNs overlaid on a common brain and VNC template by non-rigid registration. Related to Figure 4B.

4.7.3 Supplemental Experimental Procedures

4.7.3.1 Fly genetics

Split-GAL4 derivatives for *TL-1-GAL4*, *TLA-1-GAL4* and *TLA-2-GAL4* split-combinations were obtained from *VT20742-GAL4*, *VT33047-GAL4*, *125F10-GAL4* and *113C10-GAL4* parental lines and inserted into the *attP2* or *attP40* landing sites by phiC31 mediated recombination. Other stocks used were *UAS-TNT-E* [1]; *MDN-1* [2]; *20XUAS-CsChrimson-mVenus* (attP18) [3,5]; *pJFRC300-20XUAS-FRT>dSTOP-FRT>-CsChrimson::mVenus* (attP18) [3,4]; *hs-FLP-PESTOpt* (attP3) [3,4]; *UAS-syt-GFP* [6] (Bloomington #6925); *pJFRC22-10XUAS-IVS-myr::tdTomato* (attP2) [7] (Bloomington #32221); *5XUAS-CsChrimson::mCherry (su(Hw)attP5)* [3]; *LexAop2-IVS-GCaMP6m-p10 (VK00005)*, Bloomington stock #44276 [3,8], *BPZpGAL4DBD* (attP2) [7], *BPp65ADZp* (attP40) [7] and *Canton S.*

All flies were raised at 25°C and 50% relative humidity. For silencing experiments with TNT, male flies were raised in a 12hr:12hr dark:light cycle on semidefined media and aged for 4-6 days prior to experiments. For silencing experiments in the linear and ring assays, groups of 12-15 flies were collected at eclosion and tested in presence of light at early morning or dusk, Zeitgeber time. For silencing experiments in the Flybowl, groups of 20-30 flies were collected at eclosion and tested in the dark. For optogenetic activation and stochastic labeling experiments with CsChrimson, all flies were raised in the dark on cornmeal-molasses food supplemented with all-trans retinal (0.2 mM prior to eclosion and 0.4 mM post-eclosion) and tested in the dark. For optogenetic activation experiments in Figures 1 and 2, groups of 20-25 male flies were collected at eclosion, aged for 5-6 days and tested in groups. For stochastic activation experiments, flies of both sexes were heat-shocked at adult stage for 2.5 hrs, tested individually in the dark in Flybowl and later retrieved for anatomical characterization.

4.7.3.2 Behavioral assays and analysis

Linear and ring assays and analysis
Linear and ring assays and computer tracker used are same as described in Chapter 3 Supplemental Methods.

Flybowl optogenetic activation assay and analysis
Optogenetic activation assay was conducted as in [3] (Supplemental Methods, Chapter 2), using the identical rig. All flies were allowed to walk for 1 minute before the first optogenetic stimulation. For the optogenetic activation experiments described in Figures 1C and 2E-F, around 20-25 flies were loaded in the chamber for 5 trials of optogenetic stimulation using red light of intensity ~ 25.2 mW/cm^2. Each trial comprised 4 s of optogenetic stimulation followed by a 30 s light-off period. For the stochastic activation experiments described in Figure 2B-C and Figure S1, flies of both sexes were individually loaded in the arena and illuminated with red light of increasing intensities – 5.6 mW/cm^2, 11.9 mW/cm^2, 25.2 mW/cm^2, 33.5 mW/cm^2, 41.5 mW/cm^2. The first batch of experiments used a protocol with 1 trial per intensity (total of 5 trials for 5 intensities) while subsequent batches used a protocol with 2 trials per intensity (total of 10 trials for 5 intensities). Datasets from all batches were pooled for the analysis shown but the conclusion drawn from the pooled dataset was independently true for the individual datasets.
Videos of freely walking flies were tracked as in [3]. We only analyzed tracking data for flies that were continuously tracked throughout the video. The tracking fit an ellipse to the fly and

forward velocity, centroid and head-extremity (nose) of the fly were calculated as in [9] for every frame. Forward velocity (referred to in figures and henceforth as 'translational velocity') was defined as the projection of the fly's velocity on its orientation direction. Time-series plots of translational velocity for optogenetic experiments show a window centered on the stimulation period, comprising 4 s before, 4 s during and 4 s after optogenetic stimulation. Backward translation upon optogenetic stimulation was calculated by integrating the area under the translational velocity versus time plots whenever translational velocity was negative. Trajectories of flies upon optogenetic stimulation were generated by plotting the centroid positions of the fly at every frame of the stimulus window. The orientations of flies were denoted as dashes joining the head of the fly to the centroid for every alternate frame in the stimulus window (15 fps).

Flybowl silencing assay and analysis

All experiments were conducted in the dark to eliminate visual cues. To analyze backward translation distances and trajectories of flies in response to wall-touch, we first detected instances of fly-wall encounters. We defined head-on collisions with wall as events when the fly faced the wall, its centroid was <1 mm away from the wall, and the head-direction was $<\pm 22.5^{\circ}$ to the normal to the wall. Encounters lasted for several frames before the fly turned away or backed up from the wall. We hence defined an encounter-bout to last for 100 frames from the initial point of contact and identified a single-frame 'wall-touch' event as the time point within each bout when the fly was closest to the wall. We calculated the trajectories and backward translation distances for the subsequent 180 ms (6 frames) starting from the frame of wall-touch.

4.7.3.3 Immunohistochemistry and imaging

Immunohistochemistry and imaging used identical protocols as in Chapter 3 Supplemental Methods, with the exception that we stained flies expressing *20XUAS-CsChrimson-mVenus* using the protocol described in https://www.janelia.org/sites/default/files/Project%20Teams/Fly%20Light/FL%20Protocol%20-%20Adult%20IHC%20-%20Anti-GFP.pdf. Flies expressing *5XUAS-CsChrimson::mCherry LexAop2-IVS-GCaMP6m-p10* in Figure 4C were stained using the protocol described in https://www.janelia.org/sites/default/files/FL%20Protocol%20-%20Adult%20IHC%20-%20Polarity%20Sequential.pdf with the modifications that we used chicken anti-GFP (1:1500, Abcam), rabbit anti-dsRed (1:1000, Clontech Laboratories), and secondary AF488 anti-chicken (1:800, Thermo Fisher Scientific), Cy3 anti-rabbit (1:1000, Jackson ImmunoResearch), and Cy5 anti-mouse (1:1000, Jackson ImmunoResearch) antibodies. Movies showing segmentations of TLAs and overlaid segmentations of MDNs and TLAs onto a reference brain or ventral nerve cord template were generated using Fluorender [10], an image-renderings software.

4.7.3.4 Calcium imaging and analysis

Calcium imaging experiments used identical protocols as in [3] (Supplemental Methods, Chapter 2) and were analyzed similarly with the following modifications: The LED light source (~660 nm) for optogenetic activation was targeted to the mesothoracic ganglia in the VNC in an attempt to specifically target TLAs in the VNC without activating Cluster 7. Each fly was tested for 12 trials of optogenetic stimulation and each trial comprised 5-sec of red-light activation followed by 35 sec of light-off period. For each time-series experiment, $\Delta F/F_0$ values were calculated for 4 distinct regions of interests (ROIs) in MDN processes – 2

ROIs/side of the brain. The 2 ROIs were located in the branches of MDNs located in the upper and lower lateral accessory lobe (LAL).

4.7.4 Supplemental References

1. Sweeney, S.T., Broadie, K., Keane, J., Niemann, H., and O'Kane, C.J. (1995). Targeted expression of tetanus toxin light chain in Drosophila specifically eliminates synaptic transmission and causes behavioral defects. Neuron *14*, 341–351.

2. Bidaye, S.S., Machacek, C., Wu, Y., and Dickson, B.J. (2014). Neuronal control of *Drosophila* walking direction. Science *344*, 97–101.

3. Sen, R., Wu, M., Branson, K., Robie, A., Rubin, G.M., and Dickson, B.J. (2017). Moonwalker descending neurons mediate visually evoked retreat in *Drosophila*. Curr. Biol. *27*, 766–771.

4. Wu, M., Nern, A., Williamson, W.R., Morimoto, M.M., Reiser, M.B., Card, G.M., and Rubin, G.M. (2016). Visual projection neurons in the *Drosophila* lobula link feature detection to distinct behavioral programs. eLife *5*, e21022.

5. Klapoetke, N.C., Murata, Y., Kim, S.S., Pulver, S.R., Birdsey-Benson, A., Cho, Y.K., Morimoto, T.K., Chuong, A.S., Carpenter, E.J., Tian, Z., *et al.* (2014). Independent optical excitation of distinct neural populations. Nat. Methods *11*, 338–346.

6. Zhang, Y.Q., Rodesch, C.K., and Broadie, K. (2002). Living synaptic vesicle marker: synaptotagmin-GFP. Genesis. *34*, 142–145.

7. Pfeiffer, B.D., Ngo, T.-T.B., Hibbard, K.L., Murphy, C., Jenett, A., Truman, J.W., and Rubin, G.M. (2010). Refinement of tools for targeted gene expression in *Drosophila*. Genetics *186*, 735–755.

8. Chen, T.-W., Wardill, T.J., Sun, Y., Pulver, S.R., Renninger, S.L., Baohan, A., Schreiter, E.R., Kerr, R.A., Orger, M.B., Jayaraman, V., *et al.* (2013). Ultrasensitive fluorescent proteins for imaging neuronal activity. Nature *499*, 295–300.

9. Kabra, M., Robie, A.A., Rivera-Alba, M., Branson, S., and Branson, K. (2012). JAABA: interactive machine learning for automatic annotation of animal behavior. Nat. Methods *10*, 64–67.

10. Wan, Y., Otsuna, H., Chien, C.-B., and Hansen, C. (2012). FluoRender: an application of 2D image space methods for 3D and 4D confocal microscopy data visualization in neurobiology research. IEEE Pac. Vis. Symp. Proc. IEEE Pac. Vis. Symp., 201.

Discussion

The moonwalker descending neurons (MDNs) are 2 pairs of 'command' neurons that are necessary and sufficient for backward locomotion in *Drosophila* [1]. The discovery of MDNs provided a key toehold in our inroads to understanding locomotion circuits in *Drosophila*. In this work, I have extended our understanding of backward locomotion by characterizing additional neurons important for backward walking. At least a subset of these identified neurons constitutes inputs or putative outputs of MDNs.

Historically, the MDNs were identified in an unbiased neuronal activation screen for directed walking. Upon thermogenetic activation, flies expressing a heat-sensitive cation channel in MDNs walked several millimeters backwards. By designing an assay chamber where flies navigated down a narrow constricted groove to a dead-end, we were able to trigger backward locomotion in a more natural setting. Wild-type flies walked backwards in this scenario; however, silencing the activity of MDNs resulted in flies getting stuck at the end of the grooves. These results proved that MDNs were necessary for backward locomotion in flies. Furthermore, this assay formed the basis for our search for additional neurons involved in backward walking. The discovery of MDNs was a vital starting point, but several important questions remained: for instance, what is the nature of sensory cues that triggers MDN activation in an ethological context? And how exactly does MDN activity translate into coordinated backward-stepping of all six legs? In this work, I presented some inroads to both these questions.

Towards the first question, I mapped two sensory inputs to MDNs: visual and mechanosensory. The visual input corresponds to a population of visual projection neurons – the lobula columnar 16 cells (LC16) [2] that encode visual threats and the mechanosensory input corresponds to neuronal pathways that convey tactile information from anterior-body touch. The latter possibly includes a pair of ascending neurons – the Twolumps ascending neurons (TLAs) – that are functionally connected to MDNs and important for backward locomotion triggered by head-on collisions with physical obstructions. Towards the second question, I used our groove assay to conduct a large unbiased neuronal silencing screen using the split-GAL4 intersectional system, which provided an extensive list of hits labeling sparse to moderate populations of neurons important for backward locomotion. Interestingly, the expression patterns of these hits were enriched in the VNC, suggesting the involvement of a relatively large number of premotor circuits in the VNC for the execution of backward

locomotion. A notable hit from this screen was a cluster of 4 local interneurons in the metathoracic ganglia – the John Cleese Neurons (JCNs) – that are necessary for backward locomotion and appear to trigger hindleg extensions. We speculate that the latter could be important for the swing phase of backward walking.

5.1 Sensory cues and neuronal circuits that activate MDNs

Generally, it is thought that backward locomotion is an evasive action [1–13]. In most of these cases, backward locomotion is accompanied by a turn which results in a reorientation away from the perceived threat. In *Drosophila*, behavioral studies have indicated that flies can be triggered to walk backwards by vision and touch [1,9,10,13]. However, the circuitry for these sensory inputs had remained undiscovered. Our work has made the first significant inroads into the circuits that underlie these sensory inputs. We find that visual input is conveyed to MDNs by a set of neurons known as the LC16 cells [2]. In addition, our screen uncovered neurons (the TLAs) that are putative mechanosensory inputs to backward walking. Importantly, both of the LC16 visual input and the TLA mechanosensory input signal via MDNs. Artificial activation of either LC16 or TLAs resulted in a large turning component to the backward walking – consistent with the turning component seen during natural evasive responses.

MDNs receive inputs from threatening visual stimuli

Wild-type fruit flies are known to retreat from ambush predators (such as nymphal praying mantids) by walking a few steps backwards and steering away [9]. In laboratory conditions, a synthetic predator-mimicking looming stimulus elicits similar backward walking retreat in flies. The LC16 population responds to artificial looming stimuli, and furthermore, optogenetic activation of these cells elicits backward turning that resembles behavioral features of the loom-triggered retreat [13]. In Chapter 2 [2], we presented data from behavioral epistasis, functional imaging and stochastic activation experiments to prove that MDNs are necessary for LC16-triggered backward locomotion and that asymmetric activation of the left and right MDNs could elicit backward turns. Based on these results, we infer that LC16 and MDNs are critical circuit elements that transduce threatening visual stimuli to directed locomotor output during visually evoked retreat.

MDNs receive mechanosensory inputs from anterior-body touch

Foraging flies can reach high densities in food (>1 fly/cm^2) [14]. We speculated that flies might frequently bump into each other in crowded conditions, thereby requiring them to back-up and steer away in response to head-on collisions. We predicted that MDNs might play a key role in such reflexive avoidance turns. In our behavioral assays, head-on encounters with physical obstructions (for example other flies or arena walls) elicited transient backward turning in walking flies. In Chapter 4, we showed that silencing the activity of MDNs significantly reduced back-ups triggered by such wall encounters. We also identified a pair of ascending neurons (from our unbiased silencing screen) – the TLAs – that likely conveys the mechanosensory information from anterior-body touch to MDNs. TLAs provide functional inputs to MDNs and bilateral optogenetic activation of TLAs elicits backward locomotion that matches behavioral features of wall-triggered back-ups in wild-type flies. Furthermore, like in MDNs, silencing the activity of TLAs significantly reduces total backward locomotion triggered by head-on wall encounters.

MDNs independently control left and right leg movement during backward turning

Overall, our results suggest that MDNs receive multimodal aversive sensory stimuli and mediate evasive walking in specific ethological contexts. Previously, activation of MDNs had been shown to trigger straight backward locomotion [1]. However, we observed that evasive backward walking in response to either wall touch or a looming stimulus involved only a few backward steps, and included a turning component that allowed reorientation to a new direction away from the aversive cue. Likewise, we found that artificial bilateral activation of either LC16 or TLAs resulted in a large turning component. One possibility is that slight asymmetries existed in the delivery of optogenetic stimuli in our assays, resulting in asymmetric activation of the two sides of the nervous system and a lateralization of movement. However, bilateral activation of MDNs in the same assay elicited straight backward locomotion in flies, with little turning. Hence it is possible that the turning component of LC16 and TLAs existed regardless of the asymmetry of the stimuli – suggesting that the underlying circuit is biased to generate an asymmetric output. Two questions are important to answer in order to understand these observations: 1) is the turning component conveyed through MDNs or via a parallel pathway, and 2) what are the circuit elements that reinforce the asymmetry during LC16 and TLA activation?

Our stochastic activation experiments showed that activation of a single MDN cell (1 out of 4) elicited transient backward walking, with a turning component, followed by forward

locomotion – suggesting that weak MDN activation (i.e activation of a single cell in the cluster) could be sufficient to trigger transient backward locomotion (Chapter 2, Figure 4; 1/0 MDN trajectories). Furthermore, asymmetric activation of MDNs elicited contralateral turns (with respect to the MDN soma in the brain), suggesting that MDNs can trigger backward translation with a directed turning component. We speculate that under natural conditions, a visual threat (conveyed by LC16) or mechanical obstruction (perhaps conveyed by TLAs) might asymmetrically activate MDNs leading to an evasive or avoidance turn. We infer that the major turning component seen in LC16 and TLA-triggered backward locomotion is most likely conveyed via MDNs rather than via a separate pathway.

MDNs comprise 4 cells – two on each side of the brain. Are all of these cells identical or could the turning component come from distinct functions of each of the 4 cells? Bilateral activation of 4 (2/2) MDNs results in straight backward locomotion; bilateral activation of 2 (1/1) results in a slight lateralization of backward movement (Chapter 2, Figure 4; compare 1/1 MDN trajectories with 2/2 MDN trajectories). Could this be attributed to the fact that in the cases where we stochastically labeled 1/1 MDNs, we ended up activating only 1 functional cell that triggered backward translation? In approximately half of our samples labeling only 1 MDN cell, a careful analysis of MDN anatomy revealed a missing branch in the metathoracic ganglia – thus, anatomically the 4 cells are not completely identical. However, further careful analysis revealed that optogenetic activation of any single MDN resulted in comparable backward translational distances and angles turned (Appendix; Chapter 2). So, despite subtle differences in anatomy, the 4 MDNs are likely to be functionally equivalent, at least within the detection limits of our locomotion in our assay.

Bilateral optogenetic activation of all four MDNs triggered straight backward locomotion; bilateral activation of either LC16 or TLAs elicited backward walking with a strong turning component. How does a symmetric trigger delivered to LC16 or TLAs result in what looks like an asymmetric output from MDNs? Interestingly, the answer could be different for LC16 and TLAs based on their respective anatomy and our results from unilateral optogenetic activation experiments.

Like asymmetric MDN activation, asymmetric activation of LC16 cells results in contralateral turns. We can therefore infer that the asymmetric activation of LC16 is faithfully conveyed to asymmetric MDN activation, leading to directed withdrawal from a perceived visual threat. Consistent with this observation, the anatomy of LC16 shows that it does not project across the left and right brain hemispheres. But why does symmetric LC16 activation result in asymmetric output from MDNs? LC16 is not directly synaptically

connected to MDNs. We could imagine two broad (not mutually exclusive) scenarios: Simply by virtue of being one or a few synapses away from MDNs, small inter-hemispheric differences in the activity of LC16 can get amplified in the downstream synapse(s) leading to unilateral MDN activation. Alternatively, intervening circuits between LC16 and MDNs might include mutually inhibitory neurons that augment the small left-right differences in the activity of LC16 to cause asymmetric activation at the level of MDNs.

Optogenetic activation of TLAs in ex-planted nervous system elicits calcium responses in MDNs. Much like the LC16 cells, symmetric activation of the TLAs results in a strong turning component. These observations imply that MDNs could be asymmetrically activated even in the lack of asymmetric TLA activation. However, a few notable differences exist between LC16 and TLAs. First, TLAs are anatomically closer to MDNs and the synaptic processes of TLAs follow the dendritic arbors of both left and right MDNs in the brain. The anatomy of the TLAs do not immediately imply asymmetric inputs to MDNs, at least not in the same manner as LC16. Furthermore, while asymmetric activation of LC16 results in contralateral turns [13], asymmetric activation of TLAs show backward turning without any directional bias (as observed in our stochastic activation experiments in Chapter 4, data not shown). Unlike LC16, the spatial information from TLAs is not faithfully conveyed to the MDNs. Our stochastic activation experiments suggest that while activation of all 4 MDNs elicits straight backward walking, bilateral activation of 2 versus 4 MDN cells can result in relatively more turning, the latter having no directional bias (compare trajectories of 1/1 versus 2/2 MDNs in Chapter 2, Figure 4; trajectories are more curved for 1/1 MDNs). These results suggest that weak bilateral MDN activation can already lead to a weak turning component. We speculate that TLAs may provide such weak excitatory drive to MDNs to trigger turning without any directional bias.

5.2 Putative downstream neurons to MDNs and VNC control of backward locomotion

How are the motor commands of MDNs implemented to execute backward walking and turning? Quiescent headless flies expressing CsChrimson in MDNs show coordinated backward locomotion upon optogenetic activation (Chapter 3, Figure 7). Once the optogenetic activation of MDNs is removed, flies cease to move backwards (Chapter 3, Movies M8 and M9). Stochastic asymmetric activation of MDNs leads to contralateral turns. The observation of coordinated backward locomotion in headless flies demonstrates that the

circuitry for executing backward locomotion largely resides within the VNC. The termination of backward walking upon stimulus removal shows that the VNC circuits require tonic input to remain active. The contralateral turns upon asymmetric MDN activation demonstrate that MDNs can independently control the left and right sides of the body. These observations give us the first cursory characteristics of MDN output. However, the circuit level details remain a mystery. We do not know if fruitflies use autonomous pattern generators (so-called central pattern generators (CPGs) i.e, circuits that produce a rhythmic output without receiving a rhythmic input) for generating rhythmic limb movements. If these CPGs do exist, we will need to understand how MDNs trigger their activity. We will also need to understand how MDNs operate in conjunction with sensory feedback to maintain and coordinate backward locomotion. While we do not have answers to these questions, we have made advances towards identifying VNC circuit elements thanks to the results from our neuronal silencing screen.

Our unbiased neuronal silencing screen used the split-GAL4 intersectional strategy (Chapter 3) to look for intersections which when used to express TNT impaired backward walking. This screen generated an extensive list of split-GAL4 hits that label sparse to moderate populations of neurons. We further characterized the hits from our screen by using an unbiased clustering approach. Specifically, this allowed us to cluster the hits into distinct silencing phenotypes – likely reflecting circuit elements that contained common elements. Intersections with interesting locomotion phenotypes included several neurons in the VNC, comprising local interneurons, intersegmental neurons, ascending neurons and putative mechanosensory neurons. Indeed, we observed an overall enrichment of hits with expression in the VNC, suggesting that a relatively rich set of computations must occur in the premotor VNC circuits to execute backward locomotion. The discovery of the MDNs provided a key inroad into our understanding of backward locomotion. Likewise, we believe that the hits from our unbiased screen open up the possibility to address several outstanding questions in locomotion. Amongst these questions we feel that at least three deserve a more extensive discussion. First, how does a fly switch between forward and backward locomotion? Second, how is inter-leg and intra-leg coordination achieved during locomotion? And finally, how do forward and backward locomotor circuits interact to ensure that competing modes of locomotion do not clash?

Switch between forward and backward locomotion

We can imagine two broad scenarios for the VNC circuits downstream MDNs: 1) There could exist two (or more) stable states (attractor-like states) of VNC network activity, corresponding to forward and backward walking. MDNs could switch the bias of this bi-stable circuit to backward walking state. 2) Alternatively, MDNs could trigger a distinct pattern-generating circuit, largely non-overlapping with the pattern-generator mediating forward walking.

What can we glean from studies of locomotion in other organisms? In humans, it has been suggested that motor pattern generators controlling forward and backward locomotion are largely non-overlapping [15] and independently adaptable (challenging a previous study [16] that argued for a common locomotor CPG). The primitive tetrapod salamander has also been proposed to use two autonomous pattern generators for forward and backward locomotion [17]. However, it has been proposed in stick insects by theoretical studies [19] and demonstrated in lampreys experimentally [20,21] that a common locomotor pattern generator is responsible for both forward and backward locomotion. The switch from forward to backward locomotion takes place because the common locomotor pattern generator exists in a bistable state.

We do not yet have evidence on which of these models is true for *Drosophila*, but hits from our silencing screen might provide some insights. In future studies, if one were to find that MDNs trigger a pattern-generator that is specialized for backward locomotion, silencing components of this pattern-generator would specifically affect backward locomotion with no effect on forward locomotion. Furthermore, tonic activation of MDNs would produce rhythmic activity in these neurons even in a 'brain on a dish' preparation. By contrast, one might find that the MDNs reverse walking direction by causing a state-dependent switch in the network activity of VNC without employing specialized CPGs. In such a case, we would expect the involvement of higher order neurons in the VNC for the actual reversal of walking direction – ones that flip the switch of the bi-stable VNC circuit, as those seen in stick insects. Silencing the activity of these neurons would result in a specific defect in backward locomotion but, in contrast to putative elements of CPGs, these neurons should lack intrinsic rhythmic properties. Several intersections in our silencing screen yielded flies with specific backward locomotion defects that had no impairment in forward walking. Many of these intersections label interneurons spatially restricted to the VNC. Future experiments can resolve whether these VNC interneurons correspond to neurons with intrinsic rhythmic

properties (i.e. CPG elements) or correspond to higher-order neurons that switch the bias of the bi-stable network activity in the VNC.

The change in walking direction may not simply require a reversal of limb motion but instead might require distinct limb movements that are truly unique to the walking state. Our screen yielded evidence that just such a unique leg movement does exist during backward locomotion. We observed that joint movements in hindlegs initiate backward locomotion (Chapter 3, Movie M9). A notable hit from our silencing screen includes a cluster of 4 local interneurons in the metathoracic ganglia – the John Cleese Neurons – that are necessary for backward locomotion and appear to trigger hindleg extensions during the swing phase of backward locomotion. Such elaborate hindleg extensions are rarely observed during the stance phase of forward locomotion. Along with the JCNs, it is of course possible that additional VNC interneurons identified in our screen might constitute subsets of neurons controlling specific joint movements unique for backward locomotion and dispensable for forward walking.

Coordination of backward locomotion

Optogenetic activation of MDNs switches the phase of muscle activation in individual legs but in a way that the individual segments of legs are appropriately coordinated within each step cycle. Flies with activated MDNs walk with a coordinated, reversed metachronal gait [1]. What is the nature of the computations that maintains inter-leg and intra-leg coordination during backward walking? And what are the relative contributions of sensory feedback and central circuits in coordinating backward locomotion in *Drosophila*? In the lamprey spinal cord, central circuits play a prominent role in coordinating the motor outputs of segmental CPGs [21–25]. Stick insects, on the other hand, predominantly rely on sensory feedback for intra-leg and inter-leg coordination (for review see [18,19,26–38]). It has been suggested that stick insects are more tuned to sensory feedback as they operate on low frequency cycles during walking and have to cope with the challenges of moving through rugged terrain. In contrast to stick insects, fast swimming lampreys move through a largely homogeneous substrate and need a fast central predictive component to maintain their speed on a cycle-to-cycle basis [39]. Lampreys, thus, rely less on sensory feedback and more on prominent central control for coordinated swimming.

How do flies compare to stick insects and lampreys? Flies walk faster than stick insects and may thus have different relative contributions of sensory feedback and central circuits for coordination. Maintaining rapid movement might, for instance, involve less autonomy in the

CPGs (i.e, more coupling between CPGs of the different joints) in *Drosophila* compared to stick insects. On the other hand, the importance of proprioceptive feedback for limb coordination in *Drosophila* is also clearly seen in our experiments. Specifically, we observed a dramatic difference in leg movements during backward locomotion triggered in suspended versus non-suspended flies – coordination among legs was severely impaired (Chapter 3) in the absence of contact with a substrate. Interestingly, the hindlegs in suspended flies still showed some rhythmic activity; depression, levation, extensions, and retractions were still interspersed with low-amplitude protractions and flexions even in the absence of ground contact. These observations suggest that coordination of backward locomotion in *Drosophila* might rely on a combinatorial input of central computations and sensory feedback – sensory feedback might be more important for inter-leg coordination than intra-leg coordination, while the latter might rely more on central circuits. However, the nature of the neuronal computations and the identity of underlying circuits responsible for inter-leg and intra-leg coordination in *Drosophila* still remain unknown. A careful analysis of joint movements and gait upon silencing the activity of neurons labeled by our silencing screen hits will, in future, give us important inroads to anatomically and functionally dissect these circuits.

5.3 Control of backward versus forward locomotion

Apart from providing an extensive list of hits labeling neurons important for backward locomotion, our silencing screen also identified hits that had defects in forward locomotion. These might include common elements between forward and backward locomotion – such as components of a common locomotor pattern generator. Alternatively, these might constitute higher order neurons that mediate interactions between forward and backward locomotion or circuit elements specific for forward locomotion. While our screen was not specifically designed to identify such components, we can postulate why they might have been found. In general, in our screen, flies do not tend to walk backwards until they reach the end of the linear assay chamber – reaching the dead-end provides the trigger to initiate backward walking. A fly with reduced forward locomotion will therefore take longer to reach the end of the chamber and would be triggered less frequently to reverse direction, resulting in an overall decrease in backward locomotion (hence being identified as a hit in our screen). However, we predict (based on studies in *C. elegans* where forward and backward circuits have been defined at a circuit level [3,40]) that there exist extensive synaptic connections between the forward and backward circuits. In *C. elegans*, reciprocal connections between

these circuits serve to ensure that the organism exists in one of two states [3,41–43]. While we don't currently know the circuits for forward locomotion in *Drosophila*, we can predict that once they are found they will have extensive interplay with the backward circuit. We can further postulate some of the hits that display defects in forward locomotion form part of this interconnected network – specifically, we anticipate that if we identified a neuron that was needed for the mutual inhibition between the circuits, the forward and backward walking circuits would be equally active, leading to clashing signals and defects in both forward and backward locomotion. The hits from our screen might contain some of these neurons that mediate the interactions between the circuits controlling forward and backward locomotion.

Consideration of whether distinct pattern-generators exist for backward and forward locomotion will further inform the search for putative neurons that mediate interactions between forward and backward walking circuits. For example, if there are CPGs that are specific to backward and forward locomotion, it follows that one set of CPGs must be shut down while the other is active to prevent clashing motor output. Presynaptic sites of MDNs are present in the leg neuropils as well as the arbors in the subesophageal ganglia (SEZ). The outputs in the SEZ might represent the sites of interaction with the forward walking circuits. If the synapses in the SEZ represent the sites through which forward walking CPGs are turned off, it would demonstrate that the inhibition is MDN-mediated and takes place in the brain. Alternatively, the mutual inhibition might take place via MDN-mediated recruitment of higher order neurons in the VNC. Of course, the reciprocal inhibition between forward and backward circuits is also likely to occur if common locomotor CPGs control both forward and backward walking. Nonetheless, due to the convergence on a single circuit element, the mutual inhibition need not be as complete in order to get a coordinated output – all that would be necessary would be a pattern generator that preferentially exists in one of two states. CPGs that exist in a small number of stable states have been described in numerous organisms (for reviews see [44–46]). In this example, MDNs would not need to actively inhibit forward walking circuits, but could instead shift the bias of the common bistable locomotor CPGs.

5.4 Concluding remarks

Overall, this study has laid the groundwork to gain a circuit level understanding of backward locomotion in *Drosophila*. Our results suggest that MDNs process multimodal aversive stimuli to mediate evasive backward walking in specific contexts. We conducted an unbiased

neuronal silencing screen and identified several small to moderate populations of neurons that are critical for the execution of backward locomotion in the VNC. Some of the VNC interneurons identified in our screen are specifically involved in backward locomotion and hence provide tools to dissect the VNC pathways that implement the commands of MDNs. Additionally, other hits retrieved from this screen label neurons implicated in forward locomotion and provide inroads to understanding how the forward and backward walking circuits interact. Using backward locomotion as a model, our studies provide a framework within which we can address the larger question of how sensory information is converted into appropriate motor action and how animals execute complex and flexible locomotor patterns in nature.

5.5 References

1. Bidaye, S.S., Machacek, C., Wu, Y., and Dickson, B.J. (2014). Neuronal control of drosophila walking direction. Science *344*, 97–101.

2. Sen, R., Wu, M., Branson, K., Robie, A., Rubin, G.M., and Dickson, B.J. (2017). Moonwalker descending neurons mediate visually evoked retreat in drosophila. Curr. Biol. *27*, 766–771.

3. Chalfie, M., Sulston, J.E., White, J.G., Southgate, E., Thomson, J.N., and Brenner, S. (1985). The neural circuit for touch sensitivity in *Caenorhabditis elegans*. J. Neurosci. *5*, 956–964.

4. Graham, D., and Epstein, S. (1985). Behaviour and motor output for an insect walking on a slippery surface: II. backward walking. J. Exp. Biol. *118*, 287–296.

5. Kaplan, J.M., and Horvitz, H.R. (1993). A dual mechanosensory and chemosensory neuron in *Caenorhabditis elegans*. Proc. Natl. Acad. Sci. U. S. A. *90*, 2227–2231.

6. Hilliard, M.A., Bergamasco, C., Arbucci, S., Plasterk, R.H., and Bazzicalupo, P. (2004). Worms taste bitter: ASH neurons, QUI-1, GPA-3 and ODR-3 mediate quinine avoidance in *Caenorhabditis elegans*. EMBO J. *23*, 1101–1111.

7. Kass, J., Jacob, T.C., Kim, P., and Kaplan, J.M. (2001). The egl-3 proprotein convertase regulates mechanosensory responses of *Caenorhabditis elegans*. J. Neurosci. *21*, 9265–9272.

8. McClellan, A.D. (1989). Control of locomotion in a lower vertebrate, the lamprey: brainstem command systems and spinal cord regeneration. Integr. Comp. Biol. *29*, 37–51.

9. Parigi, A., Porter, C., Cermak, M., Pitchers, W.R., and Dworkin, I. (2014). How predator hunting-modes affect prey behaviour: capture deterrence in drosophila melanogaster. Biorxiv, 10330.

10. Ramdya, P., Lichocki, P., Cruchet, S., Frisch, L., Tse, W., Floreano, D., and Benton, R. (2014). Mechanosensory interactions drive collective behaviour in *Drosophila*. Nature *519*, 233–236.

11. Sambongi, Y., Takeda, K., Wakabayashi, T., Ueda, I., Wada, Y., and Futai, M. (2000). *Caenorhabditis elegans* senses protons through amphid chemosensory neurons: proton signals elicit avoidance behavior. NeuroReport *11*, 2229–2232.

12. Troemel, E.R., Chou, J.H., Dwyer, N.D., Colbert, H.A., and Bargmann, C.I. (1995). Divergent seven transmembrane receptors are candidate chemosensory receptors in *C. elegans.* Cell *83*, 207–218.

13. Wu, M., Nern, A., Williamson, W.R., Morimoto, M.M., Reiser, M.B., Card, G.M., and Rubin, G.M. (2016). Visual projection neurons in the *Drosophila* lobula link feature detection to distinct behavioral programs. eLife *5*, e21022.

14. Schneider, J., Atallah, J., and Levine, J.D. (2012). One, two, and many--a perspective on what groups of *Drosophila melanogaster* can tell us about social dynamics. Adv. Genet. *77*, 59–78.

15. Choi, J.T., and Bastian, A.J. (2007). Adaptation reveals independent control networks for human walking. Nat. Neurosci. *10*, 1055–1062.

16. Lamb, T., and Yang, J.F. (2000). Could different directions of infant stepping be controlled by the same locomotor central pattern generator? J. Neurophysiol. *83*, 2814–2824.

17. Ashley-Ross, M.A., and Lauder, G.V. (1997). Motor patterns and kinematics during backward walking in the pacific giant salamander: evidence for novel motor output. J. Neurophysiol. *78*, 3047–3060.

18. Akay, T., Ludwar, B.C., Göritz, M.L., Schmitz, J., and Büschges, A. (2007). Segment specificity of load signal processing depends on walking direction in the stick insect leg muscle control system. J. Neurosci. *27*, 3285–3294.

19. Toth, T.I., Knops, S., and Daun-Gruhn, S. (2012). A neuromechanical model explaining forward and backward stepping in the stick insect. J. Neurophysiol. *107*, 3267–3280.

20. Islam, S.S., Zelenin, P.V., Orlovsky, G.N., Grillner, S., and Deliagina, T.G. (2006). Pattern of motor coordination underlying backward swimming in the lamprey. J. Neurophysiol. *96*, 451–460.

21. Matsushima, T., and Grillner, S. (1992). Neural mechanisms of intersegmental coordination in lamprey: local excitability changes modify the phase coupling along the spinal cord. J. Neurophysiol. *67*, 373–388.

22. Buchanan, J.T. (1999). Commissural interneurons in rhythm generation and intersegmental coupling in the lamprey spinal cord. J. Neurophysiol. *81*, 2037–2045.

23. Buchanan, J.T., and Grillner, S. (1987). Newly identified "glutamate interneurons" and their role in locomotion in the lamprey spinal cord. Science *236*, 312–314.

24. Cangiano, L., and Grillner, S. (2003). Fast and slow locomotor burst generation in the hemispinal cord of the lamprey. J. Neurophysiol. *89*, 2931–2942.

25. Grillner, S., Cangiano, L., Hu, G.-Y., Thompson, R., Hill, R., and Wallén, P. (2000). The intrinsic function of a motor system — from ion channels to networks and behavior. Brain Res. *886*, 224–236.

26. Akay, T., Haehn, S., Schmitz, J., and Büschges, A. (2004). Signals from load sensors underlie interjoint coordination during stepping movements of the stick insect leg. J. Neurophysiol. *92*, 42–51.

27. Bässler, U. (1986). Afferent control of walking movements in the stick insect *Cuniculina impigra*. J. Comp. Physiol. A *158*, 351–362.

28. Bässler, U. (1988). Functional principles of pattern generation for walking movements of stick insect forelegs: the role of the femoral chordotonal organ afferences. J. Exp. Biol. *136*, 125–147.

29. Bässler, U., and Wegner, U.T.A. (1983). Motor output of the denervated thoracic ventral nerve cord in the stick insect carausius morosus. J. Exp. Biol. *105*, 127–145.

30. Borgmann, A., Toth, T.I., Gruhn, M., Daun-Gruhn, S., and Büschges, A. (2011). Dominance of local sensory signals over inter-segmental effects in a motor system: experiments. Biol. Cybern. *105*, 399–411.

31. Bucher, D., Akay, T., DiCaprio, R.A., and Büschges, A. (2003). Interjoint coordination in the stick insect leg-control system: the role of positional signaling. J. Neurophysiol. *89*, 1245–1255.

32. Büschges, A. (1995). Role of local nonspiking interneurons in the generation of rhythmic motor activity in the stick insect. J. Neurobiol. *27*, 488–512.

33. Büschges, A., and Gruhn, M. (2007). Mechanosensory feedback in walking: from joint control to locomotor patterns. In Advances in Insect Physiology Insect Mechanics and Control., J. Casas and S. J. Simpson, eds. (Academic Press), pp. 193–230.

34. Daun-Gruhn, S. (2011). A mathematical modeling study of inter-segmental coordination during stick insect walking. J. Comput. Neurosci. *30*, 255–278.

35. Ekeberg, Ö., Blümel, M., and Büschges, A. (2004). Dynamic simulation of insect walking. Arthropod Struct. Dev. *33*, 287–300.

36. Hess, D., and Büschges, A. (1999). Role of proprioceptive signals from an insect femur-tibia joint in patterning motoneuronal activity of an adjacent leg joint. J. Neurophysiol. *81*, 1856–1865.

37. Zill, S.N., Büschges, A., and Schmitz, J. (2011). Encoding of force increases and decreases by tibial campaniform sensilla in the stick insect, *Carausius morosus*. J. Comp. Physiol. A *197*, 851–867.

38. Zill, S.N., Keller, B.R., and Duke, E.R. (2009). Sensory signals of unloading in one leg follow stance onset in another leg: transfer of load and emergent coordination in cockroach walking. J. Neurophysiol. *101*, 2297–2304.

39. Buschges, A. (2004). Sensory control and organization of neural networks mediating coordination of multisegmental organs for locomotion. J. Neurophysiol. *93*, 1127–1135.

40. White, J.G., Southgate, E., Thomson, J.N., and Brenner, S. (1986). The structure of the nervous system of the nematode *Caenorhabditis elegans*. Phil Trans R Soc Lond B *314*, 1–340.

41. Lee, R.Y., Sawin, E.R., Chalfie, M., Horvitz, H.R., and Avery, L. (1999). EAT-4, a homolog of a mammalian sodium-dependent inorganic phosphate cotransporter, is necessary for glutamatergic neurotransmission in *Caenorhabditis elegans*. J. Neurosci. Off. J. Soc. Neurosci. *19*, 159–167.

42. Wicks, S.R., Roehrig, C.J., and Rankin, C.H. (1996). A dynamic network simulation OF THE nematode tap withdrawal circuit: predictions concerning synaptic function using behavioral criteria. J. Neurosci. *16*, 4017–4031.

43. Zheng, Y., Brockie, P.J., Mellem, J.E., Madsen, D.M., and Maricq, A.V. (1999). Neuronal control of locomotion in c. Elegans is modified by a dominant mutation in the glr-1 ionotropic glutamate receptor. Neuron *24*, 347–361.

44. Dickinson, P.S. (2006). Neuromodulation of central pattern generators in invertebrates and vertebrates. Curr. Opin. Neurobiol. *16*, 604–614.

45. Harris-Warrick, R.M. (2011). Neuromodulation and flexibility in central pattern generator networks. Curr. Opin. Neurobiol. *21*, 685–692.

46. Marder, E., and Bucher, D. (2007). Understanding circuit dynamics using the stomatogastric nervous system of lobsters and crabs. Annu. Rev. Physiol. *69*, 291–316.